INVESTIGATION TOWARD LARGE ANGLE, LARGE AREA ATOM INTERFEROMETER

by
Ying Tan
B.S. Physics, Tongji University (July, 1989)

Submitted to the Department of Physics in partial
fulfillment of the requirements for the degree of

Doctor of Philosophy

at the

MASSACHUSETTS INSTITUTE OF TECHNOLOGY

September 2001

Author……
Department of Physics
August 3,2001

Certified by……
Shaoul Ezekiel
Professor of Aeronautics and Astronautics, Thesis Supervisor

Certified by……
Selim Shahriar
Research Scientist of Research Laboratory of Electronics, Thesis Co-Supervisor

Certified by……
David E. Pritchard
Professor of Physics, Thesis Co-Supervisor

Accepted by……...
Thomas J. Greytak
Professor of Physics, Associate Department Head for Education

INVESTIGATION TOWARD LARGE ANGLE, SINGLE ORDER ATOM INTERFEROMETER

Abstract

by

Ying Tan

We have proposed a scheme for large angle two-dimensional atom interferometers based on multiple Raman pulses which will produce a two-dimensional pattern with independent choice of grating spacings in each direction. The feature size of this pattern is on the order of a few nm.

Our experimental effort in implementing the multiple pulses Raman atom interferometer was interrupted by an accident out of our control. In order to continue our experiment in a reasonable time frame, we built a small and compact atomic beam. In the process of resuming our work on this compact atomic beam, we observed the atomic interference in a way we didn't expect.

In addition, we have developed a numerical procedure for modeling our interferometer and have proposed a novel atom interferometer based on single Raman pulse.

Thesis Supervisor : Shaoul Ezekiel, Professor of Aeronautics and Astronautics
Thesis Co-Supervisor : Selim Shahriar, Research scientist of Research Laboratory of Electronics
Thesis Co-Supervisor : David E. Pritchard, Professor of Physics

TABLE OF CONTENTS

LIST OF FIGURES

ACKNOWLEDGMENTS

I would like to thank my advisor, Selim Shahriar, for his guidance over these years. His clear explanation of how lock-in amplifier works impressed me so much that I probably will remember it the rest of my life.

I would like to thank all members of my thesis committee. Among them, I took a short laser course with Professor Shaoul Ezekiel and listened an atomic physics course taught by Professor Wolfgang Ketterle. Both are great teachers and I learned a lot from them. I especially wish to thank my co-supervisor Professor David Pritchard. He read my progress report carefully every year and gave me some very valuable suggestions. Without his encouragement, this work might not have been possible or might have taken a lot longer.

I am indebted to Philip R. Hemmer. I am grateful that I had the luck to work with him for some time. It was such a pleasure to watch him doing things in the lab. I still remember once that we were trying to install one of the nozzle screws for the atomic beam. He was trying to adjust its position by looking at the reflection from the mirror. I was so impressed since I can never do it well. I tried to cut my own hair by looking into the mirror and I always messed up. He told me that he was really good at doing things by looking at mirror images because he spent enough time playing that with his son. It seemed to me that he always had a good suggestion for any problems I ever had in the lab. For a long time, I had the habit of thinking about physics in equations. He once told me that experimentalists could understand physics better since they don't have time to solve complicated equations or they don't feel comfortable to do so, they usually will try to simplify the problem at hand as much as possible and ultimately they will get the essence of the problem. That is really a new way for me.

I also would like to thank my co-workers.

John Kierstead is such a pleasant person to work with. He showed me that a capable and relaxed person could work much more efficiently. Work with him was not rushed but were always beautifully done. It seems to me that he could always come up with some genius solution for mechanical problems and electronic problems. I still remember once that we needed to repair a big diffusion pump in our vacuum system. We needed to lower the monster and to move it out But the space there was so limited. John came up with such a great idea that I will never forget. He just used a big piece of aluminum plate and put four threaded holes at four corners. We just used that plate and four screws to raise and lower the big diffusion pump.

Dr. Timothy Grove taught me pretty much every lab technique when I first joined the group. I guess I will definitely pass on the Grove's method of aligning the saturation absorption setup if I ever get a chance.

I worked with Dr. Xiao-Wei Xia during the initial stage of the experimental setup. Most of our work back then were mechanical. I have some fond memory about that part too. Sometimes he would sing songs while we tightened the screws for the vacuum system. He had a beautiful voice.

Dr. A. Kumarakrishnan was another very knowledgeable postdoc in our group. He taught me pretty much everything I know about electro optical components. However,

the most valuable thing he taught me was how to tackle a problem, especially an experimental problem, systematically.

Dr. Alexey Turukhin was in some sense my mentor. It will be hard for me to forget those countless lunch conversations. I was always amazed how many jokes he could remember and how many of them are physics related. He is very easy-going and is very compassionate. Through my interaction with him, I realized that I really enjoy doing technical work and got some ideas from him on how to pursue my career along this line.

Jacob Morzinski is my fellow graduate student. He is the smartest person I've ever met. On top of that, he is very polite and he always goes extra miles to help other people. I feel I am very privileged to have been working with him. I was fascinated by his brain, often wondered how he could make those associations among various ideas so quickly.

Chapter One:

Introduction

1.1 Atom interferometer[1,2,3]

The atom interferometer is an apparatus that takes advantage of the wave nature of atoms. It is very similar to optical interferometers. In both cases, the wave is split in two coherent parts and recombined later to produce interferences. However, since the equations of motion for photons and for atoms are not the same and because there are some other differences between photons and atoms, the atom interferometer has some special features. For example, atoms are a lot heavier than photons; atoms have a much shorter de Broglie wavelength; atoms can be deposited to substrates, etc. In addition, atom interferometers can be applied to some areas which optical interferometers are not appropriate or not as good. For example, the atomic interferometer can be used to study atomic properties, because for different internal structure, different mass, different magnetic moment, different absorption frequencies, and different polarizability, the atomic interference might be different. The atomic interference might also be different with other atoms nearby. It can also be used to explore fundamental issues such as measuring the inertial effects. For practical applications, the atomic interferometer is very useful too. For example, it can be used as a good gyroscope or a gravity gradiometer. It can also be used to deposit quantum dots and nano-scale lithography on substrates. Since it has such a rich variety of applications, people are strongly motivated to build better and better atom~~ic~~ interferometers.

Another difference between atomic interferometers and optical ones is that different types of beam splitters and mirrors are used. Furthermore, while some people use nano-fabricated slits or diffraction gratings as atomic beam splitters and mirrors, using material structures or periodic light field, others take advantage of the fact that the internal and external degree of freedoms in atoms can be related. In our group, we adopt the second approach.

An atomic beam splitter, which involves internal states, is based on the interaction of a two level atom with a standing wave light field. The disadvantage of that method is that the atom wave packet scatters into multiple orders since the phase grating is sinusoidal. Alternatively, people also use magneto-optic beam splitters and bichromatic standing wave beam splitters[4]. Both methods provide a triangular phase grating so the momentum separation of the splitting components of the wave packet is much larger than the momentum spread of each component. For the former scheme, because the triangular shape only extends to the scale of the wavelength, there are still a number of significant higher orders. The latter one would have a potential remaining triangular for all the dressed state and extending over many wavelengths. However, for both of them, since the excited states are involved, if the interaction time is longer than the lifetime of the excited states, spontaneous emission would limit the splitting.

1.2 Application in Rotation Sensing

For commercial applications, optical and mechanical gyroscopes are good enough. The motivation behind our atom interferometer is to test the fundamentals of physics.

Atomic gyroscopes as well as optical gyroscopes use the Sagnac effect, a rotation dependent phase shift, to measure the rotation rate.

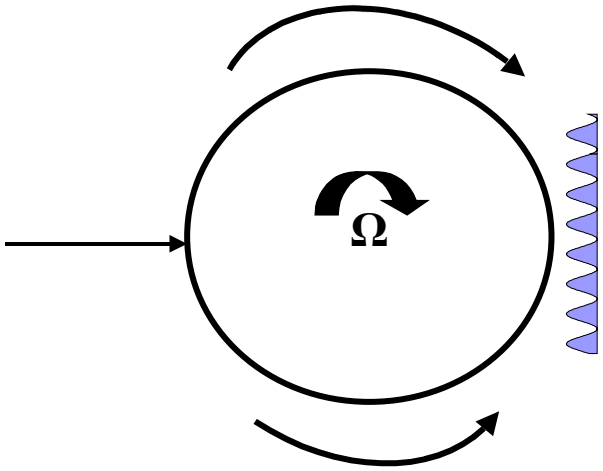

Sagnac effect

$(\Delta\Phi)_{atomic} = 2m\boldsymbol{\Omega}\cdot\mathbf{A}/h$

$(\Delta\Phi)_{optical} = 4\pi\boldsymbol{\Omega}\cdot\mathbf{A}/(\lambda c)$

Figure 1.1 *Interferometer as gyroscope*

See Figure 1.1., if an interferometer, with the top and bottom half circles as its two legs, is placed in a frame of reference with rotation rate Ω, the phase accumulated for the top path and bottom path are

$$k(\pi R + R\Omega t) \qquad \text{(eq. 1.1)}$$

$$k (\pi R - R \Omega t) \quad \text{(eq. 1.2)}$$

respectively, where R is the radius of the circle and $t = \pi R/v$. The phase difference is $\Delta\Phi = 2 k R \Omega t = 2 k R \Omega \pi R / v = 2 k \mathbf{\Omega} \cdot \mathbf{A} /v$, where **A** is the area of the loop.

In the optical case,

$$v = c, \quad \text{(eq. 1.3)}$$

$$k = 2 \pi / \lambda, \quad \text{(eq. 1.4)}$$

$$(\Delta\Phi)_{optical} = 4\pi \mathbf{\Omega} \cdot \mathbf{A} / (\lambda c), \quad \text{(eq. 1.5)}$$

in the atomic case,

$$\hbar k = p = m v, \quad \text{(eq. 1.6)}$$

$$(\Delta\Phi)_{atomic} = 2m \mathbf{\Omega} \cdot \mathbf{A} / \hbar. \quad \text{(eq. 1.7)}$$

Given the same rotation rate **Ω** and the same enclosed area **A**, the ratio

$$(\Delta\Phi)_{atomic} / (\Delta\Phi)_{optical} = m c^2 / \hbar \omega. \quad \text{(eq. 1.8)}$$

For example, using Rubidium atoms and using visible optical wavelength around 600 nm, $m c^2 / \hbar \omega$ is on the order of 10^{11}. The sensitivity of the gyros is proportional to the phase shift. We see that atom interferometers have an 11 orders of magnitude advantage over optical interferometers if all else is equal. However, optical interferometer gyros can have much larger enclosed areas and have much larger signal to noise ratio. At present, the performance of the best atomic gyro is comparable to the best optical gyro. The best atom interferometer gyro reported to date has enclosed area about 22 mm^2 and flux about 10^8 /second [5], which can measure 3×10^{-8} rad/second[6]. In our scheme , we ultimately hope to

use trapped atoms as the source, which could give us an enclosed area of about 0.5 m^2 and a flux 10^{10} atoms/second. This scheme could measure the rotation rate about 10^{-13} rad/second.

1.3 Application in lithography[7]

An atom can be considered a de Broglie wave packet. For example, the Rubidium atom we use in our experiment, at about 300 ^oC has de Broglie wavelength $\lambda=h/mv=0.0153$ nm. If we split the de Broglie wave packet and then recombine them, we will get interference fringes, just as in the optical case.

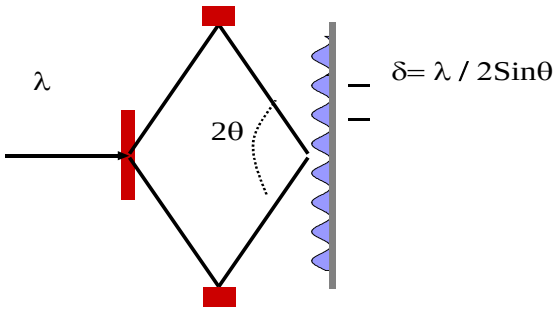

Figure 1.2 *Lithography application*

For the following discussion refer to Figure 1.2. The fringe spacing is $\lambda/2\sin\theta$. The smaller the wavelength and the bigger the splitting angle, the finer the fringes will be. General optical lithography, in the visible range, can reach a feature size on the order of 100 nm. There are other means to push the feature size down by using x rays, electron beams, STM (Scanning Tunneling Microscope), MBE(molecular beam epitaxy). However, they either have many problems at the current stage or they are very slow and only one-dimensional.

Atom interferometry in the application of lithography offers some advantages over general optical lithography. Using Rubidium, the de Broglie wavelength is more than four orders of magnitude smaller than that of visible light. The difficult part in lithography using atom interferometry is the wave packet splitting angle. In the optical case, the splitting angle can easily be as large as 90 ^{o} and still will generate the smallest fringe spacings at that wavelength. In the atomic case, we need good mirrors and good beam splitters. Only the transverse components (θ =90 ^{o}) contribute to the interference fringes. In the atomic case, momentum is related to wavelength. If for example we were to use Rubidium atoms, the optical transition wavelength is λ_o=780 nm; if part of the atom wave packet receives n photon recoils in the transverse direction, the momentum in that direction is n$\hbar$k , where k=2π/ λ_o. The effective de Broglie wavelength is λ=2π/nk= λ_o/n. If we want to get the atom lithography feature size down to the order of 10 nm, we need to have roughly n=80. In our scheme we hope to achieve on the order of 100 photon recoils. This could produce uniform one-dimensional and two-dimensional structures with feature size less than 10 nm, which can be used as a quantum dot array. We also hope to generate two-dimensional arbitrary patterns with feature size down to 10 nm. What limits us to get down to even smaller structures are some technical difficulties. For example, more splitting requires more laser power and the Raman-Nath limit comes into play. Also, when the atom receives too many photon recoils, because of the Doppler effect, it's not in resonance with the laser beam any longer and a more complicated scheme has to be designed to solve this problem.

1.4 Overview of the thesis

We investigate the possibility of building large angle and large area one-dimensional and two dimensional atom interferometers. We also investigate the possibility of building a guided wave atom interferometer via binary phase masking of the optical field.

Initially, we tried to realize our atom interferometer by using the bichromatic standing wave method[8], which produces triangular potential field for atoms, like blazed gratings. It turned out that this scheme required too much laser power and still suffered from spontaneous emission since atoms are in the excited states half of the time. This scheme is ok for a small area interferometer but not good for a large area interferometer because part of the atom is in the excited state even during the free flight as well.

Then we realized that the physical mechanism of the bichromatic standing wave method is essentially multiple π pulses. The alternative is to use a bichromatic standing wave method in a Λ system. This is equivalent to multiple Raman pulses and is an extension of the Raman interferometer of Chu's group[9]. Using a Λ system for an atom interferometer, we have the options of adiabatic following[10] and multiple Raman pulses. The adiabatic following doesn't work with $m_F = 0$ level. It also has some other difficulties. The multiple Raman pulses method[11] has an additional feature necessary for spatial interference and can be extended to two-dimensional atom interferometer and this is the method we are using in this work.

While we were attempting the $\pi/2$- π- $\pi/2$ interferometer, the first step of multiple Raman pulse interferometer experiment, an accident happened. Our lab was shutdown for the removal of asbestos on the floor for one day. The next morning I was notified that

something was smoking around our experimental apparatus while we were kept out of the lab. I went to check and found out that our vacuum system was completely destroyed. After failing to recover the vacuum system, we had to take each diffusion pump off and test it separately. Eventually we replaced each one of them. The experimental effort along the line of the multiple Raman pulses was stopped and instead we built a smaller scale atomic beam machine.

Before we attempt the $\pi/2$- π- $\pi/2$ interferometer experiment on this new atomic beam machine, we tried to see whether we can use one single counter-propagating Raman to get atomic interference since we believe that the one Raman pulse approach is the same as $\pi/2$- π- $\pi/2$ interferometer with the distance set to zero between Raman pulses. We did see the atomic inference. Further numerical simulations show that we can design a new type of atomic interferometers based on one single Raman pulses by manipulating the phases of different parts of the Raman beam.

This thesis is organized in six chapters. Chapter one covers the general introduction and overview. Chapter two describes the theory of Raman interaction, one-dimensional atom interferometers using multiple Raman pulses and the extension to two-dimensional atom interferometers. Chapter three covers the experimental investigation of one dimensional atom interferometers using multiple Raman pulses. Chapter four is about the experimental investigation of a new type of atom interferometer using single Raman pulse. Chapter five contains the numerical simulations and the investigation of the possibility of designing a new type of atom interferometer using single Raman pulse. Chapter six is the conclusion and the future work.

Chapter Two:

Raman Interaction and One-Dimensional Atom Interferometer Using Multiple Raman Pulses

2.1 Basic ideas of one-dimensional atom interferometer using atom-light interaction as beam splitters and beam deflectors, using two-level system to demonstrate the principles[12,13]

The basic idea Borde[14] of using Raman pulses to realize the atom interferometer was proposed by C. J. in 1989.

Our beam splitters and deflectors are based on the near resonance atom-light interaction. If a ground state two-level atom absorbs a near-resonance photon, it would transit to the excited state. At the same time it will also absorb the momentum of the photon and pick up a recoil momentum in the same direction and with the same value as that of the incident photon. An excited atom will either emit a photon stimulated by an incident photon or spontaneously emit a photon and go back to the ground state. In the former case, the emitted photon would be identical to the stimulating photon and the recoil momentum that the atom picks up would be exactly the same value as that of the incident photon but in the opposite direction. In the latter case, the momentum of the emitted photon would follow a probability distribution determined by the energy levels

involved so the direction of the recoil momentum that the atom picks up is not fixed. We see that there is a correspondence between the internal state (distribution of the electrons relative to the nucleus) and external state (momentum) of the atom. If we use atom-light interaction to manipulate an atom's internal state, then at the same time we can also change its momentum. However, spontaneous emission doesn't let us manipulate the momentum of the atom in the way we want. It actually contributes noises to this type of atom interferometer and so it should be avoided.

2.1.1 Rabi flopping

There is an analytical way to calculate the time evolution of a wave function that is to transform the basis to an eigenstate basis representation where the time evolution is very easy to calculate and then to transform back. Here is the example with the two level system:

A two-level atom[15] with ground state $|g\rangle$, energy E_g, and excited state $|e\rangle$, energy E_e, interacts with a laser beam with detuning $\delta = (\omega - \omega_{eg})$, where $\omega = 2\pi f$, f is the laser frequency, $\omega_{eg} = \omega_e - \omega_g$ and $\omega_e = E_e / \hbar$, $\omega_g = E_g / \hbar$. The Hamiltonian for the interaction is

$$H = \hbar \omega_e |e\rangle\langle e| + \hbar \omega_g |g\rangle\langle g| - \mathbf{d} \cdot \mathbf{E} \qquad \text{(eq. 2.1)}$$

where **d i**s the dipole moment of the atom and **E** is the laser field,

$$\mathbf{E} = \mathbf{E_0} \cos(\omega t + \varphi). \qquad \text{(eq. 2.2)}$$

In matrix form

$$H = \hbar \begin{bmatrix} \omega_e & -\Omega \cos(\omega t + \varphi) \\ -\Omega^* \cos(\omega t + \varphi) & \omega_g \end{bmatrix} \qquad \text{(eq. 2.3)}$$

where

$\Omega = \langle e | \mathbf{d} \cdot \mathbf{E_0} | g \rangle / \hbar$ (eq. 2.4)

is the Rabi frequency. After rotating wave approximation[16], we get

$$H = \hbar \begin{bmatrix} \omega_e & -\frac{\Omega}{2} e^{-i(\omega t+\varphi)} \\ -\frac{\Omega^*}{2} e^{i(\omega t+\varphi)} & \omega_g \end{bmatrix} \quad \text{(eq. 2.5)}$$

The atom generally is in state

$|\psi > = a_g |g > + a_e |e>,$ (eq. 2.6)

applying Schrödinger equation

$$i\hbar \frac{\partial}{\partial t} | \Psi > = H | \Psi >, \quad \text{(eq. 2.7)}$$

we get

$$i \begin{bmatrix} \dot{a}_e \\ \dot{a}_g \end{bmatrix} = \begin{bmatrix} \omega_e & -\frac{\Omega}{2} e^{-i(\omega t+\varphi)} \\ -\frac{\Omega^*}{2} e^{i(\omega t+\varphi)} & \omega_g \end{bmatrix} * \begin{bmatrix} a_e \\ a_g \end{bmatrix} \quad \text{(eq. 2.8)}$$

that is

$$\begin{cases} i\dot{a}_e = \omega_e a_e - \frac{\Omega}{2} e^{-i(\omega t+\varphi)} a_g \\ i\dot{a}_g = \omega_g a_g - \frac{\Omega^*}{2} e^{i(\omega t+\varphi)} a_e \end{cases} \quad \text{(eq. 2.9)}$$

If we factor out the fast varying part, let

$$\begin{cases} a_e = c_e e^{-i\omega_e t} \\ a_g = c_g e^{-i\omega_g t} \end{cases} \qquad \text{(eq. 2.10)}$$

we get

$$\begin{cases} i\dot{c}_e = -\frac{\Omega}{2} e^{-i(\delta t+\varphi)} c_g \\ i\dot{c}_g = -\frac{\Omega^*}{2} e^{i(\delta t+\varphi)} c_e \end{cases}. \qquad \text{(eq. 2.11)}$$

In the new basis $\{|e'>= e^{-i\omega_e t}|e>, |g'>= e^{-i\omega_g t}|g>\}$,

$$|\psi> = c_g |g'> + c_e |e'>, \qquad \text{(eq. 2.12)}$$

$$i\hbar\frac{\partial}{\partial t}|\Psi>= H'|\Psi>, \qquad \text{(eq. 2.13)}$$

$$H' = \hbar\begin{bmatrix} 0 & -\frac{\Omega}{2} e^{-i(\delta t+\varphi)} \\ -\frac{\Omega^*}{2} e^{i(\delta t+\varphi)} & 0 \end{bmatrix}. \qquad \text{(eq. 2.14)}$$

Now we want to make a rotating wave transformation so that the transformed Hamiltonian H_R would be time independent and real. In matrix form,

$$|\psi> = \begin{bmatrix} c_e \\ c_g \end{bmatrix}, \qquad \text{(eq. 2.15)}$$

$$|\psi>_R = \begin{bmatrix} d_e \\ d_g \end{bmatrix}, \qquad \text{(eq. 2.16)}$$

and the transformation matrix is

$$R = \begin{bmatrix} e^{\frac{i(\delta t+\phi)}{2}} & 0 \\ 0 & e^{-\frac{i(\delta t+\phi)}{2}} \end{bmatrix}, \qquad \text{(eq. 2.17)}$$

$$|\psi>_R = R\,|\psi>. \qquad \text{(eq. 2.18)}$$

Assume

$$\Omega = |\Omega|\, e^{-i\varphi'} \qquad \text{(eq. 2.19)}$$

and

$$\phi = \varphi + \varphi' \qquad \text{(eq. 2.20)}$$

so

$$H' = \hbar \begin{bmatrix} 0 & -\frac{|\Omega|}{2} e^{-i(\delta t+\phi)} \\ -\frac{|\Omega|}{2} e^{i(\delta t+\phi)} & 0 \end{bmatrix}. \qquad \text{(eq. 2.21)}$$

and

$$H'_R = RH'R^+ = \frac{\hbar}{2}\begin{bmatrix} 0 & -|\Omega| \\ -|\Omega| & 0 \end{bmatrix}, \qquad \text{(eq. 2.22)}$$

where

$$R^{+} = R^{-} = \begin{bmatrix} e^{-\frac{i(\delta t+\phi)}{2}} & 0 \\ 0 & e^{\frac{i(\delta t+\phi)}{2}} \end{bmatrix}. \qquad \text{(eq. 2.23)}$$

We can derive the Hamiltonian for the new representation from the Schrödinger equation.

$$i\hbar\frac{\partial}{\partial t}|\Psi>=H'|\Psi>, \qquad \text{(eq. 2.24)}$$

$$|\psi> = \mathrm{R}^{+}|\psi>_{\mathrm{R}}, \qquad \text{(eq. 2.25)}$$

so we have

$$i\hbar\frac{\partial}{\partial t}(R^{+}|\Psi>_{R}) = H'R^{+}|\Psi>_{R}, \qquad \text{(eq. 2.26)}$$

$$i\hbar\frac{\partial}{\partial t}(R^{+})|\Psi>_{R} + R^{+}i\hbar\frac{\partial}{\partial t}|\Psi>_{R} = H'R^{+}|\Psi>_{R}. \qquad \text{(eq. 2.27)}$$

Multiplying R from the left, we get

$$i\hbar R\frac{\partial}{\partial t}(R^{+})|\Psi>_{R} + RR^{+}i\hbar\frac{\partial}{\partial t}|\Psi>_{R} = RH'R^{+}|\Psi>_{R} = H'_{R}|\Psi>_{R}, \qquad \text{(eq. 2.28)}$$

$$i\hbar\frac{\partial}{\partial t}|\Psi>_{R} = (H'_{R} - i\hbar R\frac{\partial}{\partial t}(R^{+}))|\Psi>_{R} = H_{R}|\Psi>_{R}, \qquad \text{(eq. 2.29)}$$

$$-i\hbar R\frac{\partial}{\partial t}(R^{+}) = \hbar\begin{bmatrix} -\frac{\delta}{2} & 0 \\ 0 & \frac{\delta}{2} \end{bmatrix}, \qquad \text{(eq. 2.30)}$$

$$H_{R} = (H'_{R} - i\hbar R\frac{\partial}{\partial t}(R^{+})) = \frac{\hbar}{2}\begin{bmatrix} -\delta & -|\Omega| \\ -|\Omega| & \delta \end{bmatrix}. \qquad \text{(eq. 2.31)}$$

The eigenvalues of H_R are

$$\lambda_{\pm} = \pm\frac{\hbar}{2}\Omega_r \qquad \text{(eq. 2.32)}$$

where

$$\Omega_r = \sqrt{\delta^2 + |\Omega|^2}\ . \qquad \text{(eq. 2.33)}$$

We can find the eigenstates by a matrix transformation.

$$|\Psi>_D = D\,|\Psi>_R \qquad \text{(eq. 2.34)}$$

where

$$D = \begin{bmatrix} \cos\theta & -\sin\theta \\ \sin\theta & \cos\theta \end{bmatrix} \qquad \text{(eq. 2.35)}$$

is the matrix which should diagonalize H_R.

$$H_D = DH_R D^{-}$$
$$= \frac{\hbar}{2}\begin{bmatrix} -\delta\cos^2\theta + 2|\Omega|\sin\theta\cos\theta + \delta\sin^2\theta & -2\delta\sin\theta\cos\theta - |\Omega|\cos^2\theta + |\Omega|\sin^2\theta \\ -2\delta\sin\theta\cos\theta + |\Omega|\sin^2\theta - |\Omega|\cos^2\theta & -\delta\sin^2\theta - 2|\Omega|\sin\theta\cos\theta + \delta\cos^2\theta \end{bmatrix}$$
(eq. 2.36)

If H_D is diagonalized, then

$$\delta\sin 2\theta + |\Omega|\cos 2\theta = 0 \qquad \text{(eq. 2.37)}$$

that is

$$
\begin{aligned}
tg2\theta &= -\frac{|\Omega|}{\delta} \\
\sin 2\theta &= -\frac{|\Omega|}{\Omega_r} \\
\cos 2\theta &= \frac{\delta}{\Omega_r} \\
0 \le 2\theta &\le \pi
\end{aligned}
\qquad \text{(eq. 2.38)}
$$

The eigenstates are

$$
\begin{cases}
|\lambda_- >= \cos\theta\,|e>_R - \sin\theta\,|g>_R \\
|\lambda_{+-} >= \sin\theta\,|e>_R + \cos\theta\,|g>_R
\end{cases}
\qquad \text{(eq. 2.39)}
$$

So the time evolution of the wave function can be expressed as

$$
|\Psi(t_0+t)>= R^{-1}(t_0+t)(e^{-\frac{i\lambda_+ t}{\hbar}}\,|\lambda_+><\lambda_+| + e^{-\frac{i\lambda_- t}{\hbar}}\,|\lambda_-><\lambda_-|)R(t_0)\,|\Psi(t_0)>
\qquad \text{(eq. 2.40)}
$$

If we use matrix form,

$$
|\Psi(t_0+t)>= \begin{bmatrix} c_e(t_0+t) \\ c_g(t_0+t) \end{bmatrix},
\qquad \text{(eq. 2.41)}
$$

$$
|\Psi(t_0)>= \begin{bmatrix} c_e(t_0) \\ c_g(t_0) \end{bmatrix},
\qquad \text{(eq. 2.42)}
$$

$$
R(t_0) = \begin{bmatrix} e^{\frac{i(\delta t_0+\phi)}{2}} & 0 \\ 0 & e^{-\frac{i(\delta t_0+\phi)}{2}} \end{bmatrix}
\qquad \text{(eq. 2.43)}
$$

$$R^{-}(t_0+t)=\begin{bmatrix} e^{-\frac{i(\delta(t_0+t)+\phi)}{2}} & 0 \\ 0 & e^{\frac{i(\delta(t_0+t)+\phi)}{2}} \end{bmatrix} \quad \text{(eq. 2.44)}$$

$$|\lambda_{+}>=\begin{bmatrix}\sin\theta\\ \cos\theta\end{bmatrix}, \quad \text{(eq. 2.45)}$$

$$|\lambda_{-}>=\begin{bmatrix}\cos\theta\\ -\sin\theta\end{bmatrix}, \quad \text{(eq. 2.46)}$$

$$<\lambda_{+}|=\begin{bmatrix}\sin\theta & \cos\theta\end{bmatrix}, \quad \text{(eq. 2.47)}$$

$$<\lambda_{-}|=\begin{bmatrix}\cos\theta & -\sin s\theta\end{bmatrix}. \quad \text{(eq. 2.48)}$$

After some simple but tedious algebra, we get

$$c_e(t_0+t)=e^{-i\frac{\delta t}{2}}\{c_e(t_0)[\cos(\frac{\Omega_r t}{2})+i\sin(\frac{\Omega_r t}{2})\cos(2\theta)]+c_g(t_0)e^{-i\delta t_0-i\phi}[-i\sin(2\theta)\sin(\frac{\Omega_r t}{2})]\} \quad \text{(eq. 2.49)}$$

$$c_g(t_0+t)=e^{i\frac{\delta t}{2}}\{c_e(t_0)e^{i\delta t_0+i\phi}[-i\sin(2\theta)\sin(\frac{\Omega_r t}{2})]+c_g(t_0)[\cos(\frac{\Omega_r t}{2})-i\cos(2\theta)\sin(\frac{\Omega_r t}{2})]\} \quad \text{(eq. 2.50)}$$

Rabi flopping is a special case. Assume that the initial conditions are

$t_0=0$, (eq. 2.51)

$c_g(t_0) = 1$, (eq. 2.52)

$c_e(t_0) = 0$, (eq. 2.53)

that is the atom is in the ground state to start with, and with zero detuning, $\delta=0$, we get

$$c_e(t) = -i\sin(\frac{\Omega t}{2})e^{-i\phi} \quad \text{(eq. 2.54)}$$

$$c_g(t) = \cos(\frac{\Omega t}{2}) \quad \text{(eq. 2.55)}$$

$$\rho_{ee} = |c_e|^2 = \frac{1}{2}[1-\cos(\Omega t)] \quad \text{(eq. 2.56)}$$

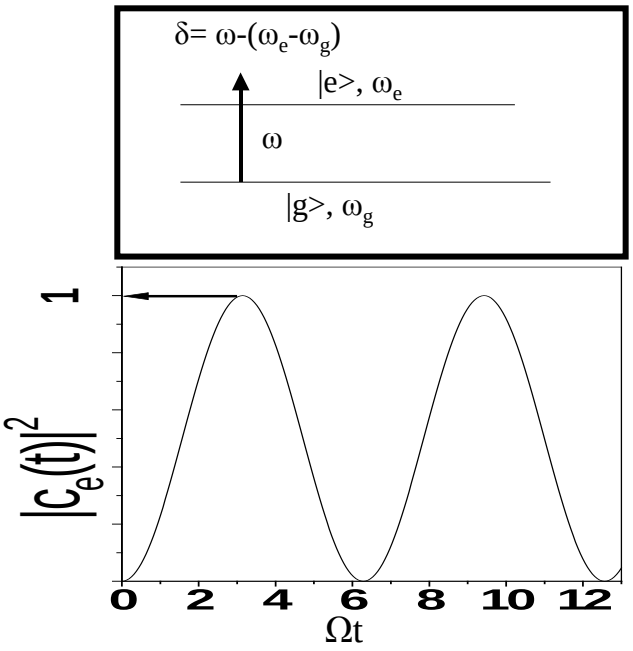

Figure 2.1 *Two level system Rabi flopping*

Figure 2.1 shows the probability of the transition to the excited state as a function of time. This is called Rabi flopping. We see that when

$$\Omega t = \pi, \quad \text{(eq. 2.57)}$$

$$c_e(\frac{\pi}{\Omega}) = -i\sin(\frac{\pi}{2})e^{-i\phi} = -ie^{-i\phi} \quad \text{(eq. 2.58)}$$

$$c_g(\frac{\pi}{\Omega}) = \cos(\frac{\pi}{2}) = 0 \qquad \text{(eq. 2.59)}$$

$$\rho_{ee}(\frac{\pi}{\Omega}) = 1, \qquad \text{(eq. 2.60)}$$

the probability of the transition to the excited state is unity. The " pulse " with Ωt= π is usually called a π pulse. When

$$\Omega t = \frac{\pi}{2}, \qquad \text{(eq. 2.61)}$$

$$c_e(\frac{\pi}{2\Omega}) = -i\sin(\frac{\pi}{4})e^{-i\phi} = -i\frac{\sqrt{2}}{2}e^{-i\phi} \qquad \text{(eq. 2.62)}$$

$$c_g(\frac{\pi}{2\Omega}) = \cos(\frac{\pi}{4}) = \frac{\sqrt{2}}{2} \qquad \text{(eq. 2.63)}$$

$$|\Psi(\frac{\pi}{2\Omega})> = -i\frac{\sqrt{2}}{2}e^{-i\phi}|e> + \frac{\sqrt{2}}{2}|g> \qquad \text{(eq. 2.64)}$$

$$\rho_{ee}(\frac{\pi}{2\Omega}) = \frac{1}{2}$$
$$\rho_{gg}(\frac{\pi}{2\Omega}) = \frac{1}{2} \qquad \text{(eq. 2.65)}$$

The " pulse " with Ωt= π/2 is called a π/2 pulse. We see that a π/2 pulse put atoms in a superposition state of the ground state and the excited state when they start from a pure state, ground state. The probabilities of the atom being at ground state and at the excited state are the same. Both are ½.

If we start with the excited state, that is

t_0=0, (eq. 2.66)

$c_e(t_0) = 1$, (eq. 2.67)

$c_g(t_0) = 0$, (eq. 2.68)

with also δ=0, we get

$$c_e(t) = \cos(\frac{\Omega\ t}{2}), \quad \text{(eq. 2.69)}$$

$$c_g(t) = ie^{i\phi}\sin(\frac{\Omega\ t}{2})]. \quad \text{(eq. 2.70)}$$

For

Ωt= π, (eq. 2.71)

$$c_e(\frac{\pi}{\Omega}) = \cos(\frac{\pi}{2}) = 0 \quad \text{(eq. 2.72)}$$

$$c_g(\frac{\pi}{\Omega}) = i\sin(\frac{\pi}{2})e^{i\phi} = ie^{i\phi} \quad \text{(eq. 2.73)}$$

ρ_{gg} (t) = 1. (eq. 2.74)

So the probability of the transition to the ground state from the excited state is unity. For a two level system, the π pulse can be used to flip states of the atoms, as the above description shows. When

$$\Omega t = \frac{\pi}{2}, \quad \text{(eq. 2.75)}$$

$$c_e(\frac{\pi}{2\Omega}) = \cos(\frac{\pi}{4}) = \frac{\sqrt{2}}{2} \quad \text{(eq. 2.76)}$$

$$c_g(\frac{\pi}{2\Omega}) = i\sin(\frac{\pi}{4})e^{i\phi} = i\frac{\sqrt{2}}{2}e^{i\phi} \quad \text{(eq. 2.77)}$$

$$|\Psi(\frac{\pi}{2\Omega})>= \frac{\sqrt{2}}{2}|e> + i\frac{\sqrt{2}}{2}e^{i\phi}|g> \quad \text{(eq. 2.78)}$$

$$\rho_{ee}(\frac{\pi}{2\Omega}) = \frac{1}{2}, \quad \rho_{gg}(\frac{\pi}{2\Omega}) = \frac{1}{2} \quad \text{(eq. 2.79)}$$

so for a two-level system, when an atom starts with either the ground state or the excited state, a π/2 pulse puts the atoms in a superposition state of the ground state and the excited state with equal probability in either state.

2.1.2. Principle of one dimensional atom interferometer

This kind of atom interferometer is based on the atom-light interactions. As we described in the section 2.1, when an atom and light interact, there's a correlation between the atom's internal state and its external state. We can control the atom's external motion by manipulating the atom's internal states if we can limit the interaction to absorption and stimulated emission while the spontaneous emission is negligible. There are two situations where we can consider ignoring spontaneous emission. One is when the energy levels involved are very sharp, such as the hyperfine splitting of ground

states or metastable states. Another is when the inverse of the Rabi frequency is much shorter than the lifetime of the upper energy level.

From section 2.1.1., we see that a π pulse can be used to deflect the atom. Assume that the atom starts at the ground state, though it would work similarly if the atom were to start at the excited state. Furthermore, we ignore the spontaneous emission in the following discussion. Since the transition probability is unity, the atom will absorb a photon and transit to the excited state and at the same time it will also pick up the momentum identical to the incident photon. On the other hand, since a $\pi/2$ pulse put the atom in a superposition state of the ground state and the excited state with equal probability, we can use the $\pi/2$ pulse as a beam splitter. The ground state part of the superposition keeps its momentum and the excited part of the superposition acquires the recoil momentum identical to that of the incident photon. Ultimately, those two parts will separate in space.

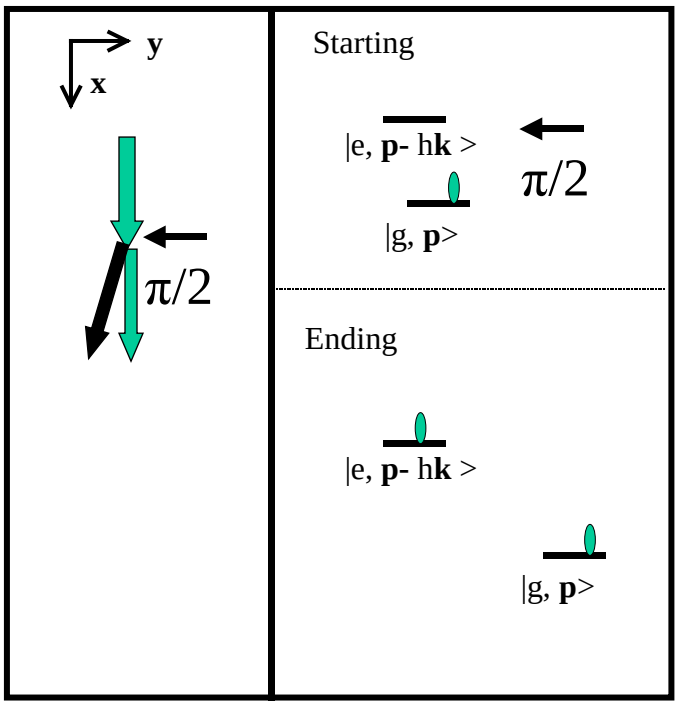

Figure 2.2 *Principle of the atom interferometer (1)*

Figure 2.2-Figure 2.8 shows how the principle of this type of atom interferometer works. In Figure 2.2 an atom starts with |g, **p**> at ground state with initial momentum **p** along **x** direction. A $\pi/2$ pulse is coming with photon momentum **-ħk** along the –**y** direction. After this $\pi/2$ pulse, the atom will be put into a superposition state of the ground state |g, **p**> with momentum **p** and the excited state |e, **p**-ħ**k**> with momentum **p**-ħ**k.** Given some time, |g, **p**> and |e, **p**-ħ**k**> will separate in space, as shown in the left half of the diagram.

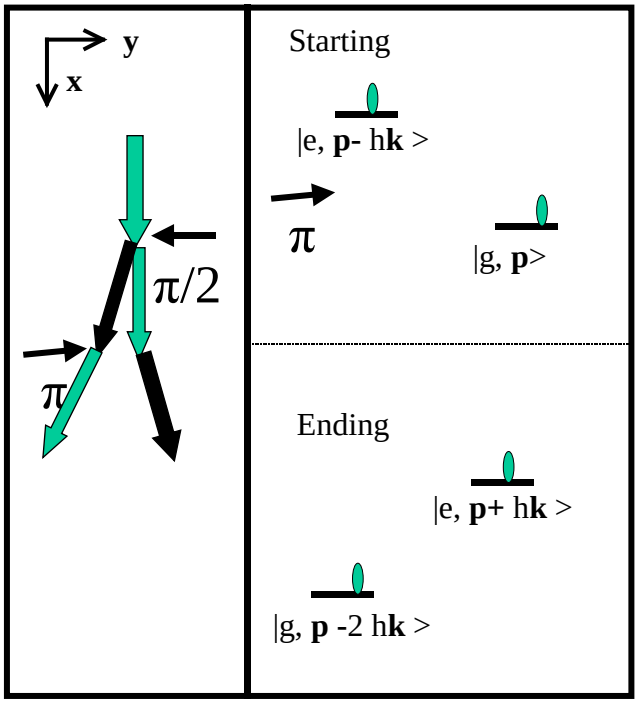

Figure 2.3 *Principle of the atom interferometer (2)*

Then we apply a π pulse from the direction opposite to the previous π/2 pulse, in the **y** direction, as in Figure 2.3. One effect of this π pulse is to flip the internal states. So we see that the ground state |g, **p**> flips to the excited state |e, **p**+ħ**k**> and the momentum of this part of the wave packet will change from **p** to **p**+ħ**k**. The excited state |e, **p**-ħ**k**> flips to the ground state |g, **p**-2ħ**k** > and the momentum of this part of the wave packet will change from **p**-ħ**k** to **p**-2ħ**k**. The split wave packets will move further apart after this π pulse, as shown in the left half of Figure 2.3.

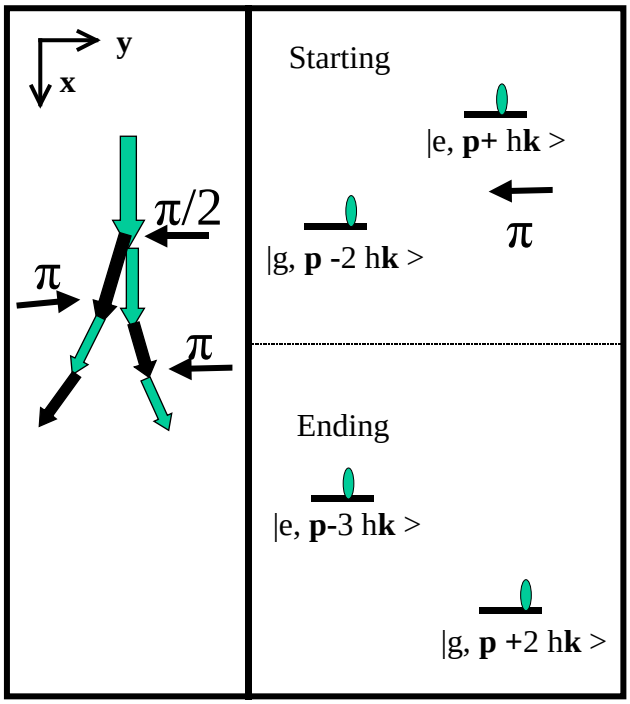

Figure 2.4 *Principle of the atom interferometer (3)*

After this first π pulse, we apply another π pulse from the opposite direction to the first π pulse, in -**y** direction, as in Figure 2.4. The second π pulse will flip state |e, **p**+ħ**k**> to the ground state |g, **p**+2ħ**k** > and the momentum of this part of the wave packet will change from **p**+ħ**k** to **p**+2ħ**k**, it will then flip state |g, **p**-2ħ**k** > to state |e, **p**-3ħ**k** > and the momentum of this part of the wave packet will change from **p**-2ħ**k** to **p**-3ħ**k**. This second π pulse also pushes the split wave packet further away, as shown in the left half of Figure 2.4. The first two π pulses which are opposite in directions can be considered as a π pulse pair. Afterwards, each such π pulse pair will push the split wave packet further apart.

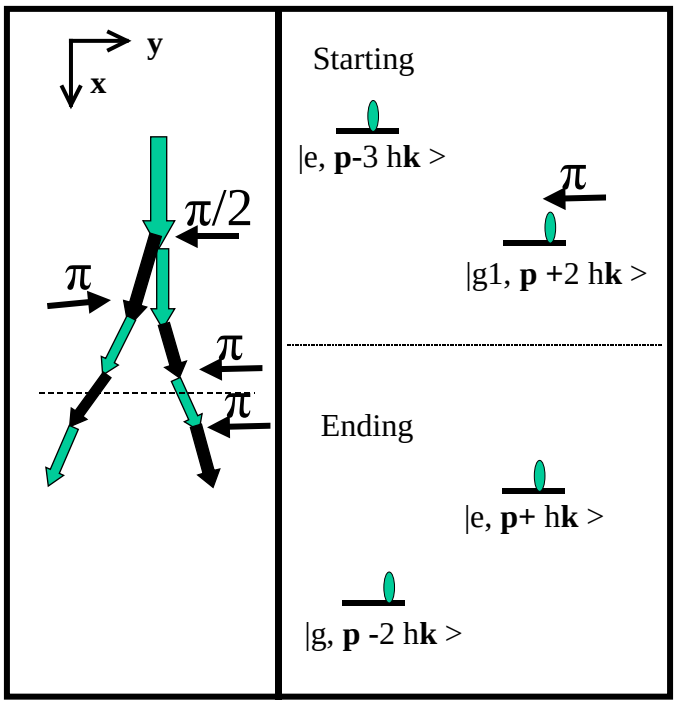

Figure 2.5 *Principle of the atom interferometer (4)*

If we want to bring the split wave packet back together and interfere, we need to apply a π pulse, which has the same direction as the previous π pulse, as shown in Figure 2.5.

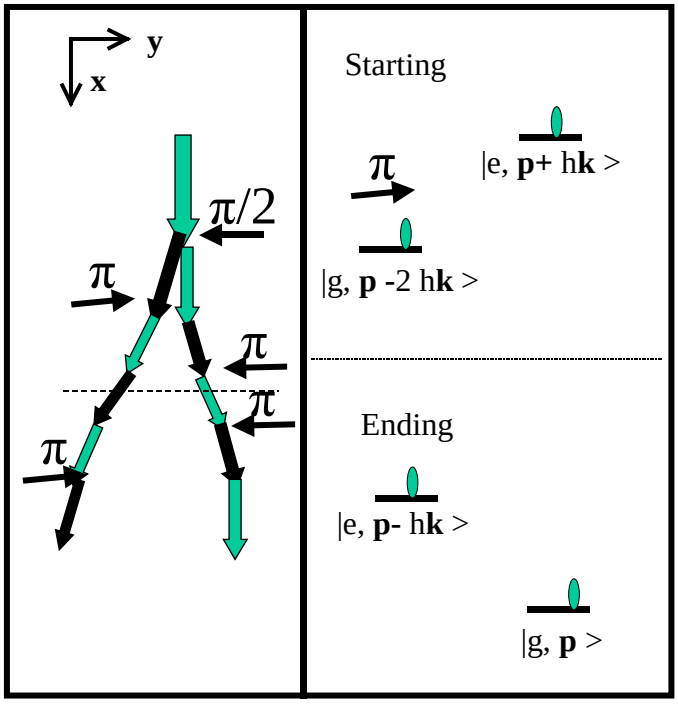

Figure 2.6 *Principle of the atom interferometer (5)*

Appling another π pulse from the opposite direction, as shown in Figure 2.6, will bring the wave packets even closer to each other. So if we apply the same number of π pulse pairs as that of the splitting π pulse pairs with directions opposite to that of the splitting π pulse pairs, we can bring the momentum states of the split components back to the identical states as were present just after the first π/2 pulse.

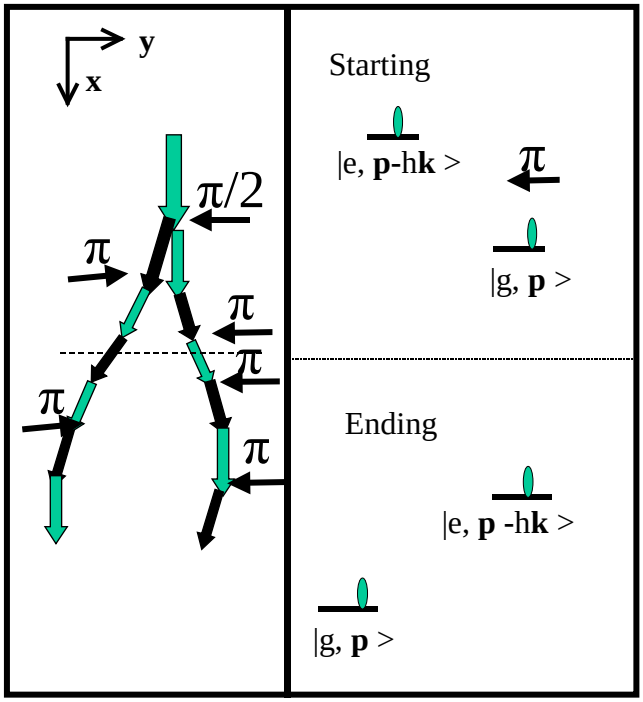

Figure 2.7 *Principle of the atom interferometer (6)*

To make them propagate toward each other, we have to apply another π pulse with the direction the same as that of the first π/2 pulse, as shown in Figure 2.7. We can eventually bring the split wave packet components back together by applying another π/2 pulse.

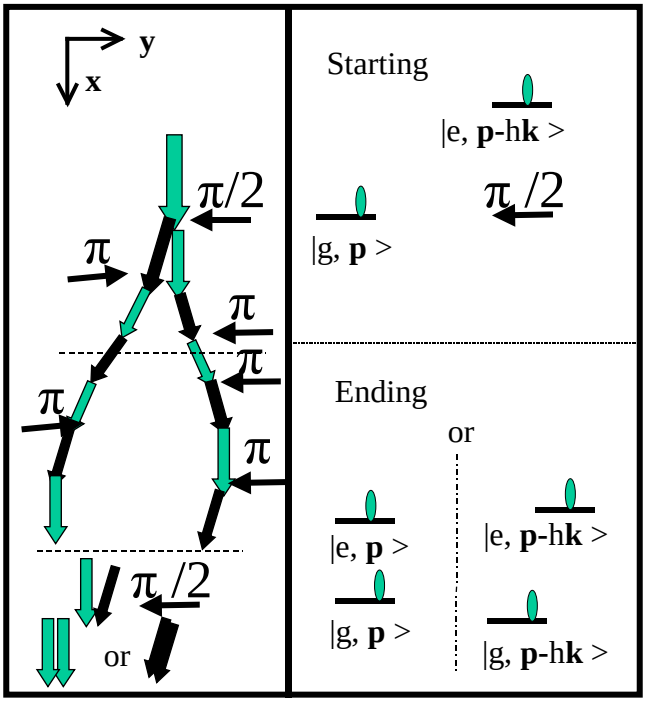

Figure 2.8 *Principle of the atom interferometer (7)*

Depending on the relative phase between the atom and the π/2 pulse, the atom will either end up at the ground state or the excited state, as shown in Figure 2.8.

Similar to optical interference, there are two ways to detect the atomic interference for different applications. The first method is to use a substrate so the atomic interference pattern can be deposited on. To use this method, some thing has to be done to make those two parts of the wave packet in the same internal states but not in the same momentum states. This is a good method for lithography applications. The second method is to apply another π/2 pulse when those two parts of the wave packet are approaching each other, as shown in Figure 2.8. The relative phase between the π/2 pulse and the atomic internal states will determine which internal state will be the final state for the atom. If we scan the phase of this π/2 pulse, we can detect the population of one

internal state as a function of the phase shift of the $\pi/2$ pulse. Since rotation sensing only depends on the fringe shift, this method is suitable for that type of applications.

2.2 Raman Interaction

Due to the selection rules, it's not always easy to find two very sharp energy levels for which spontaneous emission is negligible. For usual energy levels, to ignore the effect of spontaneous emission, either the laser beam has to be far detuned or the laser beam has to be very intense. Far detuned interaction will have very small transition probability. High laser power might not always be available.

Raman interaction can connect two stable energy levels.

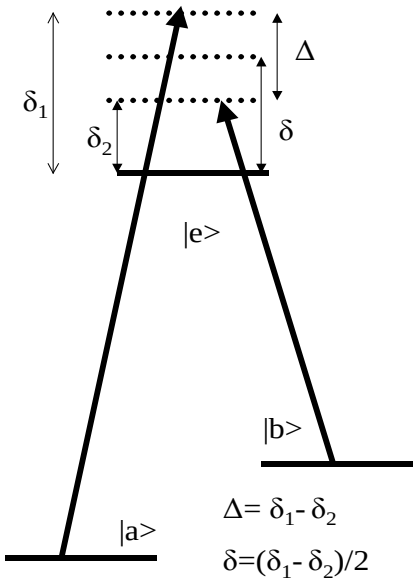

Figure 2.9 *Three level system*

2.2.1 On-Resonant Raman Interaction

Even though we don't use on-Resonant Raman interaction for our atom interferometer, it can be a very good diagnostic tool, for example, to check the frequency difference of the two stable energy levels involved and to set the Raman beam frequency difference appropriately.

We will consider a Λ system here. See Figure 2.9. The Hamiltonian for this system is

$H = \hbar \omega_e |e><e| + \hbar \omega_b |b><b| + \hbar \omega_a |a><a| - \mathbf{d} \cdot \mathbf{E}$ (eq. 2.80)

where **d i**s the dipole moment of the atom and **E** is the laser field,

$\mathbf{d}=\mathbf{d}_{ea} + \mathbf{d}_{eb}$, (eq. 2.81)

$\mathbf{E}=\mathbf{E}_{a}\cos(\omega_1 t+\varphi_1) + \mathbf{E}_{b}\cos(\omega_2 t+\varphi_2)$. (eq. 2.82)

In matrix form

$$H = \hbar \begin{bmatrix} \omega_e & -\Omega_a \cos(\omega_1 t + \phi_1) & -\Omega_b \cos(\omega_2 t + \phi_2) \\ -\Omega^*_a \cos(\omega_1 t + \phi_1) & \omega_a & 0 \\ -\Omega^*_b \cos(\omega_2 t + \phi_2) & 0 & \omega_b \end{bmatrix}$$ (eq. 2.83)

where

$\Omega_a=<e| \mathbf{d}_{ea}\bullet\mathbf{E}_{a}|a>/\hbar$ (eq. 2.84)

$\Omega_b=<e| \mathbf{d}_{eb}\bullet\mathbf{E}_{b}|b>/\hbar$. (eq. 2.85)

For on-resonance Raman interaction, we have

$\delta_1 = \delta_2 = 0$, (eq. 2.86)

$$\begin{aligned} \omega_1 &= \omega_e - \omega_a \\ \omega_2 &= \omega_e - \omega_b \end{aligned}.$$ (eq. 2.87)

After rotating wave approximation, changing the basis to the slow-varying basis, and after rotating wave transformation, as we did in section 2.1.1, we get

$$H_R = \frac{\hbar}{2}\begin{bmatrix} 0 & -\Omega_a & -\Omega_b \\ -\Omega^*{}_a & 0 & 0 \\ -\Omega^*{}_b & 0 & 0 \end{bmatrix} \qquad \text{(eq. 2.88)}$$

The basis in matrix form is

$$|e>=\begin{bmatrix}1\\0\\0\end{bmatrix}, |a>=\begin{bmatrix}0\\1\\0\end{bmatrix}, |b>=\begin{bmatrix}0\\0\\1\end{bmatrix}. \qquad \text{(eq. 2.89)}$$

We can form two orthogonal states which are superposition of two ground states |a> and |b>. They are

$$|->=\frac{1}{N}(\Omega_b\,|a> -\Omega_a\,|b>) = \begin{bmatrix} 0 \\ \frac{\Omega_b}{N} \\ \frac{-\Omega_a}{N} \end{bmatrix}$$

$$|+>=\frac{1}{N}(\Omega_a\,|a> +\Omega_b\,|b>) = \begin{bmatrix} 0 \\ \frac{\Omega_a}{N} \\ \frac{\Omega_b}{N} \end{bmatrix} \qquad \text{(eq. 2.90)}$$

where

$$N = \sqrt{\Omega^2{}_a + \Omega^2{}_b}\ . \qquad \text{(eq. 2.91)}$$

Since

$$< e | H_R | - >= \frac{\hbar}{2}\begin{bmatrix}1 & 0 & 0\end{bmatrix} * \begin{bmatrix} 0 & -\Omega_a & -\Omega_b \\ -\Omega^*_a & 0 & 0 \\ -\Omega^*_b & 0 & 0 \end{bmatrix} * \begin{bmatrix} 0 \\ \frac{\Omega_b}{N} \\ \frac{-\Omega_a}{N} \end{bmatrix} = 0 \qquad \text{(eq. 2.92)}$$

$$< e | H_R | + >= \frac{\hbar}{2}\begin{bmatrix}1 & 0 & 0\end{bmatrix} * \begin{bmatrix} 0 & -\Omega_a & -\Omega_b \\ -\Omega^*_a & 0 & 0 \\ -\Omega^*_b & 0 & 0 \end{bmatrix} * \begin{bmatrix} 0 \\ \frac{\Omega_a}{N} \\ \frac{\Omega_b}{N} \end{bmatrix} = -\frac{\hbar}{2}N \qquad \text{(eq. 2.93)}$$

$$< - | H_R | + >= \frac{\hbar}{2}\begin{bmatrix}0 & \frac{\Omega_b}{N} & -\frac{\Omega_a}{N}\end{bmatrix} * \begin{bmatrix} 0 & -\Omega_a & -\Omega_b \\ -\Omega^*_a & 0 & 0 \\ -\Omega^*_b & 0 & 0 \end{bmatrix} * \begin{bmatrix} 0 \\ \frac{\Omega_a}{N} \\ \frac{\Omega_b}{N} \end{bmatrix} = 0 \qquad \text{(eq. 2.94)}$$

Even if we add a phenomenological decay in the Hamiltonian so

$$H_R = \frac{\hbar}{2}\begin{bmatrix} -\frac{i}{2}\Gamma & -\Omega_a & -\Omega_b \\ -\Omega^*_a & 0 & 0 \\ -\Omega^*_b & 0 & 0 \end{bmatrix}, \qquad \text{(eq. 2.95)}$$

the above results don't change. We see that the state $|->$ doesn't couple with either the excited state $|e>$ or the ground state $|+>$. The state $|->$ is the so-called dark state. If an atom starts at either state $|a>$ or state $|b>$, there's a finite probability that after on-resonance Raman interaction, the atom will decay from excited state $|e>$ to state $|->$. When the atom ends up at state $|->$, it is trapped there and the on-resonance Raman interaction can't get it out of that state. In other words, the atom will stay in the ground state and we won't observe any fluorescence from the excited state. However, when the Raman interaction is not exactly on-resonance, we have the following Hamiltonian

$$H_R = \frac{\hbar}{2}\begin{bmatrix} -\frac{i}{2}\Gamma & -\Omega_a & -\Omega_b \\ -\Omega^*{}_a & \delta_a & 0 \\ -\Omega^*{}_b & 0 & \delta_b \end{bmatrix} \qquad \text{(eq. 2.96)}$$

and

$$< e | H_R | -> = \frac{\hbar}{2}\begin{bmatrix} 1 & 0 & 0 \end{bmatrix} * \begin{bmatrix} -\frac{i}{2}\Gamma & -\Omega_a & -\Omega_b \\ -\Omega^*{}_a & \delta_a & 0 \\ -\Omega^*{}_b & 0 & \delta_b \end{bmatrix} * \begin{bmatrix} 0 \\ \frac{\Omega_b}{N} \\ \frac{-\Omega_a}{N} \end{bmatrix} = 0 \qquad \text{(eq. 2.97)}$$

$$< - | H_R | + >= \frac{\hbar}{2} \begin{bmatrix} 0 & \frac{\Omega_b}{N} & -\frac{\Omega_a}{N} \end{bmatrix} * \begin{bmatrix} -\frac{i}{2}\Gamma & -\Omega_a & -\Omega_b \\ -\Omega^*{}_a & \delta_a & 0 \\ -\Omega^*{}_b & 0 & \delta_b \end{bmatrix} * \begin{bmatrix} 0 \\ \frac{\Omega_a}{N} \\ \frac{\Omega_b}{N} \end{bmatrix} \neq 0$$

(eq. 2.98)

We see that even if the state $|->$ is not coupled with the excited state $|e>$, it is coupled with the orthogonal ground state $|+>$. Even after the atom is in state $|->$, there's a finite probability that it will go to state $|+>$ and, therefore, goes to the excited state. This explains the on-resonance Raman dip we observed in the experiment. When on resonance, we observe no fluorescence and as we detune the Raman beams, we see fluorescence.

2.2.2 Off-Resonant Raman Interaction

For off-resonant Raman interaction, if far detuned, the excited states are almost not involved so the three-level system in this case can be simplified to a two-level system. After rotating wave approximation, changing the basis to the slow-varying basis, and after rotating wave transformation and shift the energy zero point, as we did in section 2.1.1, we get

$$H_R = \frac{\hbar}{2} \begin{bmatrix} 2\delta & -\Omega_a & -\Omega_b \\ -\Omega^*{}_a & \Delta & 0 \\ -\Omega^*{}_b & 0 & -\Delta \end{bmatrix}$$

(eq. 2.99)

In matrix form,

$$|\Psi>=\begin{bmatrix} C_e(t) \\ C_a(t) \\ C_b(t) \end{bmatrix}, \qquad \text{(eq. 2.100)}$$

$$i\hbar\frac{\partial}{\partial t}|\Psi>=H_R|\Psi>, \qquad \text{(eq. 2.101)}$$

$$\begin{bmatrix} \dot{C}_e(t) \\ \dot{C}_a(t) \\ \dot{C}_b(t) \end{bmatrix} = -i\begin{bmatrix} 2\delta & -\Omega_a & -\Omega_b \\ -\Omega^*{}_a & \Delta & 0 \\ -\Omega^*{}_b & 0 & -\Delta \end{bmatrix}\begin{bmatrix} C_e(t) \\ C_a(t) \\ C_b(t) \end{bmatrix}. \qquad \text{(eq. 2.102)}$$

We get

$$\begin{cases} \dot{C}_e(t) = -i2\delta C_e(t) + i\Omega_a C_a(t) + i\Omega_b C_b(t) \\ \dot{C}_a(t) = i\Omega^*{}_a C_e(t) - i\Delta C_a(t) \\ \dot{C}_b(t) = i\Omega^*{}_b C_e(t) + i\Delta C_b(t) \end{cases}. \qquad \text{(eq. 2.103)}$$

Since it's far detuned, we could adiabatically eliminate the excited state[17], that is, the excited-state population is very small, so that we can ignore the change of the ground states population due to the excited state decays, and approximately we get :

$$\dot{C}_e(t) = 0, \qquad \text{(eq. 2.104)}$$

so

$$C_e(t) = \frac{\Omega_a C_a(t) + \Omega_b C_b(t)}{2\delta} \qquad \text{(eq. 2.105)}$$

Substituting this into the above equation (eq. 2.106), we get

$$\begin{cases} \dot{C}_a(t) = i(\frac{|\Omega^*_a|^2}{4\delta} - \frac{\Delta}{2})C_a(t) + i\frac{\Omega^*_a\Omega_b}{4\delta}C_b(t) \\ \dot{C}_b(t) = i\frac{\Omega_a\Omega^*_b}{4\delta}C_a(t) + i(\frac{|\Omega^*_b|^2}{4\delta} + \frac{\Delta}{2})C_b(t) \end{cases} \qquad \text{(eq. 2.107)}$$

$$\begin{bmatrix} \dot{C}_a(t) \\ \dot{C}_b(t) \end{bmatrix} = -i\begin{bmatrix} \frac{\Delta}{2} - \frac{|\Omega^*_a|^2}{4\delta} & -\frac{\Omega^*_a\Omega_b}{4\delta} \\ -\frac{\Omega_a\Omega^*_b}{4\delta} & -\frac{\Delta}{2} - \frac{|\Omega^*_b|^2}{4\delta} \end{bmatrix}\begin{bmatrix} C_a(t) \\ C_b(t) \end{bmatrix} \qquad \text{(eq. 2.108)}$$

$$i\begin{bmatrix} \dot{C}_a(t) \\ \dot{C}_b(t) \end{bmatrix} = H_R'\begin{bmatrix} C_a(t) \\ C_b(t) \end{bmatrix} \qquad \text{(eq. 2.109)}$$

This is an effective two-level system where

$$H_R' = \begin{bmatrix} \frac{\Delta}{2} - \frac{|\Omega^*_a|^2}{4\delta} & -\frac{\Omega^*_a\Omega_b}{4\delta} \\ -\frac{\Omega_a\Omega^*_b}{4\delta} & -\frac{\Delta}{2} - \frac{|\Omega^*_b|^2}{4\delta} \end{bmatrix} \qquad \text{(eq. 2.110)}$$

and

$$\Omega_R = \frac{\Omega^*_a\Omega_b}{2\delta} \qquad \text{(eq. 2.111)}$$

is the effective Rabi frequency for this two-level system.

If we can adjust Ω_a and Ω_b so that AC stark shift is canceled, that is

$$\frac{|\Omega^*{}_a|^2}{4\delta} = \frac{|\Omega^*{}_b|^2}{4\delta}, \qquad \text{(eq. 2.112)}$$

then when the difference detuning

$$\Delta = 0, \qquad \text{(eq. 2.113)}$$

the system is equivalent to an on-resonant two-level system. If we scan the difference detuning Δ and detect the atom in state $|b>$ assuming the atom start at state $|a>$, the signal will be a peak centered at

$$\Delta = 0.$$

Off-Resonant Raman interaction has the advantage of involving two long live energy levels and the spontaneous emission can be ignored if far detuned. It is the interaction we use to realize the atom interferometer.

2.2.3 Raman-Ramsey Interference

Raman-Ramsey interference is the atomic interference and it is a very handy tool to optimize the system. Similar to Ramsey's original separate field microwave excitation, here we apply a $\pi/2$ pulse which lasts for time duration t in zone A and then let the atom move in the dark field for time T, after that the atom goes through zone B which is another field of $\pi/2$ pulse. We will show the principle in two-level system first. After zone B, we can detect the atom in either of the states.

From section 2.1.1., equation (eq.2.50), we got

$$c_e(t_0+t)=e^{-i\frac{\delta t}{2}}\{c_e(t_0)[\cos(\frac{\Omega_r t}{2})+i\sin(\frac{\Omega_r t}{2})\cos(2\theta)]+c_g(t_0)e^{-i\delta t_0-i\phi}[-i\sin(2\theta)\sin(\frac{\Omega_r t}{2})]\}$$

(eq. 2.114)

$$c_g(t_0+t)=e^{i\frac{\delta t}{2}}\{c_e(t_0)e^{i\delta t_0+i\phi}[-i\sin(2\theta)\sin(\frac{\Omega_r t}{2})]+c_g(t_0)[\cos(\frac{\Omega_r t}{2})-i\cos(2\theta)\sin(\frac{\Omega_r t}{2})]\}$$

(eq. 2.115)

For near resonance interaction, a $\pi/2$ pulse means $\Omega_r t = \pi/2$. If the atom starts at the ground state which is

$C_e(t_0) = 0,$ (eq. 2.116)

$C_g(t_0) = 1,$ (eq. 2.117)

$t_0 = 0,$ (eq. 2.118)

After zone A, we have

$$c_e(t)=-i\frac{\sqrt{2}}{2}e^{-i\frac{\delta t}{2}}e^{-i\phi}\sin(2\theta)$$

(eq. 2.119)

$$c_g(t)=\frac{\sqrt{2}}{2}e^{i\frac{\delta t}{2}}[1-i\cos(2\theta)]$$

In dark zone $\Omega_r t = 0$, so

$C_e(t+T) = C_e(t),$ (eq. 2.120)

$C_g(t+T) = C_g(t).$ (eq. 2.121)

At the end of zone B, we have

$$c_e(2t+T)=-ie^{-i\delta t-i\phi}e^{-i\frac{\delta T}{2}}\sin(2\theta)*$$
$$*[\cos(\frac{\delta T}{2})-\cos(2\theta)\sin(\frac{\delta T}{2})]$$

(eq. 2.122)

and

$$|c_e(2t+T)|^2 = \sin^2(2\theta) * [\cos(\frac{\delta T}{2}) - \cos(2\theta)\sin(\frac{\delta T}{2})]^2 \qquad \text{(eq. 2.123)}$$

For near resonance laser beam,

$$\delta << \Omega \qquad \text{(eq. 2.124)}$$

so

$$\begin{aligned} &\sin(2\theta) \approx 1, \\ &\cos(2\theta) \approx 0, \end{aligned} \qquad \text{(eq. 2.125)}$$

we have

$$|c_e(2t+T)|^2 = \cos^2(\frac{\delta T}{2}) = \frac{1}{2}[1+\cos(\delta T)] \qquad \text{(eq. 2.126)}$$

If we scan the detuning, we can detect the Ramsey fringes as a function of this detuning.

In three-level system far detuned case, as we see in the last section, it can be simplified to two level system. In a similar way, we can see Raman Ramsey interference fringes. If we make some changes in the above formula,

$$\begin{aligned} &e \to b, \\ &\Omega \to \Omega_R = \frac{\Omega_a * \Omega_b}{\delta_a + \delta_b} \\ &\delta \to \Delta' = \Delta - \frac{|\Omega_a|^2 - |\Omega_b|^2}{2(\delta_a + \delta_b)} \end{aligned} \qquad \text{(eq. 2.127)}$$

we get

$$|c_b(2t+T)|^2 = \cos^2(\frac{\Delta' T}{2}) = \frac{1}{2}[1+\cos(\Delta' T)]. \qquad \text{(eq. 2.128)}$$

2.3 Implementing the atom interferometer with Raman pulses

Using off-Resonance Raman pulses to implement this type of atom interferometer has a few advantages. First, since it's far detuned from excited state for each of the optical frequencies, the spontaneous emission effect is negligible. Second, it's two-photon interaction. If we arrange the Raman beams in counter-propagating configuration, the atom will get two-photon momentum recoil. Third, the alkali atoms we use in our experiment have ground state hyperfine splitting in the microwave range. Using Raman interaction, we only need to use optical frequencies therefore avoid using microwave excitation, which is not as easy to localize as optical waves. Fourth, the Raman interaction is only sensitive to difference frequency so ultra stable laser is not required. It's easier to stabilize the RF source.

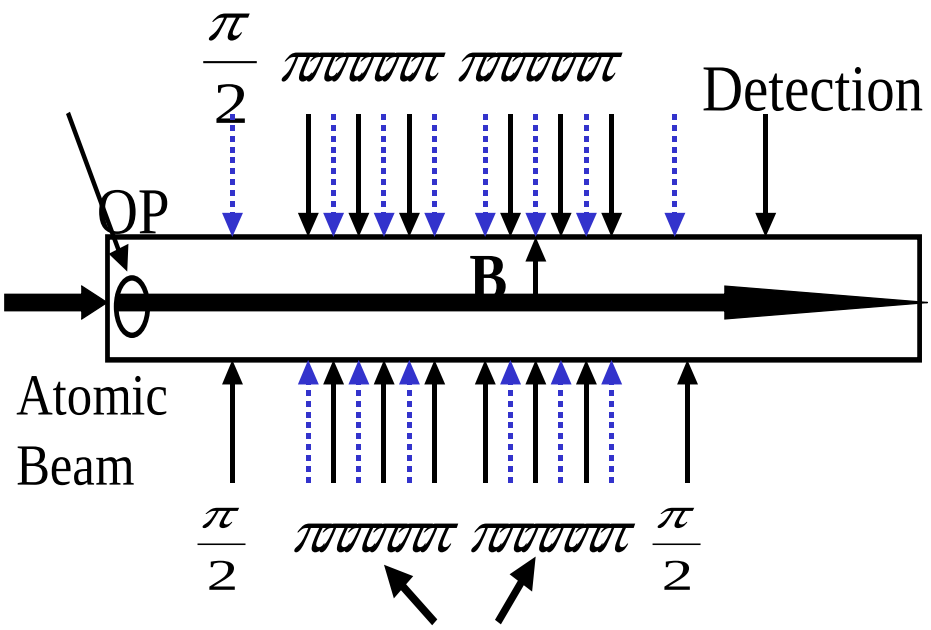

Figure 2.10 *Multi pulses in spatial domain*

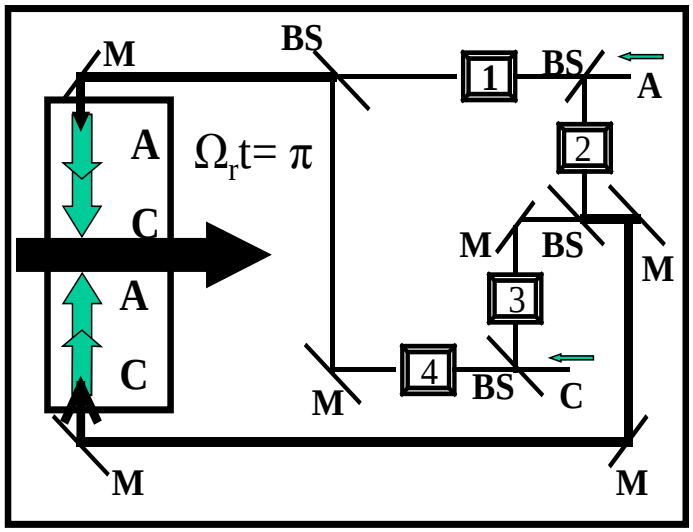

Figure 2.11 *Multi pulses in time domain, where BS is beam splitter and M is mirror.*

Experimentally, to realize multiple Raman pulses, there are two ways. One way is to deploy the Raman pulses spatially in a counter-propagating configuration, as shown in Figure 2.10. When the number of pulses is small, this method is better. However, when we need to go to larger number of pulses, the alignment of all of the pulses will become nightmare and almost impossible to accomplish. The second method is to implement Raman pulses in time domain, as shown in Figure 2.11. Two Raman beams with frequencies A and C respectively, each passes through a beam splitter then each split beam passes through a switch then goes to the experimental zone so that when all the switches are on, in experimental zone both frequencies are present from both sides. The switches 1,2, 3 and 4 are timed in a fashion so that the when the switches 1 and 3 are on for the duration of a π pulse but switches 2 and 4 are off, we have frequency A presents

from the top and C from the bottom. When the switches 2 and 4 are on for the duration of a π pulse but switches 1 and 3 are off, we have frequency C presents from the top and A from the bottom. This way we can get Raman π pulses with alternative directions. The advantage of this method is that the Raman beam alignment is a lot simpler. However, as the atom pick up recoil momentum gradually, because of the Doppler effect, the difference detuning will change and we have to chirp the Raman beam frequency to compensate this effect.

2.4 Extension to the two-dimensional atom interferometer with Raman pulses[18]

We see in section 2.12 the principle of one dimensional atom interferometer based on multiple Raman π pulses and π/2 pulses. To demonstrate the principle of two-dimensional atom interferometer, we use a concrete example here.

We consider the ^{87}Rb atom, released from an evaporatively cooled magnetic trap (or a Bose condensate) and falling under gravity. The relevant energy levels are shown in Figure 2.12. The atoms are assumed to be in state $|F=1, m_f=1\rangle$ at the onset. We excite the Raman transition, coupling $|F=1, m_f=1\rangle$ (hereafter referred to as $|a\rangle$) to $|F=2, m_f=1\rangle$ (hereafter referred to as $|c\rangle$). The beams are detuned strongly from the excited manifold of the D_2 line, but are two-photon-resonant, so that the process can be thought of as a two-level transition between the two magnetic sublevels. Here, the quantization direction, **z**, is assumed to be normal to the direction of gravity, denoted as **y**.

We assume that right after the atoms are released from their trap, they are in state $|a, p_z=0,p_x=0\rangle \equiv |a,0,0\rangle$. We apply two σ_+-polarized beams which are counter-propagating along the **z** axis, with frequencies chosen so one beam (hereafter called A) couples $|a\rangle$ to the excited state, while the other beam (hereafter called C) couples $|c\rangle$ to the same excited state. Both beams are pulsed, with pulse timing chosen so that counter-propagating pulses arrive at the atom simultaneously and leave the atom simultaneously. In our scheme, the first pulse's duration is chosen so that the pulse is a $\pi/2$ pulse, with beam A propagating in the $-\mathbf{z}$ direction and beam C propagating in the $+\mathbf{z}$ direction, so that the effect is to place the atom in an equal superposition of $|a,0,0\rangle$ and $|c,-2\hbar k,0\rangle$. This is illustrated in Figure 2.13 (solid line transitions). The second pulse pair has a longer duration, chosen so that the pulse is a π pulse, and also has the directions of beams A and C exchanged. This will cause a π-pulse transition between states $|a\rangle$ and $|c\rangle$, and the reversal of the beam direction will transfer $|a,0,0\rangle$ to $|c,+2\hbar k,0\rangle$ and $|c,-2\hbar k,0\rangle$ to $|a,-4\hbar k,0\rangle$ (dashed-line transitions in Figure 2.13). Note that the π pulses excite two Raman transitions in parallel, that momentum selection rules ensure that there is no mixing of these transitions, and that the atoms are still in an equal superposition of two states. The third pulse pair has the same duration as the second (i.e., it excites a π-pulse transition), but the directions of A and C are again exchanged. The state of the atom after this second π-pulse will now be an equal superposition of $|a,+4\hbar k,0\rangle$ and $|c,-6\hbar k,0\rangle$ (dotted-line transitions in Figure 2.13). Each subsequent pair of π-pulses again exchanges the directions of A and C, driving the atomic superposition to larger momentum splitting.

Inspection of Figure 2.13, we see the rule is that the π-pulse traveling in the +**z** direction should have the frequency that interacts with the current atomic state of the +**z**-traveling part of the atoms. After exposure to an even number N_z of these alternating-direction pairs of π-pulses, the atoms will be in an equal superposition of states $|a, +2N_z\hbar k, 0\rangle$ and $|c, -(2N_z+2)\hbar k, 0\rangle$. For example, $N_z=24$ alternating π-pulses will put the atoms in a superposition of states $|a, +48\hbar k,0\rangle$ and $|c, -50\hbar k,0\rangle$. The p_z difference of 98 $\hbar k$ corresponds to a velocity of about 0.6 m/s, and after 3.3 ms the atoms will separate into two clouds with spatial separation of 2 mm. We can now reverse the motion of the clouds by reversing the splitting scheme—choose the pulse directions so that the –**z**-traveling pulse has the frequency that interact with the +**z**-traveling atoms, and then continue to exchange pulse directions each time a π-pulse exchanges the atomic states. $N_z=24$ of these reversed pulses would bring the atoms back to the equal superposition of $|a,0,0\rangle$ and $|c,-2\hbar k,0\rangle$, and a further 25 pulses (for a total of 49) would put the atoms in a superposition of states $|c, -50\hbar k, 0\rangle$ and $|a, +48\hbar k, 0\rangle$, moving the two halves of the cloud back towards each other.

While the spatially separated components of the superposition state are moving toward each other, we can apply a pair of linearly polarized beams, co-propagating along the **x** direction, causing a Raman transition between $|a\rangle$ and $|c\rangle$ (dotted-line transitions in Figure 2.12). The duration of this pulse pair is chosen such that a π-pulse is induced on the two-photon transition coupling $|a\rangle$ and $|c\rangle$, and the location of the beam is chosen so that it only affects the component of the cloud that corresponds to the state $|c,-50\hbar k,0\rangle$.

The atom is now in an equal superposition of the states $|a,-50\hbar k,0\rangle$ and $|a,+48\hbar k,0\rangle$, since the co-propagating fields give no net momentum transfer in the **x** direction. If left alone these components will come together in about 3.3 ms and form fringes with a peak-to-peak spacing of about 8 nm. But before that happens we will split (and later recombine) each component further along the **x**-axis. We will use a pair of linearly polarized beams with frequencies A and C, counter-propagating in the **x** direction. In a manner analogous to the splitting in **z** direction, we first apply a $\pi/2$ pulse, interacting with both components of the split cloud, which produces an equal superposition of four states: $\{|a, -50\hbar k,0\rangle, |c, -50\hbar k,-2\hbar k\rangle\}$ separated spatially in the **z** direction from $\{|a, 48\hbar k,0\rangle, |c, 48\hbar k,-2\hbar k\rangle\}$. This is followed by a series of N_x direction-alternating π-pulse pairs, producing a set of four states. For even N_x, the states are:

$\{ |a,-50\hbar k,2N_x\hbar k\rangle, |c,-50\hbar k,-(2N_x+2)\hbar k\rangle\}$ and $\{ |a,48\hbar k,2N_x\hbar k\rangle, |c,48\hbar k,-(2N_x+2)\hbar k\rangle\}$.

The two clouds in curly brackets are spatially separate from each other in the **z** direction, while inside each cloud two sub clouds will now separate out in the **x** direction, with a velocity of 1.2 m/s if $N_x=2N_z=48$. Thus, after about 1.7 ms, the separation in the **x** direction will be about 2 mm in each cloud. At this point, $2N_x=96+1$ π-pulses will be applied in the **x** direction, with the pulse directions chosen to reverse the momentum splitting in the **x** direction. This will produce an equal superposition of the four states:

$\{ |a, -50\hbar k,-98\hbar k\rangle, |c, -50\hbar k,96\hbar k\rangle\}$ and $\{ |a, 48\hbar k,-98\hbar k\rangle, |c, 48\hbar k,96\hbar k\rangle\}$.

When these states merge their interference fringe spacing would be on the order of a few nanometers, which would be difficult to detect by optical grating diffraction. To observe

the interference and optimize the amplitude in real time, we could scan the phase of one of the laser pulses and detect the atoms either in state |a> or in state |c>. The population in either state is a function of the optical phase scan. This is the internal state interference and the sensitivity of this interference is independent of the splitting angle.

Finally, after optimizing the internal state interference, a **z** directed pair of co-propagating, circularly polarized beams are now used to excite a π transition between |a> and |c>, but located spatially so as to affect only the |c> sub cloud of each **z** separated cloud. The separation of 2 mm in the **x** direction makes this selective excitation possible. After this pulse sequence, we have four sub clouds, converging toward one another in both **x** and **z** directions, and each in the internal state |a>:

{ |a, -50$\hbar$k,-98$\hbar$k>, |a, -50$\hbar$k,96$\hbar$k>} and { |a, 48$\hbar$k,-98$\hbar$k>, |a, 48$\hbar$k,96$\hbar$k>}.

Note that the sub clouds are now separated in the **z** direction by 1 mm, and in the **x** direction by 2 mm. Similarly, the speed of convergence in the **z** direction (about 0.6 m/s) is half of the convergence speed in the **x** direction. As such, all four components of the cloud will come together in another 1.7 ms, forming a 2 dimensional matter wave grating pattern. The spacing of these patterns are determined by the values of N_z and N_x: for the rubidium transition wavelength of about 800 nm, the peak-to-peak separation in the **z** direction is approximately $100/N_z$ nm, and the separation in the **x** direction is $100/N_x$ nm. For the parameters chosen here, we would have a grating with about 4 nm spacing in the **x** direction, and 8 nm spacing in the **z** direction. Structures as small as 2 nm seem feasible given the source particles' parameters considered here. The number of spots, and uniformity of height thereof, are determined largely by the coherence length of the

sample. For a Bose condensed source, the coherence length is of the order of 300 μm, so that up to 10^{10} structures can be produced and deposited over an area of 300 μm diameter.

In the discussion above, we considered only the state with zero initial momentum. To see the effect of wave packet evolution on the interference pattern, we start with a Gaussian wave packet and Fourier transform it into momentum space. We take into account the initial momentum in the **x** and **z** directions and average the interference process over the initial wave packet. Figure 2.14 shows schematically the steps involved in producing the two-dimensional beam splitting and recombining. At point S, right after atoms are released from the trap, assume the initial momentum state is $|\psi_0\rangle=|a, p_{ox}\hbar k, p_{oz}\hbar k\rangle$. In what follows, we assume that the duration of the interaction with the laser pulses is negligible compared to the free evolution time of the wave-packet. Components of the wave-packet following the four distinct paths S-A-A1-E, S-A-A2-E, S-B-B1-E and S-B-B2-E will accumulate phase factors given by the following expressions:

$$\alpha=\mathrm{Exp}\{i(-\hbar k^2/2m)t[(p_{oz}-2N_z-2)^2 + (p_{oz}+2N_z)^2 + (p_{ox}+2N_x)^2 + (p_{ox}-2N_x-2)^2]\}, \quad \text{(eq. 2.129)}$$

Here t is the time from S to A or B. At point E, the momentum state becomes:

$$|\varphi(p_{ox},p_{oz})\rangle=1/2\alpha_1 (|a,(p_{oz}+2N_z-2)\hbar k, (p_{ox}-2N_x)\hbar k\rangle+ |a, (p_{oz}+2N_z-2)\hbar k, (p_{ox}+2N_x-2)\hbar k\rangle + |a, (p_{oz}-2N_z)\hbar k, (p_{ox}-2N_x)\hbar k\rangle+ |a, (p_{oz}-2N_z)\hbar k, (p_{ox}+2N_x-2)\hbar k\rangle) \quad \text{(eq. 2.130)}$$

The whole wave packet is then given by:

$$|\varphi\rangle=\iint dp_{ox}dp_{oz}\frac{2\delta}{\sqrt{2\pi}}\exp[-\delta^2(p_{ox}^{\ 2}+p_{oz}^{\ 2})k^2]^*|\varphi(p_{ox},p_{oz})\rangle \quad \text{(eq. 2.131)}$$

where δ is the standard deviation of the initial packet. The interference pattern is given by $P(x,z)\equiv\psi(x,z)^*\,\psi(x,z)$, where $\psi(x,z)=\langle a, z, x|\varphi\rangle$ is the spatial wave function.

P(x,z)=

$$\frac{4a^2}{2\pi(a^4+\frac{\hbar^2k^2}{m^2})}\cos^2[(2N_z+1)kz]\cos^2[(2N_x+1)kx]\exp[-\frac{a^2(\frac{2\hbar kt}{m}+z)^2}{2(a^4+\frac{\hbar^2t^2}{m})}]\exp[-\frac{a^2(\frac{2\hbar kt}{m}+z)^2}{2(a^4+\frac{\hbar^2t^2}{m})}] \quad \text{(eq. 2.132)}$$

From this, we can see that it is a two-dimensional interference pattern with Gaussian envelope.

Figure 2.15 shows a plot of this pattern for δ=10 nm and t=30 ns as a simple example. The relatively small size of the packet is chosen in order to ensure that both the fringe pattern and the roll-off are easily decipherable in the plot. Of course, as discussed above, the initial wave packet size could be as large as 1 mm. In that case, we will have nearly 10^{10} fringes within the envelope.

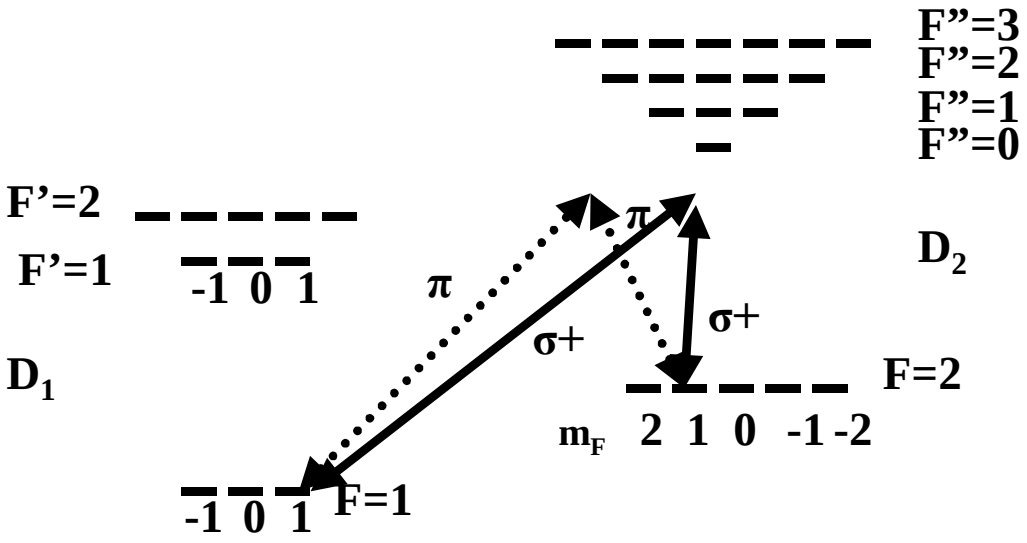

Figure 2.12 *Relevant energy level*

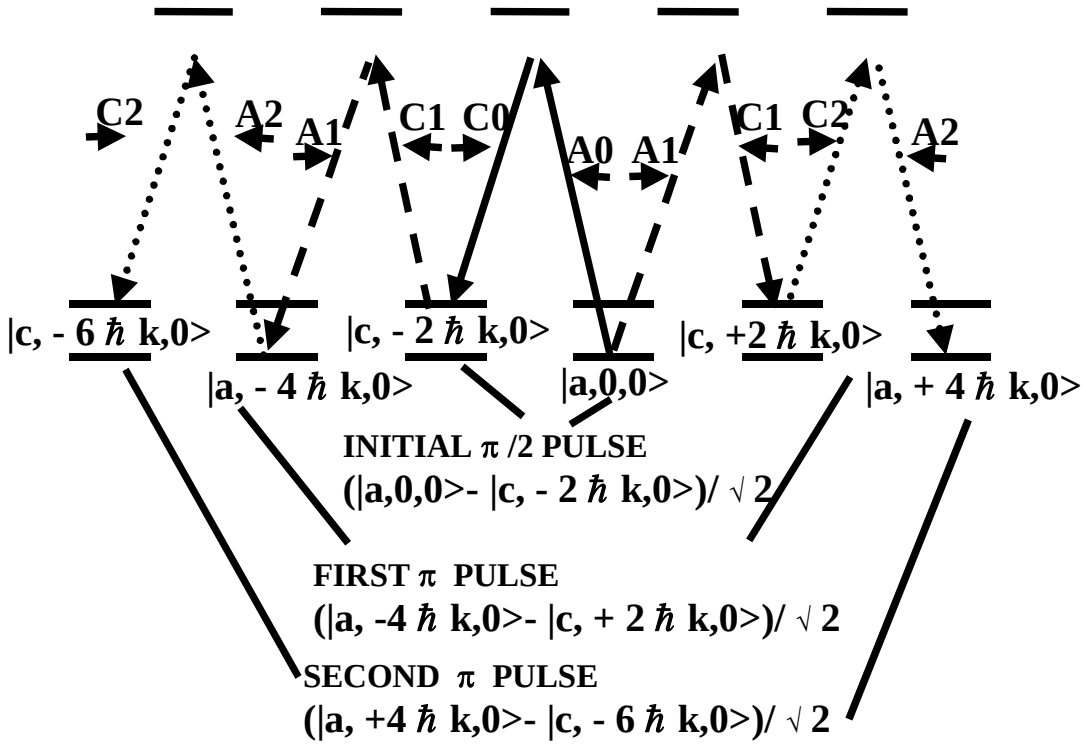

Figure 2.13 *Schematic illustration of the first three pulses in the Raman pulse beam splitter.Explicit form of the initial superposition state, after excitation with the π/2 pulse, is shown along with the superposition states resulting after the first and second π pulses are applied. Solid lines denote transitions excited with the π/2 pulse, dashed lines denote the first π pulse, dotted lines denote the second π pulse. Note that the π pulses excite two Raman transitions in parallel. Momentum selection rules ensure that there is no mixing of these transitions. For clarity, the energy shifts due to kinetic energy are omitted.*

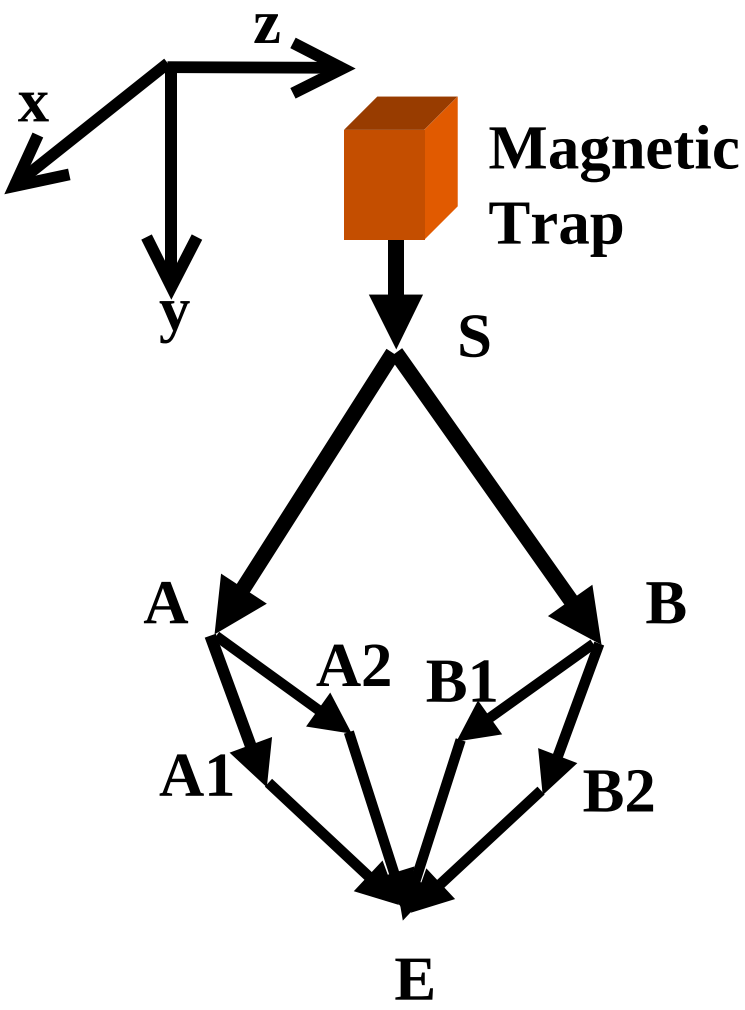

Figure 2.14 *An illustration of the steps involved in producing two-dimensional beam-splitting and recombining. For simplicity, the laser beams are not shown in the diagram.*

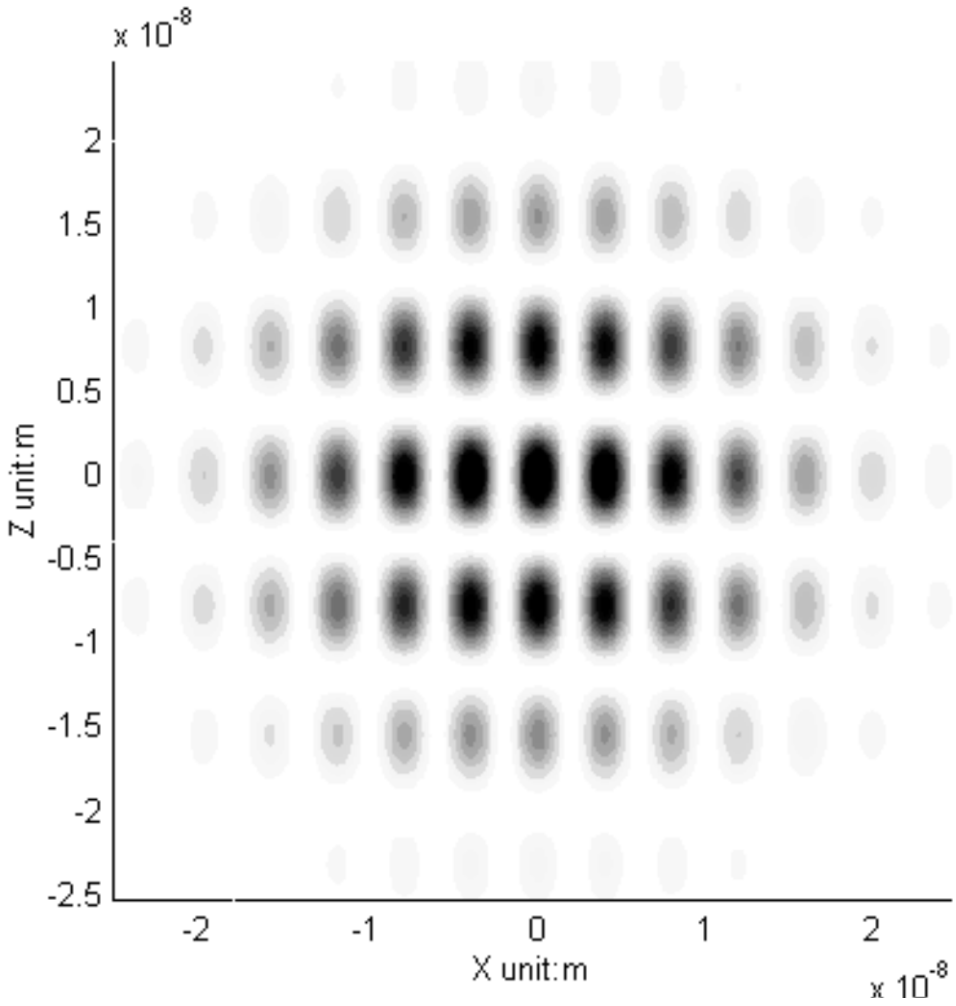

Figure 2.15 *A two-dimensional interference pattern after initial momentum averaging. This simulation assumes a 10 nm initial Gaussian wave packet size and total 60 ns propagation time.*

We can use a somewhat different approach to produce two-dimensional structures with arbitrary patterns (as illustrated in Figure 2.16). Briefly, we can draw a desired pattern (such as gears, turbines, cantilevers, etc.) in a computer graphic program Then we can convert the pattern into a bitmap file. A computer program can be written to create a

matrix which is a two-dimensional function, f(x,y), from which one computes a new function: $g(x,y)=Cos^{-1}(f(x,y))$. An optical intensity mask is then produced, corresponding to g(x,y). Consider next the atomic wave. The atoms dropped from the magnetic trap (in the form of an atom laser) is first split, using a Raman resonant pulse, with frequency **4** in Figure 2.16, into two internal states. Both internal states are then defocused using a far-red-detuned laser beam with an anti-gaussian profile, beam **1a**; this beam is pulsed on for a short time, then turned off. The expanding atomic waves are then collimated using another laser pulse with a gaussian profile, beam **2a**. A third pulse, on resonance, beam **3**, carrying the planarized intensity pattern, then interacts with only one internal state of the atoms. For a short interaction time, the laser intensity pattern acts as a linear phase mask for the atomic wave. Both internal states are then defocused and recollimated. At this point, another Raman resonant pulse, beam **4** is used to convert all the atoms into the same internal state, so that they can interfere. The interference pattern is Cos(g(x,y)), which yields the original pattern, f(x,y). However, this pattern is now on a scale much shorter than the optical wavelengths. For parameters that are easily accessible, in the case of rubidium atoms, it should be possible to produce patterns with feature sizes of as small as 10 nm. As mentioned above, these patterns can be transferred to semi-conductors or coinage metals using chemical substitution techniques. Several layers can be bonded together to yield three-dimensional structures, as is often done in current MEMS processes.

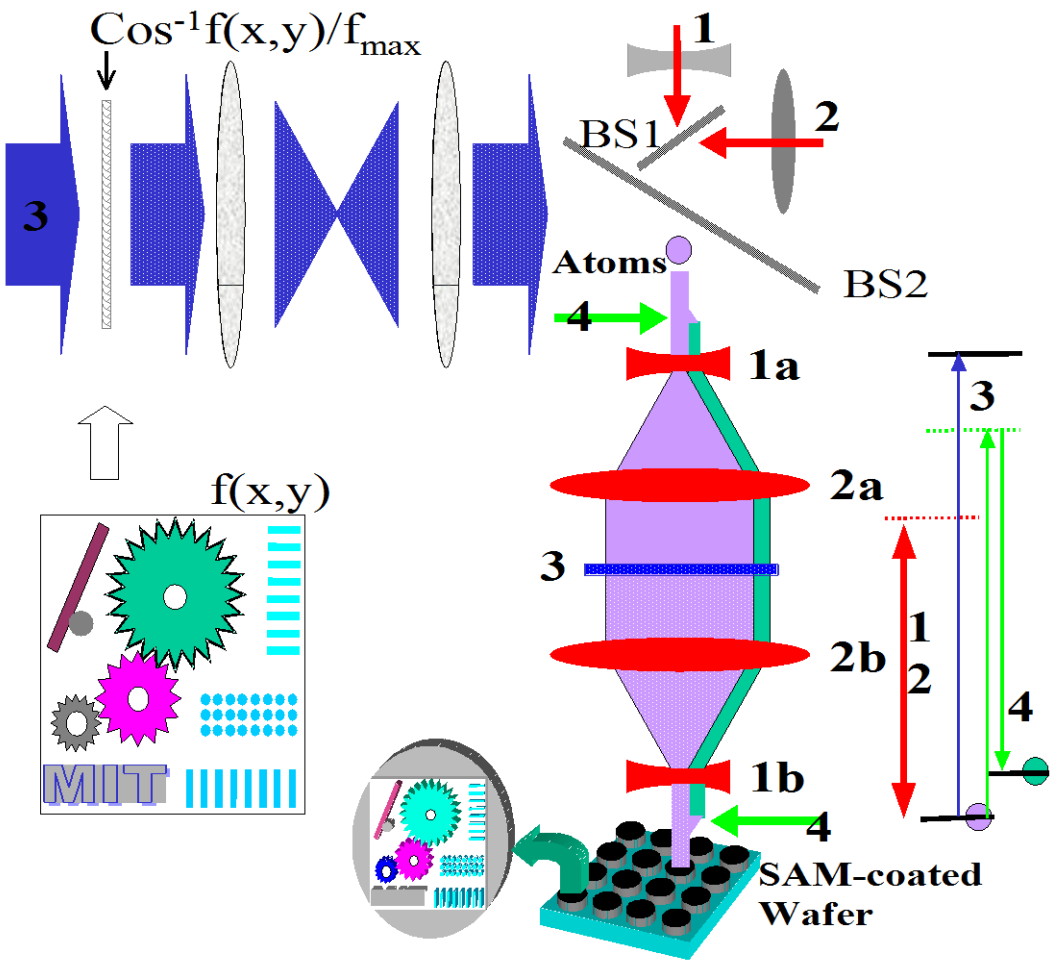

Figure 2.16*. Basic illustration of the steps involved in producing two dimensional arbitrary patterns using a combination of atom focusing/defocusing and interferometry. Here, the inverse cosine of the desired pattern is first transferred to an optical intensity mask, which in turn acts as a phase mask (via ac-stark effect) for the atomic wave packet.BS1 and BS2 are two beam splitters.*

Chapter Three:

Experimental Investigation of One Dimensional Atom Interferometer Using Multiple Raman Pulses

3.1 Experimental Setup

Our experimental setup consists of three major parts: atomic beam, optical setup and detection system. The diagram of the experimental layout of the π/2- π- π/2 atom interferometer is shown in Figure 3.1. So far the π/2- π- π/2 atom interferometer is the only multiple Raman pulses based atom interferometer we attempted because of the asbestos accident mentioned in chapter one. The apparatus is two meters long from the point of optical pumping and the point of detection.

3.1.1 Atom Source

The source of the atom we use in our experiment is Rubidium. The Rubidium atom is well studied and is commercially available. Its optical transitions are within the frequency range of our existing Ti:Sapphire lasers and its RF ground level splitting is reasonable, only about 3 GHz in the case of Rubidium 85. See Figure 3.2.

Our source is in the form of an atomic beam.

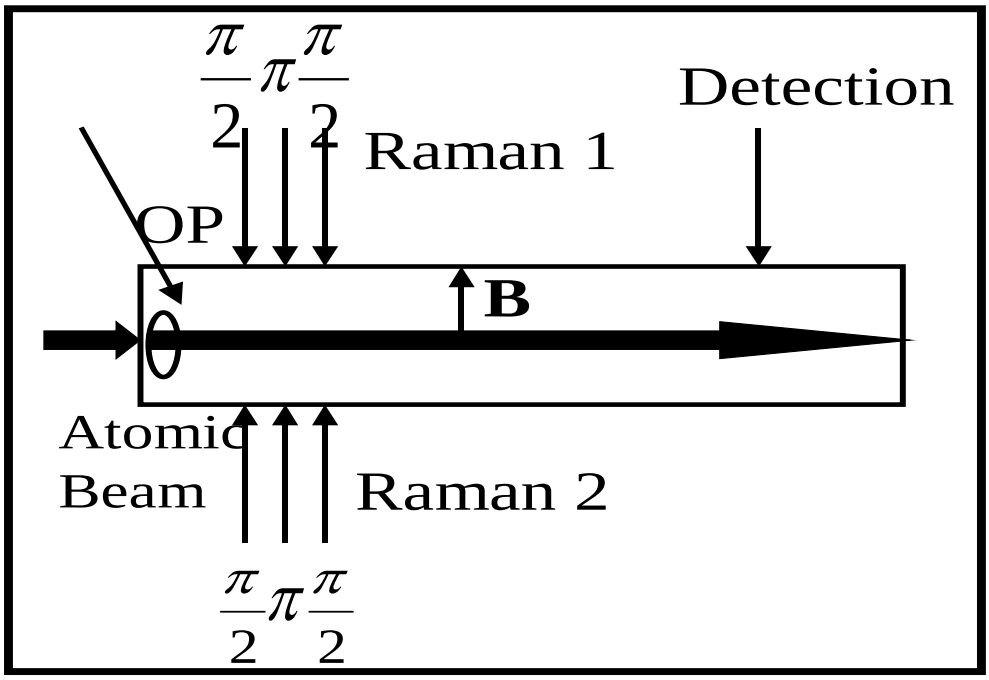

Figure 3.1 *Experimental layout*

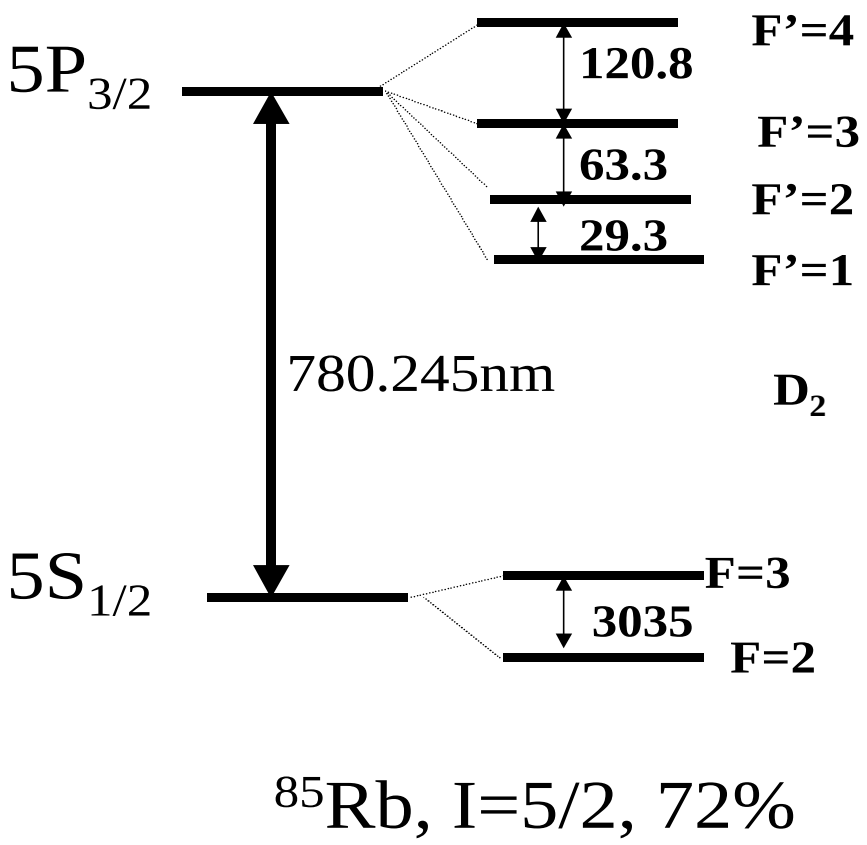

Figure 3.2 *Rubidium 85 energy levels (MHz)*

3.1.2 Oven, Atomic Beam Collimation and Aperturing

See Figure 3.3 for the oven structure: A is the oven which holds the Rubidium atoms. Above A, there is a valve V_2 so oven A can be separated from the vacuum system. When something goes wrong with any other part of the vacuum system, we can close valve V_2 to avoid the exposure of the Rubidium atoms to the air. Above valve V_2, there's a 4-way cross B. On the right of B, there is a long section of nipple C+D, then there are a

nozzle and two skimmers, which provide the collimation of the atomic beam. Originally they were designed for a supersonic beam and the first skimmer was taken out for the thermal beam. Both the nozzle and the second skimmer have 1mm diameters. The distance between the nozzle and the second skimmer is 15 cm. From the nozzle to the detection PMT, the distance is 2.3 meters. The imaging system of the detection PMT is set up such that an aperture can be used to control the field of view. We found out that by reducing the aperture size of the PMT we can detect the atoms with less transverse velocity spread. We see this effect from the width of the counter-propagating Raman signal as a function of the aperture size. Using this method, when the signal to noise level is not an important concern, we don't need to do cooling of the atomic beam to get a narrower transverse velocity spread.

On the left of B, there's another valve V_1. On the left of valve V_1, there's a view port. When the system is cooled down, we can open that valve and check whether our nozzle is clogged by illuminating it either with a laser beam or just simply a flash light.

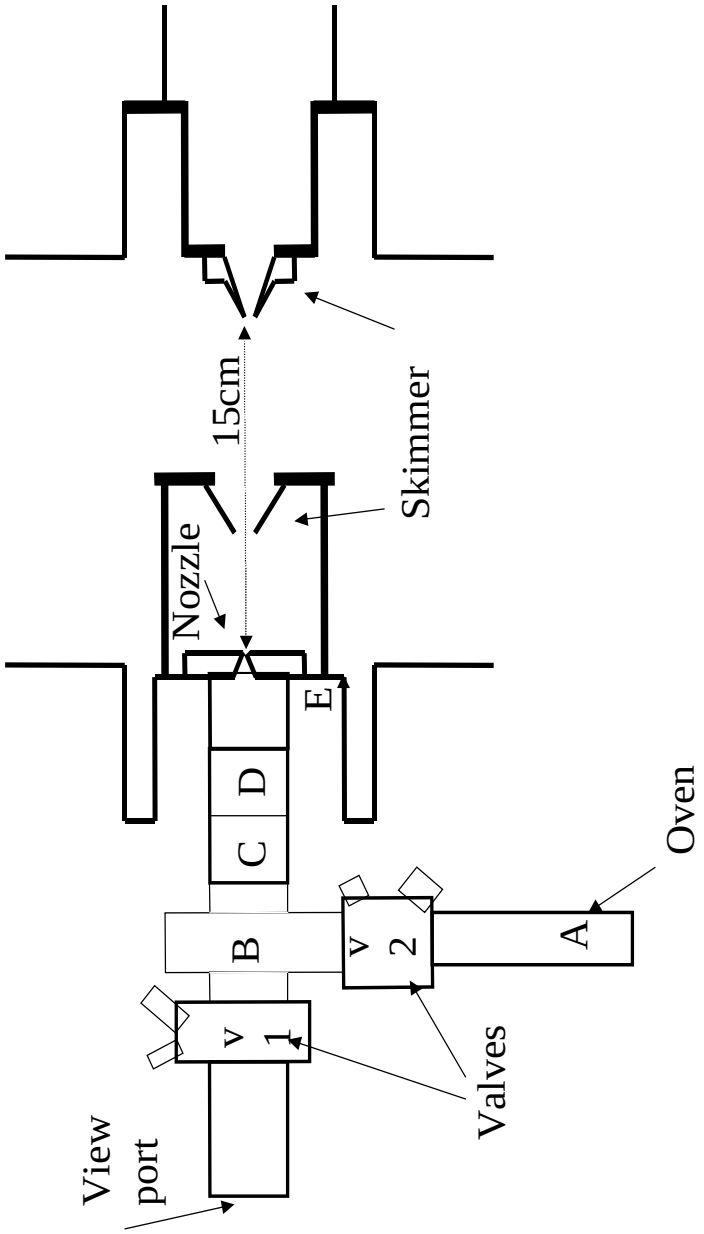

Figure 3.3 *Oven and atomic beam collimation*

There are some heaters and thermo-couples wound on parts A, B, C, D, E, V_1, V_2, respectively. The oven temperature profile is as follows:

A: 245 ^{o}C,

B:395 ^{o}C,

C:327.5 ^{o}C,

D:392.5 ^{o}C,

E:252.5 ^{o}C,

Nozzle:197.5 ^{o}C,

V2: 370 ^{o}C,

V1: 372.5 ^{o}C

3.1.3 Vacuum system

Our vacuum system has three diffusion pumps backed by three mechanical pumps. The whole system is about 3 meters long. See Figure 3.4. Most experiments were done in section 1 and detection was done in section 2.

3.1.4 Detection

A photomultiplier is mounted on top of section 2 of our vacuum system to detect the fluorescence of the atomic beam. We use F=3 to F'=4 cyclic transition as our probe beam for detection. See Figure 3.5. According to the selection rules, atoms excited to the state F'=4 can only decay back to the state F=3, so this transition is called cyclic transition.

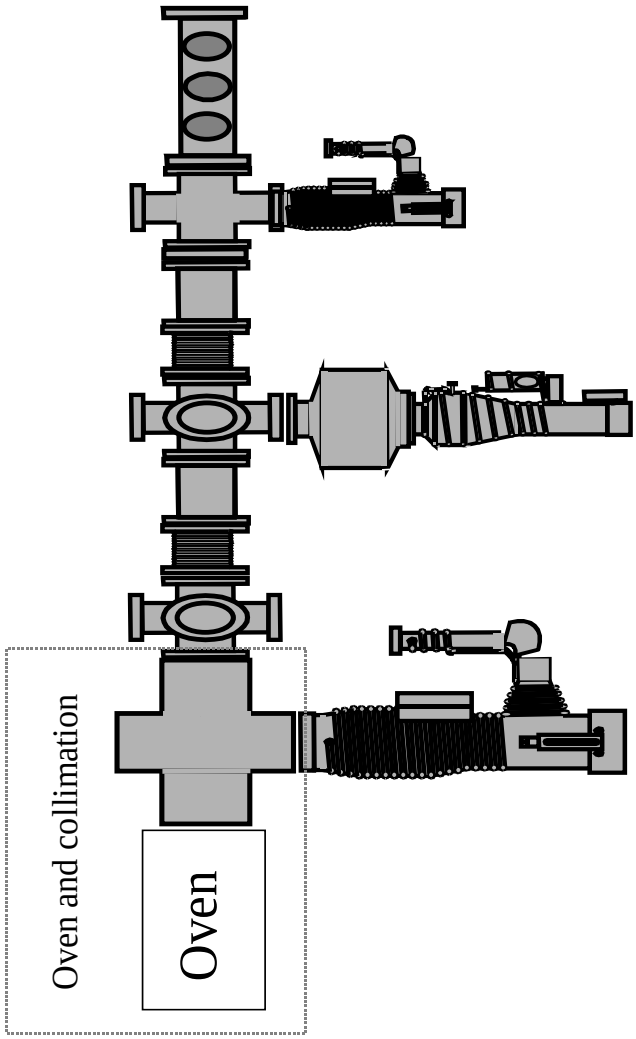

Figure 3.4 *Vacuum systems*

Cyclic transitions don't pump atoms away to other states which cannot be detected by the probe beam. So detection is more efficient using cyclic transitions.

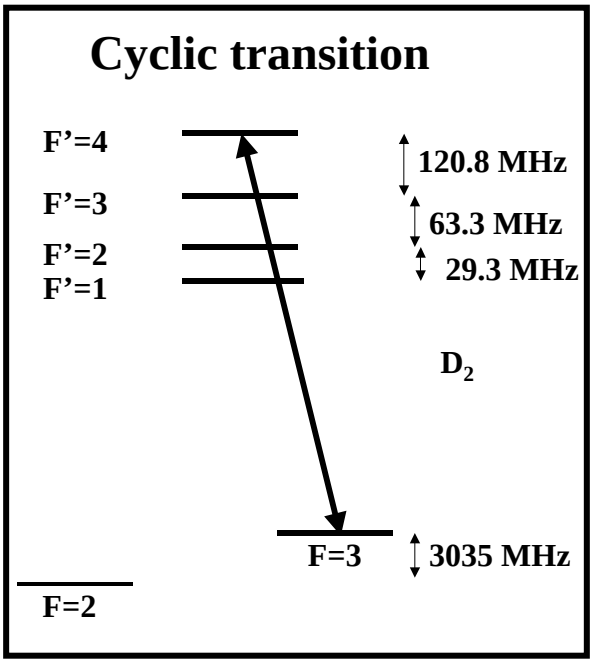

Figure 3.5 *Detection frequency*

3.1.5 State preparation

We want to prepare our atoms in a single pure state so that the later interactions are more efficient. We need a bias magnetic field, typically a few hundred mGauss, to provide us with the direction of polarization. This is accomplished by two long coil

structures sitting on each side of the atomic beam vacuum chamber. To calibrate the magnetic field with respect to the current in the coils, we apply co-propagating Raman beams. Because the propagating directions of the Raman beams are the same as the B field, we don't have the π polarized Raman beam. If we make both Raman beams circularly polarized the same way, the Raman interaction will connect magnetic sublevels with the same m_f value. So the signal shows the single peak without magnetic field, five peaks with magnetic field and the central one correspond to F=2, m_f=0 to F'=3, m_f=0. The peak to the right of this one corresponds to F=2, m_f=1 to F'=3, m_f=1. The g factor for Rubidium 85 ground state F=3 level is 1/3, and for F=2 level is –1/3, where

$$g = \left[\frac{3J(J+1)+S(S+1)-L(L+1)}{2J(J+1)}\right]\left[\frac{F(F+1)+J(J+1)-I(I+1)}{2F(F+1)}\right] \qquad \text{(eq. 3.1)}$$

With a magnetic field applied, sublevels in those two levels will shift in the opposite direction, corresponding to a shift $x=|g|\mu_B B$. The distance between peaks in the co-propagating signal would be 2x. From this distance we can deduce the magnetic field applied and the current needed for the bias magnetic field.

See Figure 3.6 for the energy levels involved for the state preparation. Rubidium 85 ground level has two hyperfine states F=2 and F=3. Our goal of state preparation is to use magnetic sublevel optical pumping to pump all, or at least most, of the atoms to the F=2, m_f=0 state.

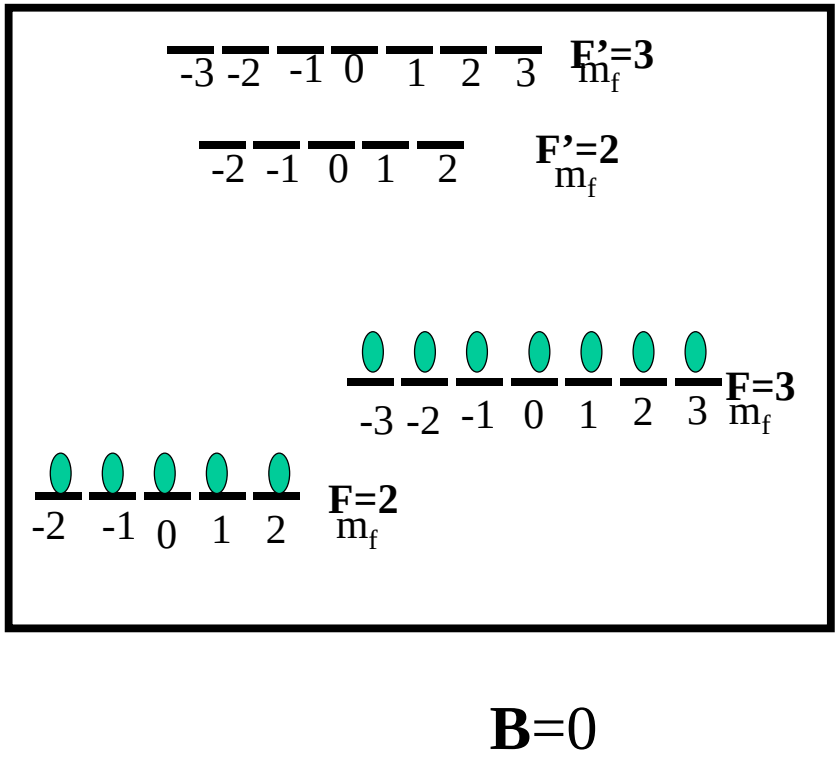

Figure 3.6 *State preparation: energy levels involved*

The bias magnetic field is about 400 mGauss. We apply a laser beam with σ^+ polarization and a F=3 to F'=3 frequency and a laser beam with π polarization and F=2 to F'=3 frequency. See Figure 3.7. According to the selection rules, the σ^+ beam excites atoms from state F = 3, m_f = 2, 1, 0, -1, -2, -3, to F' = 3, m_f' = 3, 2, 1, 0, -1, -2, respectively and the atoms can decay to state F=2, m_f = 2, 1, 0, -1, -2 and to state F=3, m_f = 3, 2, 1, 0, -1, -2, -3. The π polarization beam excites atoms from state F = 2, m_f =2, 1, -1, -2 to state F'= 2, m_f' = 2, 1,

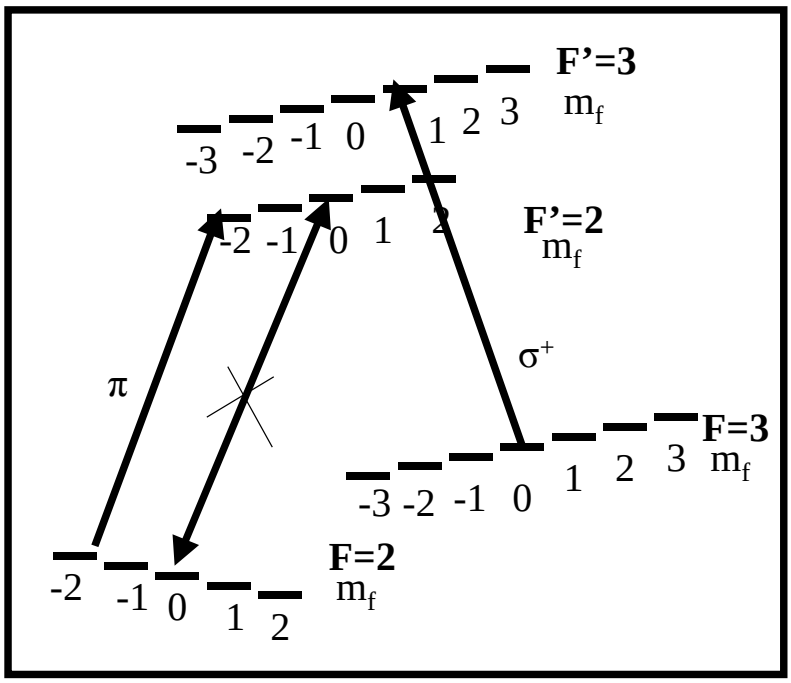

Figure 3.7 *State preparation: Magnetic sublevel optical pumping.*

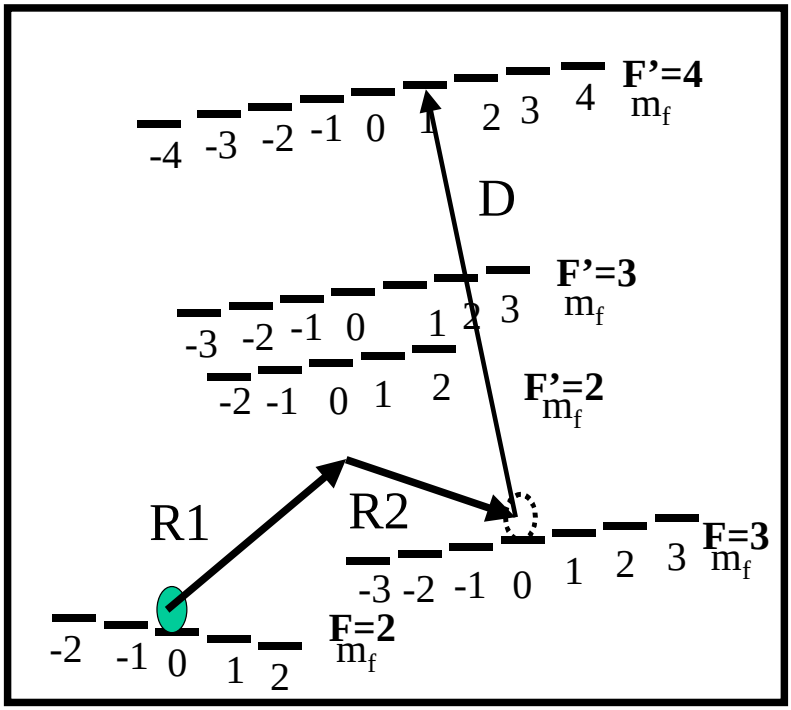

Figure 3.8 *Magnetic sublevel optical pumping detection.*

-1, -2, respectively and atoms can decay to state F = 2, m_f = 2, 1, 0, -1, -2 and state F = 3, m_f = 3, 2, 1, 0, -1, -2, -3. The transition F = 2, m_f = 0 to state F' = 2, m_f' = 0 is forbidden. Since atoms can be pumped into state F = 2, m_f = 0 but can not be pumped out, most of the atoms will be trapped in that state in a few optical pumping cycles. After pumping atoms to the pure state F=2, m_f=0 magnetic sublevel, we use a Raman transition R1+R2 to move atoms to state F=3, m_f=0 and use our cyclic transition F=3 to F'=4 to detect the optical pumping effect. See Figure 3.8.

The result is shown in Figure 3.9.

In this figure, the peaks occur when the difference frequency of two Raman beams are exactly matched with the difference frequency of the magnetic sublevels involved. We see from the figure that most of the atoms ultimately end up in the magnetic sublevel F=2, m_f=0 state after optical pumping. The small peak on the left is due to the imperfect π polarization of F=2 to F'=2 optical pumping beam.

3.1.6 Overall frequency scheme

We use the Rubidium 85 D_2 line for our experiment. The overall frequency scheme is shown in Figure 3.10. The common detuning of Raman beams can be changed.

3.1.7 The parameters of the atomic beam

We measure the average longitudinal velocity of the atomic beam by the time of flight method. See Figure 3.11. We apply a co-propagating Raman beam at point A and detect it at point E. When we turn off the co-propagating Raman at point A for 10 ms, there's delay time t_A before the detected signal decays. When we apply a co-propagating

Raman signal at point C and turn it off for 10 ms, we get the delay time t_C before the detected signal decays. The distance between A and C is L_{AC} = 1 m. So the average velocity is $V_L = (t_A - t_C) / L_{AC} =$ 388 m/s.

We deduce the transverse velocity of the atomic beam by measuring the width of the counter-propagating Raman signal. The result is consistent with the geometry of the nozzles and the aperture of the detection PMT. The counter-propagating Raman signal width is the convolution of the co-propagating Raman signal width and the transverse velocity spread.

3.1.8 Lasers and their long term frequency stabilization[19,20]

The lasers we use in our experiment are Coherent 899 Ti:sapphire ring lasers pumped by Coherent Innova 400 Argon lasers. The Ti:sapphire laser gives us about 1.8 Watt in single mode operation with the tunability of 20 GHz when pumped by 12 Watt Argon ion laser power.

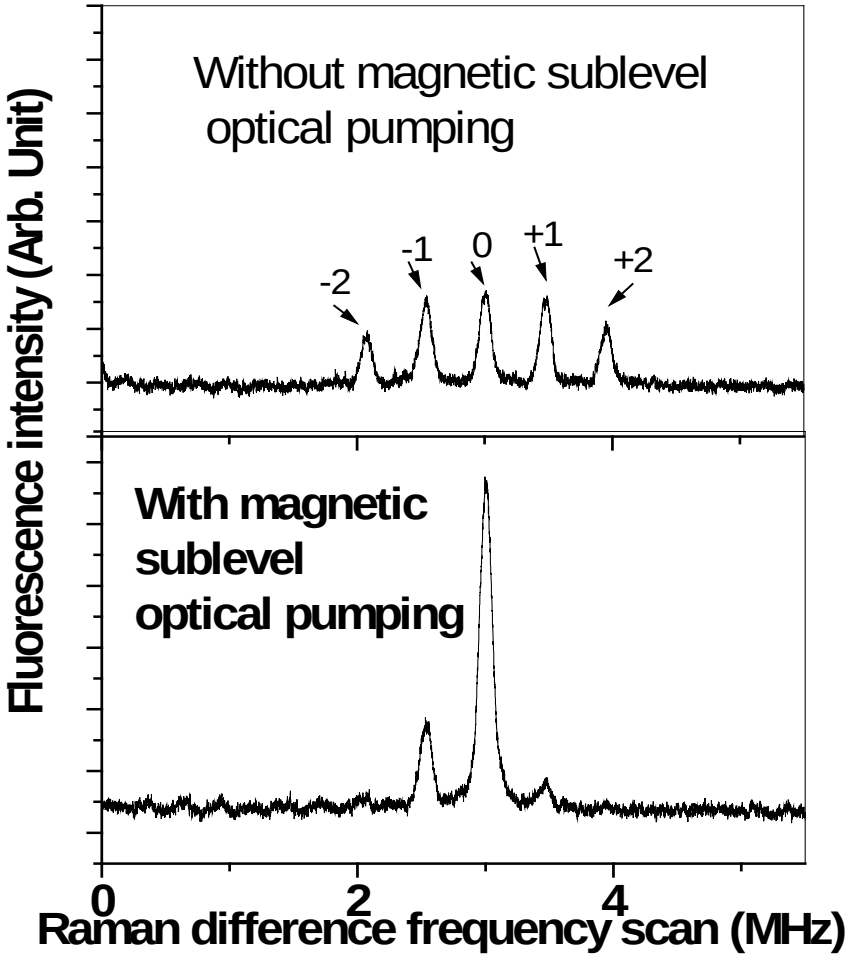

Figure 3.9 *Effect of the Magnetic sublevel optical pumping.*

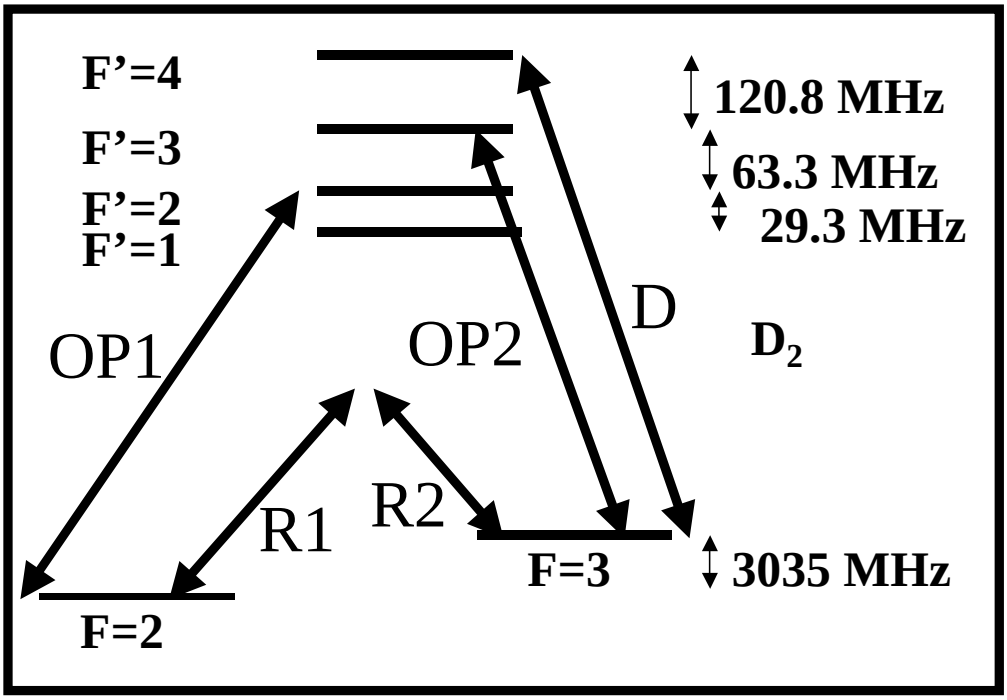

R1: Raman beam 1
R2: Raman beam 2
D: Detection beam
OP1: Optical pumping beam 1
OP2: Optical pumping beam 2

Figure 3.10 *The overall frequency scheme*

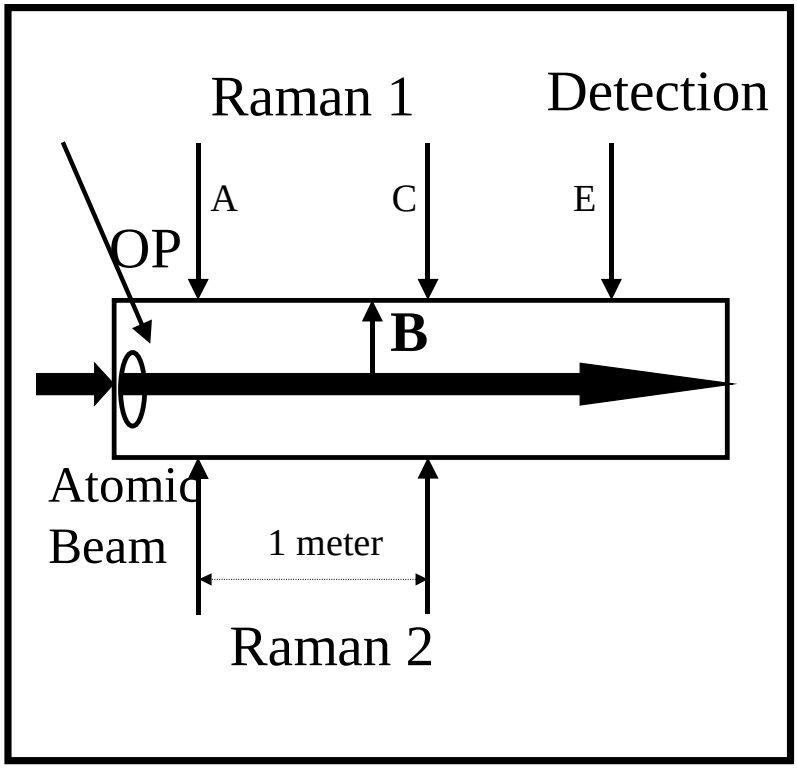

Figure 3.11 *Time of flight to measure the longitudinal velocity of the atomic beam*

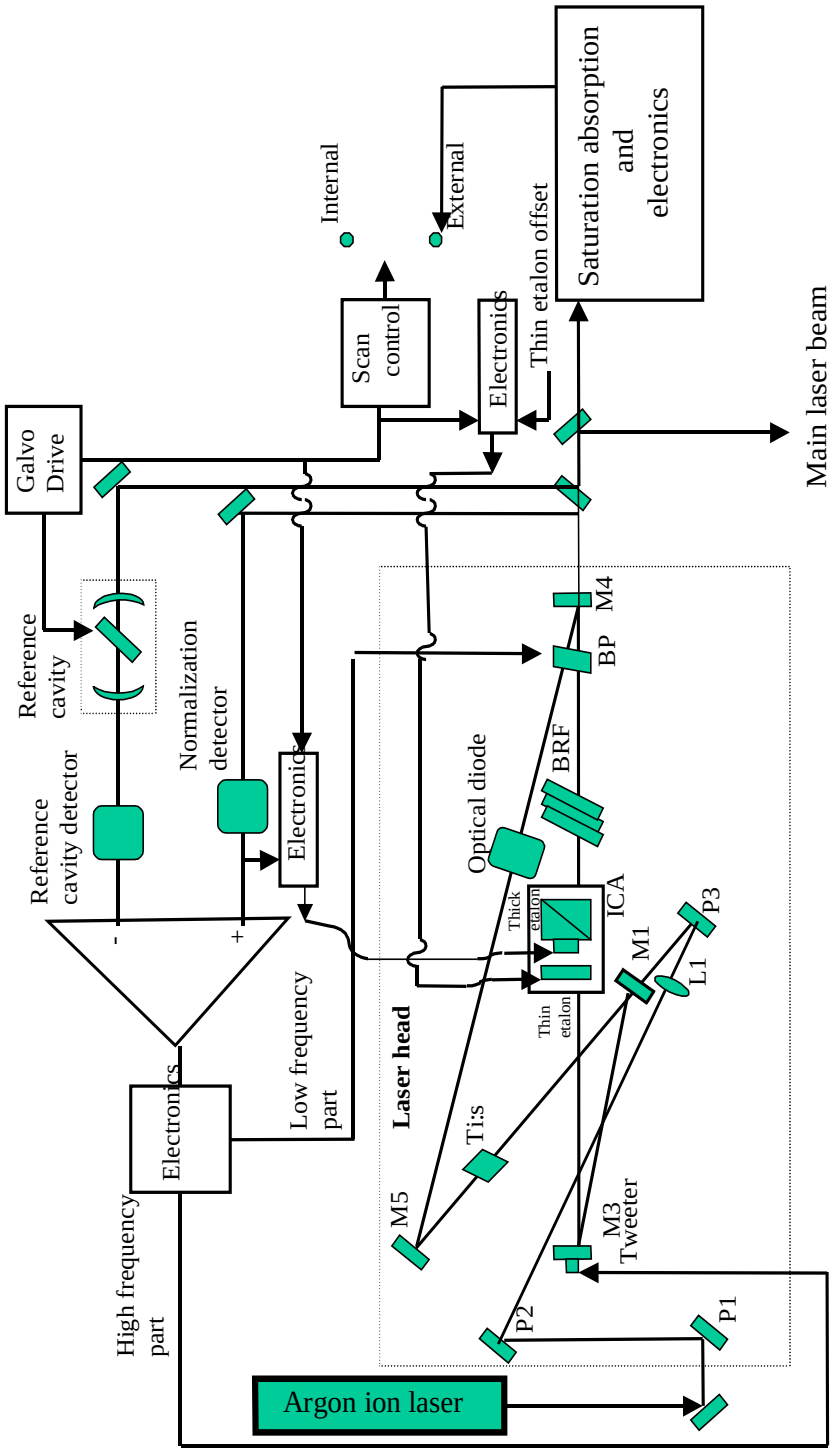

Figure 3.12 *Diagram of the Ti:sapphire laser and its lock scheme*

Figure 3.12 shows the diagram of the Ti:sapphire laser setup.

All components are mounted directly or indirectly on a two-inch Invar bar. The Invar bar has a very low coefficient of expansion, therefore, resulting in passive cavity length thermal stabilization of less than one micro/degree centigrade.

Without frequency filters in the cavity, the Ti:sapphire ring laser will lase over a broad range of longitudinal modes so long as they are covered by the Ti:sapphire crystal gain profile. The laser has a series of intracavity frequency filters to control the laser frequency passively. These include a three plate birefringent filter, an intracavity etalon assembly (ICA) that consists of a thin etalon and a thick etalon. The birefringent filter allows broadband operation with a bandwidth of 2 GHz. The ICA decreases the operational bandwidth to 10 MHz. The coated etalons are of low finesse that would allow broadband coverage.

The birefringent filter takes advantage of the fact that birefringence could induce polarization change.

In birefringent materials, if the incoming laser beam propagates along the optic axis, then the index of refraction for that beam is n_o. If the incoming beam propagates perpendicular to the optic axis, then the index of refraction for that beam is n_e when the polarization is lined up with the optic axis and it's n_o when the polarization is perpendicular to the optic axis. If the propagation direction of the incoming beam makes an angle with the optic axis, there are also two allowed polarization directions. The one that is perpendicular to the optical axis still has the index of refraction n_o. It is called the ordinary wave. The index of refraction of the other one is a function of the angle, $n_e(\theta)$. It is called the extraordinary wave.

$$1/ n_e^{\,2}(\theta) = \cos^2\theta / n_o^2 + \sin^2\theta / n_e^2 \qquad \text{(eq. 3.2)}$$

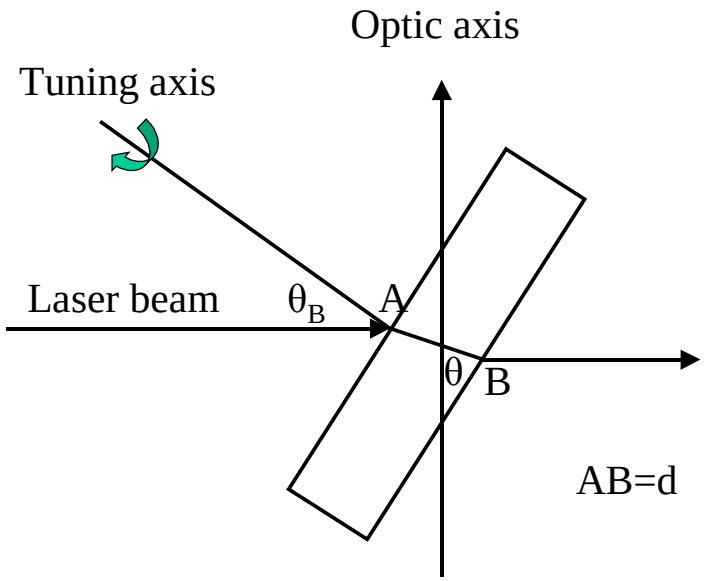

Figure 3.13 *Birefringent filter.*

In a birefringent filter, the birefringent element is placed under the Brewester angle. Many Brewster faces inside the laser cavity defines the polarization direction. When the laser beam passes through the birefringent element, the ordinary wave and the extraordinary wave have different phase velocity because their different indices of refraction. So the polarization of the laser beam will change after passing through unless the condition

$$(n_e(\theta) - n_o)d/\lambda = \text{integer} \qquad \text{(eq. 3.3)}$$

is satisfied, which is to say, that the optical path difference between the extraordinary wave and the ordinary wave should be an integer number of wavelengths. Since only the polarization direction defined by all the brewster faces would suffer no reflection loss and, therefore, would have enough gain to lase, the birefringent filter selects the frequency satisfying above condition. See Figure 3.13 for the birefringent filter. When we tune the birefringent filter, we essentially change the direction of its optic axis with respect to the direction of the incident beam. Therefore, by changing $n_e(\theta)$, and keeping the same integer in (eq. 3.3), we tune over a range of λ, i.e. a range of frequencies.

From (eq. 3.3), we can see that the birefringent element doesn't just select one frequency. It will select many of them. The bigger d, the smaller the distance between the selected frequencies. The three birefringent plates have different thicknesses but the ratios of the thickness of those three are integer numbers. For example, $d_1 = d$, $d_2 = 4\ d$, $d_3 = 16\ d$. This would give 21 peaks between birefringent filter "orders". The laser will lase on the transmission maximum that is the closest to the maximum of the crystal gain curve.

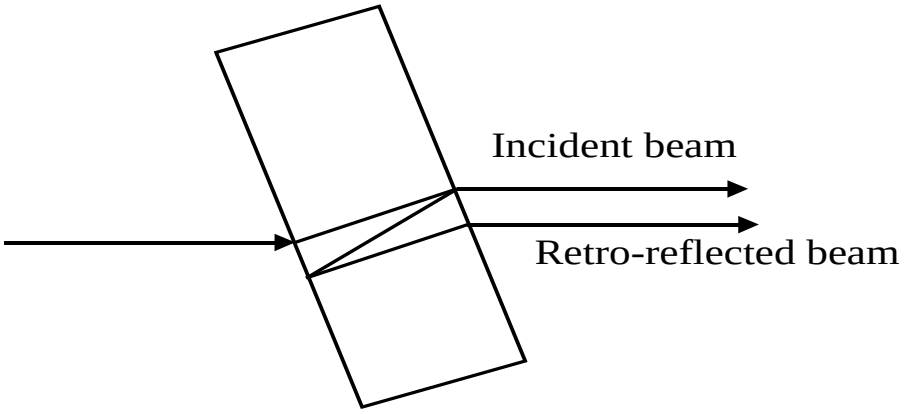

Figure 3.14 *Thin etalon*

The birefringent filter is used just for coarse tuning. The thin etalon and the thick etalon in the ICA are for frequency tuning in a narrower range. The etaton uses optical interference to filter the frequency. See Figure 3.14. When the optical path length difference between the incident beam and all the retro reflected beams is $\Delta x=n\lambda$, where n is an integer, those beams interfere constructively. All the other frequencies (or wavelengths) which don't satisfy the condition $\Delta x=n\lambda$ would interfere destructively. If we can change the thickness of the etalon in someway, we can tune the laser frequency.

The thin etalon can be tuned by a galvonameter drive which controls the tip angle. Tilting the etalon plate is effectively changing the thickness of the etalon. The thick etalon cannot be tuned the same way because of its thickness. Tilting the angle of the thick etalon, would cause the beams exiting the backside physically to separate and to induce laser power loss, the so-called "walk off". The thick etalon is the air gap between two prism wedges. See Figure 3.15 for a diagram of the thick etalon. There's a PZT attached to one of the wedges to change the spacing of the air gap.

The Ti:sapphire gain medium is tunable from 680nm to 1025nm. The birefringent filter coarsely tunes the frequency. The FWHM of the birefringent filter order is about 2 THz. The thin etalon is the finer frequency selector. The FWHM of the thin etalon is about 200 GHz. The thin etalon thickness is about 0.5 mm and the free spectral range is about 225GHz. Then comes the finest one. The thick etalon has a FWHM of about 5 GHz . It is about 10mm thick and has the free spectral range about 10 GHz. The birefringent filter's transmission order curvature imposes enough losses on the nearby orders of the thin etalon to suppress lasing in those orders. In the same way the thin etalon's

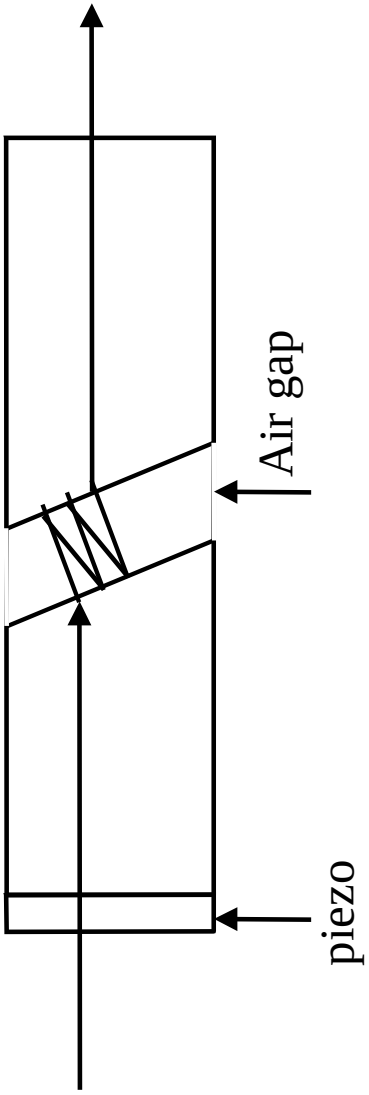

Figure 3.15 *Thick etalon*

transmission order curvature would also suppress lasing in adjacent orders of the thick etalon except one. This is how the passive frequency control works.

Active frequency control reduces the laser line width to about 500 KHz RMS. It is achieved by using an extremely stable reference cavity and an electronic servo loop. The servo consists of three elements: a reference cavity, a tweeter and a Brewster galvo.

Figure 3.16 shows the reference cavity. There is an etalon inside the reference cavity. Tilting the etalon plate changes the path length and, therefore, scans the etalon transmission. Detector B sees the interference fringes between the incident beam and the retro reflected beam. If the laser frequency changes due to the change of the main cavity length, the interference fringe pattern detector B receives changes. The signal on detector A is for reference and normalization. Other types of noise would show up at B as a reduction of signal level. The time scale of those noises is converted to frequency and an error signal is generated. The high frequency part (500 Hz~200 KHz) is applied to the tweeter to correct for fast cavity length variation. The low frequency part (0 Hz~ 500 Hz) drives the rotating Brewster's plate to compensate for the slower cavity length changes. The Brewster's plate is mounted at the vertex of the optical beam path so that during a scan the displacement of the intracavity beam is minimized.

In the Ti:sapphire laser, the single mode frequency scanning is achieved by continuously varying the cavity length with the rotating galvanometer driven by the Brewster's plate. Since wide scans could induce loss and mode hops, the servo on the thick etalon is used to prevent this. When scaning, the thick etalon keeps track of the laser frequency by varying the thickness with a piezoelectric transducer to ensure the overlap of cavity modes and the thick etalon's transmission envelope.

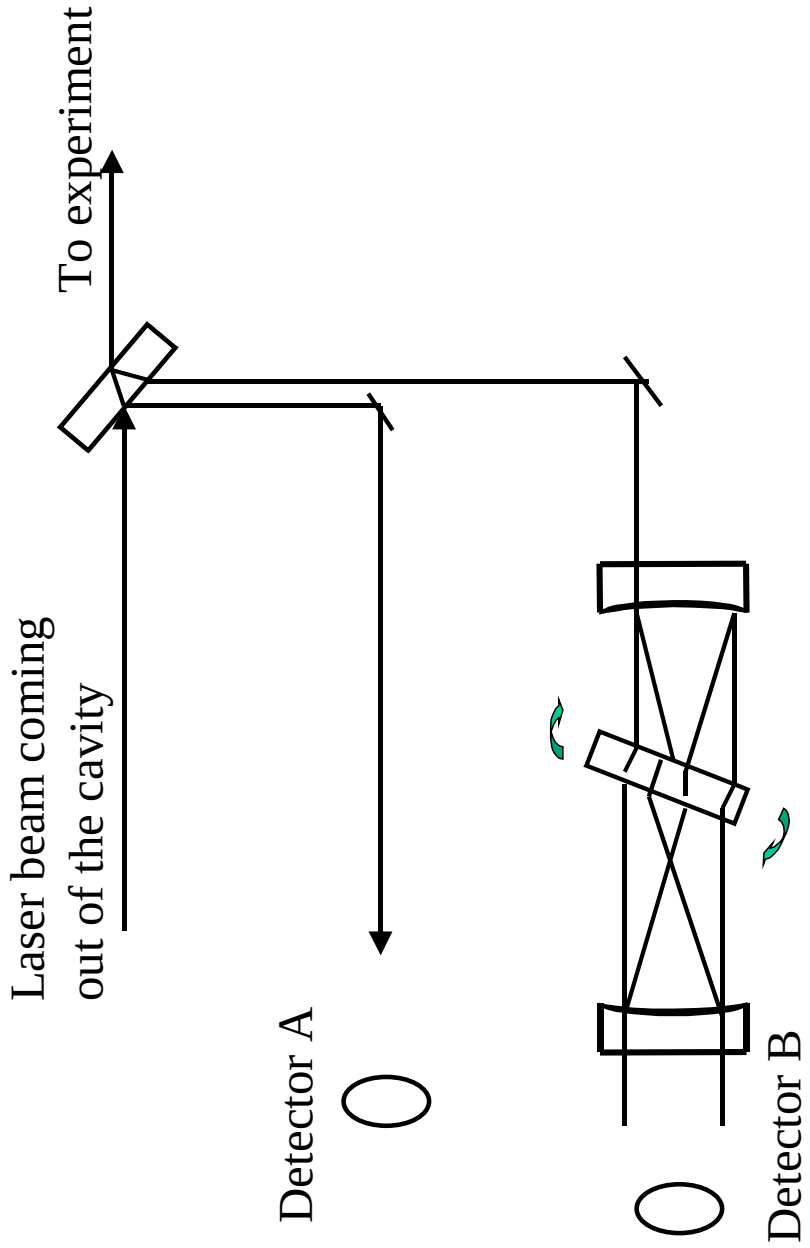

Figure 3.16 *Reference Cavity*

For unidirectional lasing, the Ti:sapphire laser has an optical diode in the cavity path. The optical diode consists of a Faraday rotator and an optical active element. In the Faraday rotator, the rotation of the polarization of the incoming beam is defined by the magnetic field direction. Whether the incoming beam propagates along the magnetic field or against the magnetic field, the polarization will rotate the same amount and along the same direction. The optical active element will rotate the polarization of the incoming beam clockwise (for d-rotatory material) or counterclockwise (for l-rotatory material) when looking in the direction of the source. In the forward direction, the optical active element will rotate the polarization by $-\theta$ and the Faraday rotator will rotate the polarization by θ; therefore, the combination of the Faraday rotator and the optical active element will keep the incoming beam polarization constant. However, in the backward direction, the combination of the Faraday rotator and the optical active element will rotate the polarization by 2θ, and the reflection loss from the intracavity Brewster plates will prevent lasing in this direction. Figure 3.17 shows how the optical diode works.

For laser long-term stabilization, we need to lock its frequency to a well-known frequency. In our experiment, we use the saturation absorption method to achieve this goal. Figure 3.18 shows the saturation absorption set up and its electronics. A part of the Ti:Sapphire laser beam goes through a piece of glass and then reflects from a mirror and a beam splitter. Two weak probe beams reflected from the front and back surfaces of the glass piece go through a Rubidium vapor cell and hit two photo detectors,

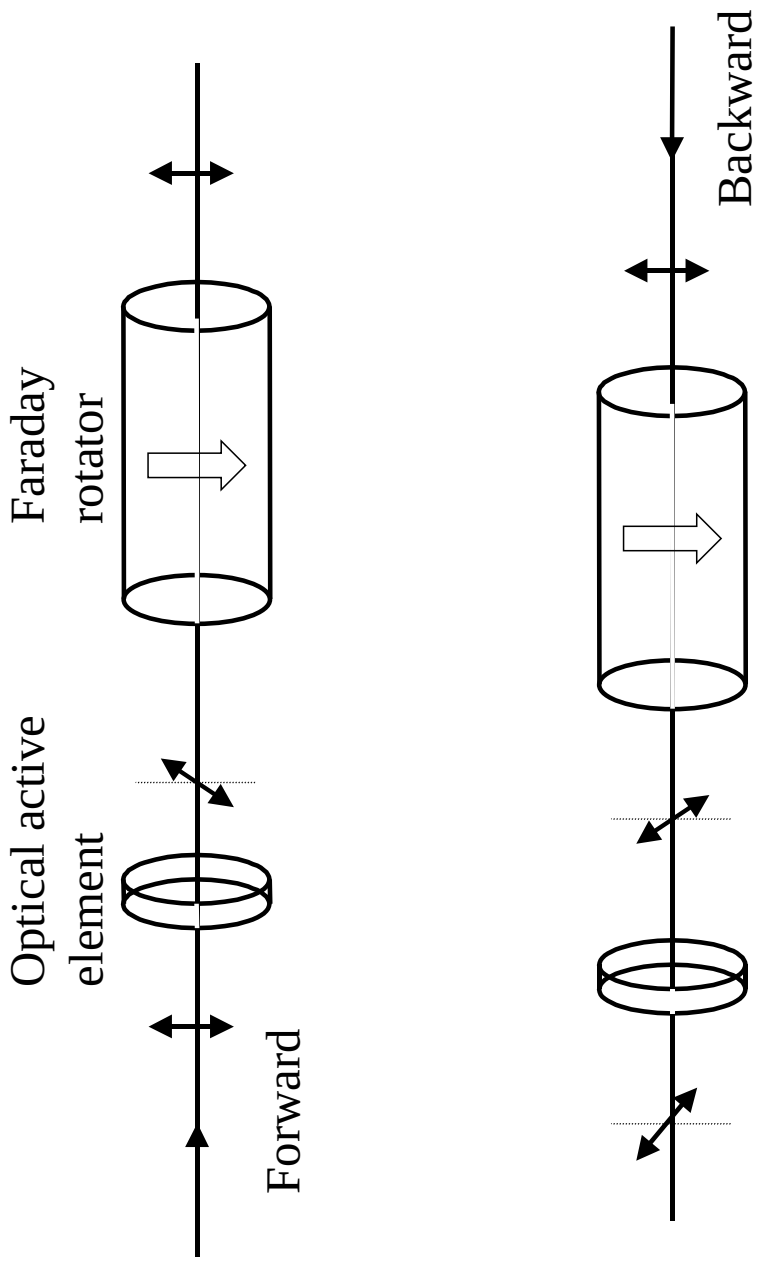

Figure 3.17 *Optical diode*

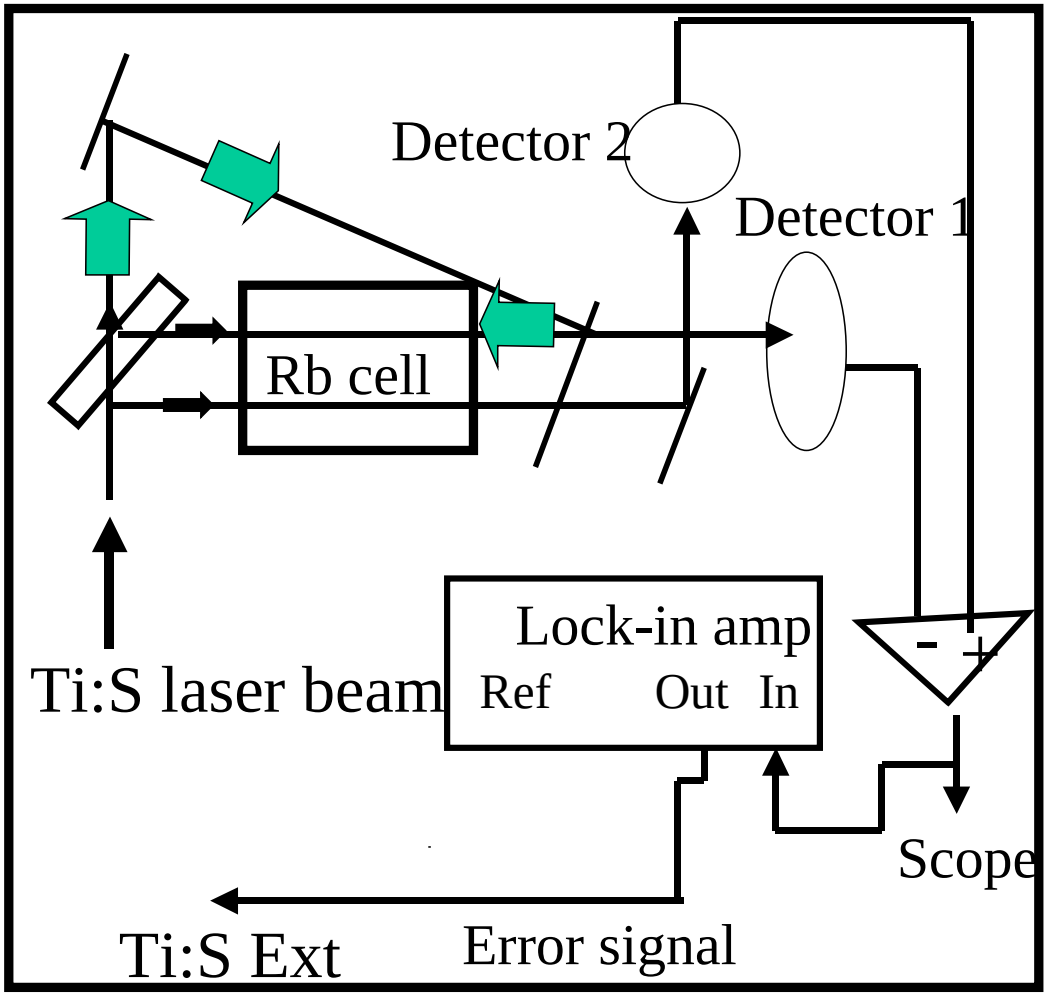

Figure 3.18 *Saturation absorption set up and electronics*

respectively. The strong pump beam reflected from the mirror and the beam splitter overlaps with one of the weak beams from the opposite direction. When we scan the Ti:Sapphire laser frequency, each of the probe beams would give us a Doppler absorption profile. The strong pump beam saturates the atoms in its path so that the probe beam overlapped with it cannot be absorbed at those frequencies that are saturated. So this probe beam gives us transmission peaks of Rubidium line profiles and some cross over peaks. Figure 3.19 shows the signals from two photo detectors when we scan the laser over only one Doppler profile. The subtraction of these two signals eliminates the Doppler background and gives the Rubidium line profiles and cross over peaks. Figure 3.20 shows the saturation absorption signal of Rubidium 85 F=3 to F' lines and cross over peaks. The cross-over peaks are caused by the Doppler effect. Assume the frequency of the laser beam is f, $\omega=2\pi f$. Since the probe beam and the pump beam propagate in opposite directions, the atoms with velocity v see the probe beam with frequency ω-kv and the pump beam with frequency ω+kv. For the group of atoms with v=0, the pump beam saturates the Rubidium transitions ω and within the Doppler absorption of the probe beam, those frequencies of ω would not get absorbed. If two transitions are close enough, their Doppler profile cannot be resolved. For example, consider a group of atoms with velocity v. If $2kv= \omega_1-\omega_2$, $\omega+kv= \omega_1$, $\omega-kv= \omega_2$, which is to say, that this group of atoms, when the laser frequency is $\omega=(\omega_1+\omega_2)/2$, is brought to resonance with transition ω_1 and ,therefore, the atoms are saturated by the pump beam. With respect to the probe beam, because of its opposite propagating direction, this group of atoms is brought to resonance with the transition $\omega 2$. Since they are already

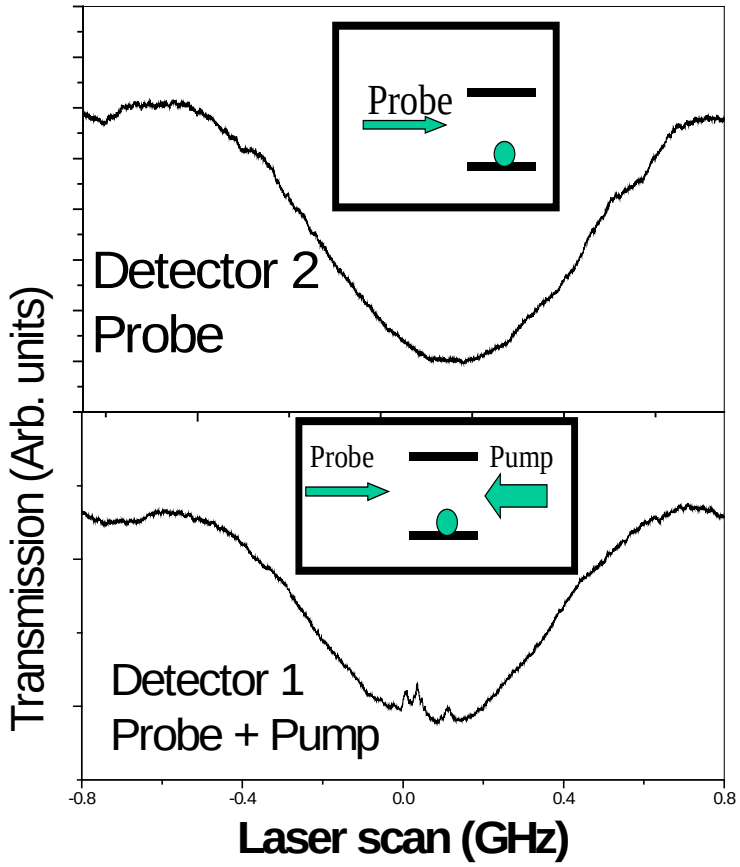

Figure 3.19 *How saturation absorption works*

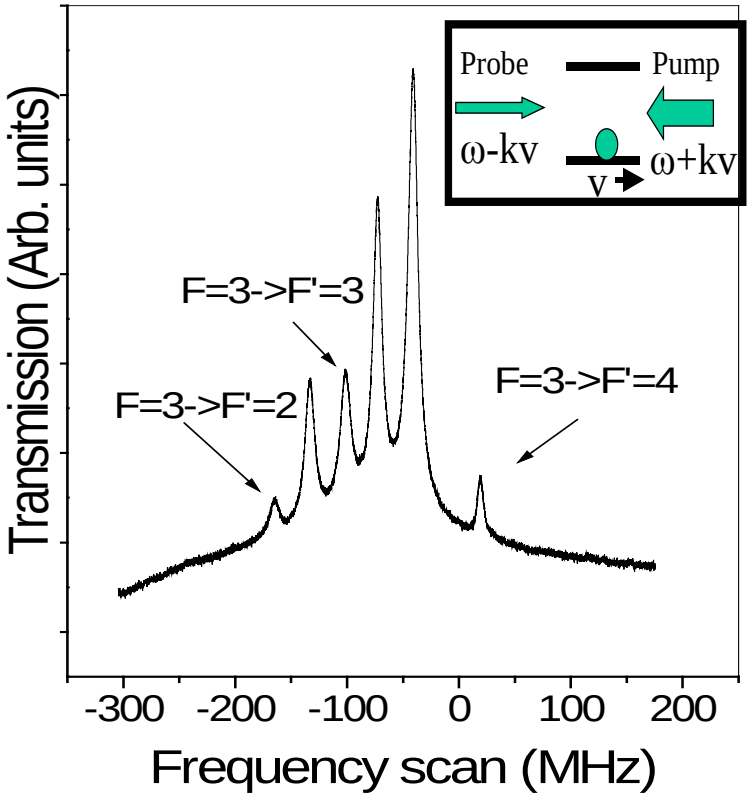

Figure 3.20 *Saturation absorption signal*

saturated, the probe beam will give us the transmission peak at $\omega=(\omega_1+\omega_2)/2$, which is a cross over peak between $\omega_1$and ω_2.

The saturation absorption signal provides us with a frequency standard. To lock the Ti:Sapphire laser to any of the peaks of the saturation absorption signal, we feed the later to the standard lock-in electronics and feed the error signal of the lock-in to the Ti:Sapphire laser Ext input. This way the Ti:Sapphire laser can be locked to the frequency we want over a few hours while we run the experiment.

3.1.9 Raman laser frequency realization

We have two ways to generate our Raman beam frequencies. But, either way, we want the difference frequency of those two Raman beams to be stable. The first method is the injection lock of the diode laser which can provide us as much power as we need and which is useful when we get to a later stage of the experiment. However, the alignment of this method is more involved. The second method is to use acoustal optic modulators to generate Raman beams. They are easy to align but the available power is limited by the damage threshold of the acoustal optic modulators. Nevertheless,this method is the prefered one for the initial stage of the experiment since we don't need that much power and since the alignment is much simpler.

3.1.9.1 Injection Lock of Diode Laser [21]

We can consider the injection locked diode laser as a laser intensity amplifier that is phase coherent with the injecting master laser beam. The requirement of the experiment is to injection lock the diode laser so that the frequency of the locked diode

laser is about 3 GHz away from the frequency of the master laser. Also when we tune the difference frequency around 3 GHz, the lock won't get destroyed and the direction of the available laser beams to the experiment won't change. A master laser beam goes through a 3 GHz Electro-Optic Modulator (EOM) (New Focus model 4431) which produces two sidebands of 3GHz above and below the incoming laser frequency. The EOM itself is driven by a 3 GHz RF source phase locked to a Rubidium clock. The sidebands and the fundamental frequency propagate along the same direction. We use a home made Fabry-Perot cavity with finesse of about 60 and a free spectral range of about 30 GHz to filter out the unwanted laser frequencies. When we scan the Fabry-Perot and find the side band we want, we lock the Fabry-Perot cavity to the side band and we inject the output of the cavity to a SDL 5412 diode laser . The challenge of locking the diode laser is to prevent the laser beam from feeding back. Because of the small cavity size, the diode laser could become very unstable due to feedback. A normal Faraday isolator could prevent feedback, however, it would also prevent the injection locking at the same time. To solve this problem, we modified a commercial Faraday isolator (from Electro-Optics Technology, Inc, which provides isolation of better than 30 dB) and we designed the polarization of all the laser beams involved carefully. See Figure 3.21 for the modified isolator.

A normal Faraday isolator has a Faraday rotator which will rotate the incoming laser beam 45^{o} with respect to the magnetic field orientation whether the incoming beam is from one side of the rotator or from the other side. On each side of the rotator, there is a

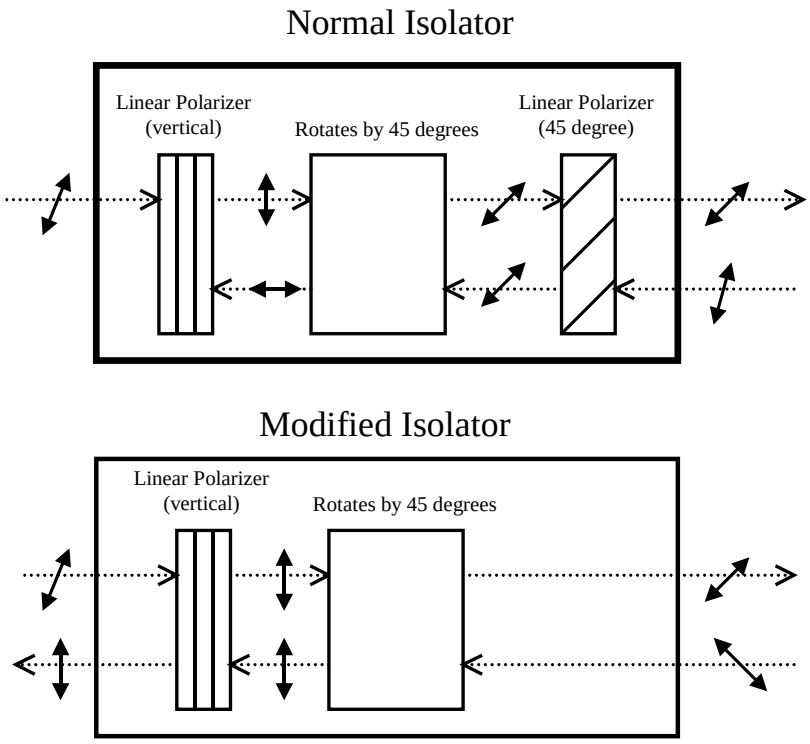

Figure 3.21 *Modified Faraday isolator*[3]

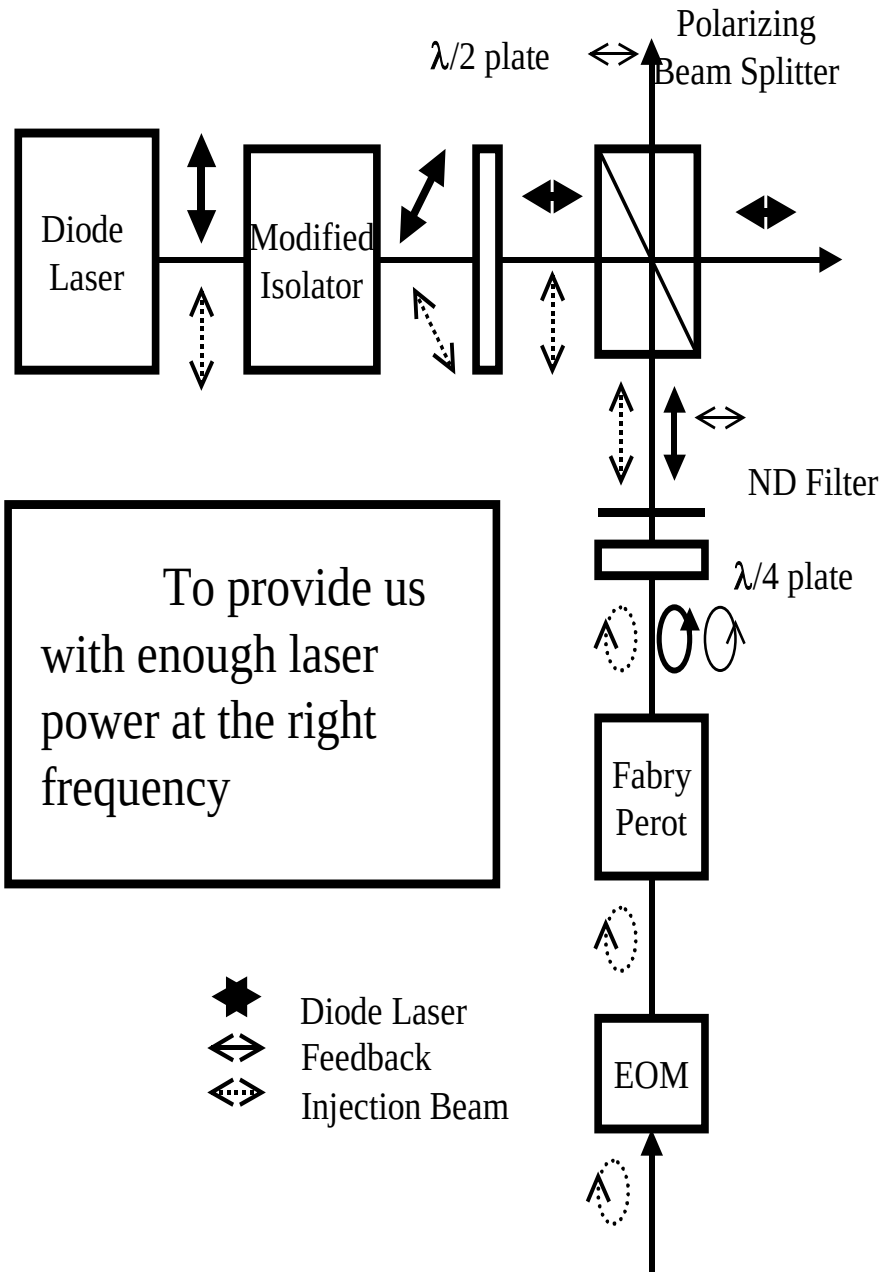

Figure 3.22 *Diode laser injection locking*[3]

linear polarizor. One side of the linear polarizor is vertical and the other side is rotated 45^o to the vertical one. When the diode laser beam first goes through the vertical linear polarizor and then through the rotator, the polarization of the beam will be 45^o to the vertical which would pass the second linear polarization without attenuation. However, when the feedback beam, passes first through the linear polarizor which is 45^o to the vertical, the Faraday rotator rotates its polarization to the horizontal and the second vertical linear polarizor would block it completely. In our modified scheme, we remove the 45^o to the vertical linear polarizor. See Figure 3.22. We have now a circularly polarized laser beam after the Fabry-Perot cavity. We then use a quarter wave plate to get a beam with vertical linear polarization. A neutral density filter is inserted after that to provide adjustment of the injecting beam intensity, therefore, the coupling between the master laser beam and the diode laser beam. A polarizing cube beam splitter in the path reflects the vertical linear polarized beam and lets the horizontal linear polarized beam through. After that a half wave plate changes the polarization from -45^o to the vertical linear, and after the modified Faraday rotator, the polarization becomes vertical again. Since the injecting beam has vertical polarization, the locked diode laser would also have a vertically polarized output laser beam. This outgoing beam goes through the modified Faraday isolator and the polarization would become 45^o to the vertical linear. The half wave plate in the path would turn it to horizontally polarized beam. If we trace the beams, we can see that there are two possible paths for feedback. One is the path going through the polarizing cube beam splitter. This would always carry the horizontal polarization past the cube, therefore, 45^o to the vertical linear between the half wave plate and the isolator, but the isolator would prevent this polarization from feeding back. Another path

originates from the cube's reflected beam. Let's trace this path. If there's some residue vertical linear polarized outgoing diode laser beam between the half wave plate and the cube, it would be reflected into the incoming master laser beam path. After passing through the quarter wave plate, it'll become circularly polarized. Afterwards it will be reflected from the cavity and passing through the quarter wave plate second time, it'll become horizontally polarized, which will go through the polarizing cube beam splitter without reflecting to the injecting locking path. Our scheme essentially separates the master laser beam path and the outgoing diode laser beam path and prevents the feedback to a very high degree.

To lock the laser, we also need to mode match the master laser and the diode laser. For horizontal mode matching, we use the temperature of the diode laser cavity for coarse tuning and the diode current for fine tuning. For transverse mode matching, we use proper collimating optics to achieve the goal.

3.1.9.2. Raman frequency produced by acoustal optic modulators

To save us the trouble of complicated alignment, we currently generate our two Raman frequencies by using acoustal optic modulators (AOM). We found AOMs from Brimrose with about 35% to 40% efficiency at 1.5 GHz and a damage threshold of 300 mW. That means we can get about 100 to 120 mW laser power at the frequency we need. This is a preferred method now since at this stage of the experiment, we are not limited by laser power. In the future when we need to implement a multi π pulse scheme, we might need to go back to diode laser injection lock and lock a chain of the diode lasers to provide us with the required laser intensity.

See Figure 3.23 for the current setup of all the laser beams needed for the experiment at the right frequencies generated by a few AOMs. We inserted proper collimating optics in the beam path to focus the laser beam. The laser beam waist is small enough to match the active aperture size of the AOM (Which is 70 μm in the 1.5 GHz AOM's case) to optimize the AOM output power. There is a beam splitter after the collimating optics. The through beam and the reflected beam each goes through a 1.5 GHz AOM with one frequency upshift and one frequency downshift. So the frequencies of the output of these two AOMs are 3 GHz apart. This scheme allows us to scan the difference frequency symmetrically.

To be able to change the common detuning of the two Raman beam, we insert a 1.2 GHz AOM with a 300 MHz tuning range in the setup. The downshift output of this AOM would serve the purpose of optical pumping, detection and locking. We upshift one of the three parts of this beam by a 60 MHz AOM to lock the laser at the crossover peak, the biggest one in the group, which is 60 MHz above the peak of F=3 to F'=3.The second part of the beam has the frequency of F=3 to F'=3 and is used for optical pumping. The third part of the beam goes through another AOM and the outgoing beam is upshifted 120 MHz in frequency. This beam serves as the detection beam, which has the frequency of F=3 to F'=4. If the 1.2 GHz AOM is driven at exactly 1.2 GHz, we have both the Raman beams red detuned from level F'=3 by about 300 MHz.

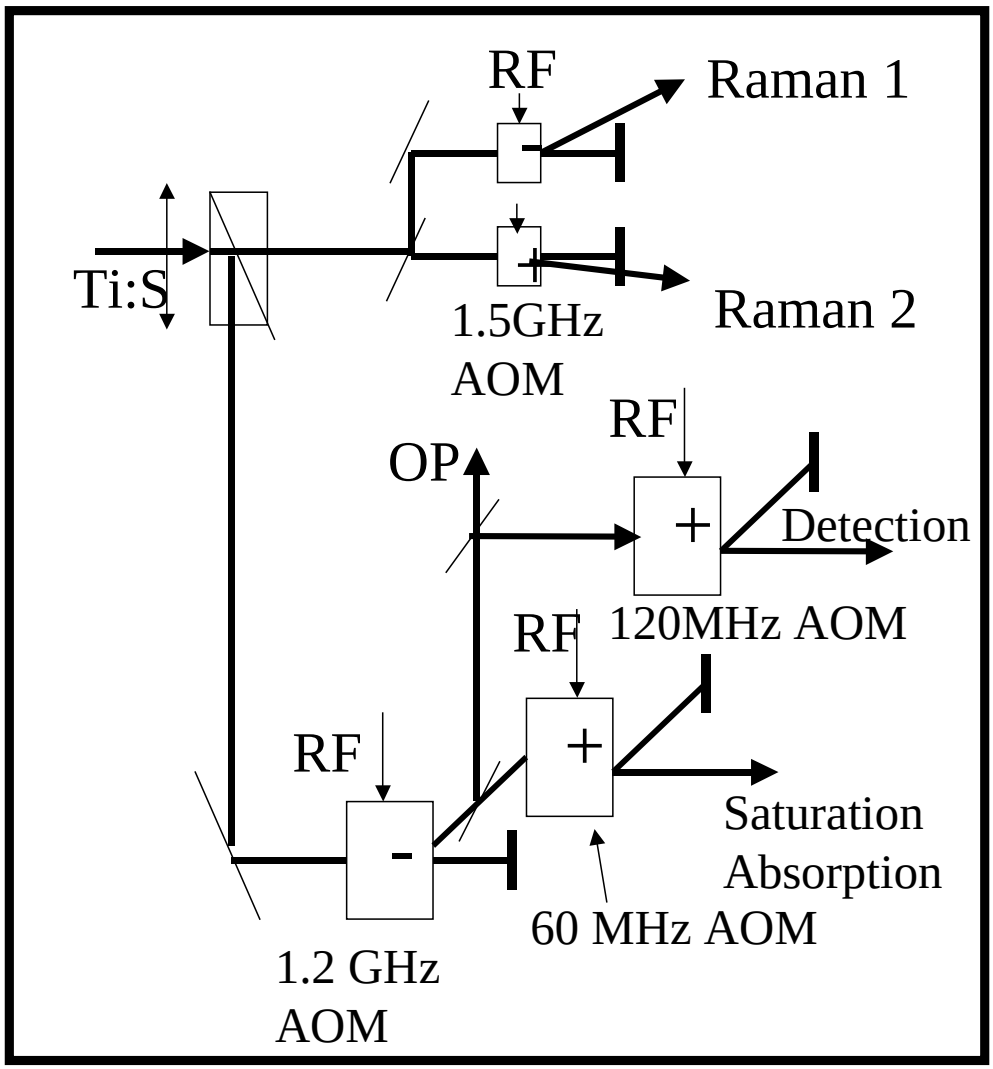

Figure 3.23 *Current setup of all the laser beams with the right frequencies generated by a few AOMs. OP stands for optical pumping beam F=3->F'=3, the other optical pumping beam is generated by a separate Ti:sapphire laser.*

3.1.10 Noise Control

3.1.10.1 Stray magnetic field gradient

Both the magnetic sublevel optical pumping and the Raman interaction are very sensitive to the laser beam polarization. It's very important that we get rid of the stray magnetic field otherwise the efficiency of the optical pumping and Raman interaction would be affected.

We put the annealed μ metal around the vacuum chamber for the atomic beam with the coils for bias magnetic field inside the μ metal. The stray magnetic field is cut down to less than 10 mGauss in the center, though there still might be some leakage around the edge.

3.1.10.2 Mechanical noise

Our atomic beam (vacuum system) was sitting on top of a Unistruct construction. On each side of the atomic beam, four ¾"x1'x1$^{1}/_{2}$' breadboards were mounted on two long Unistruct bars. Breadboards were connected with each other by a few 1"x1"x32" aluminum bars. Optics for the last part of the detection beam, Raman beams and cooling beam in their corresponding beam paths were mounted on those breadboards.

To characterize the mechanic vibration effect of the system on our experiment, we set up a Mach-Zehnder interferometer and looked at the stability of the interference fringes. See Figure 3.24 for this optical interferometer. In one of our diagnostic

experiments, $\pi/2$-π-$\pi/2$ counter propagating Raman experiment, we use the first $\pi/2$ and the second $\pi/2$

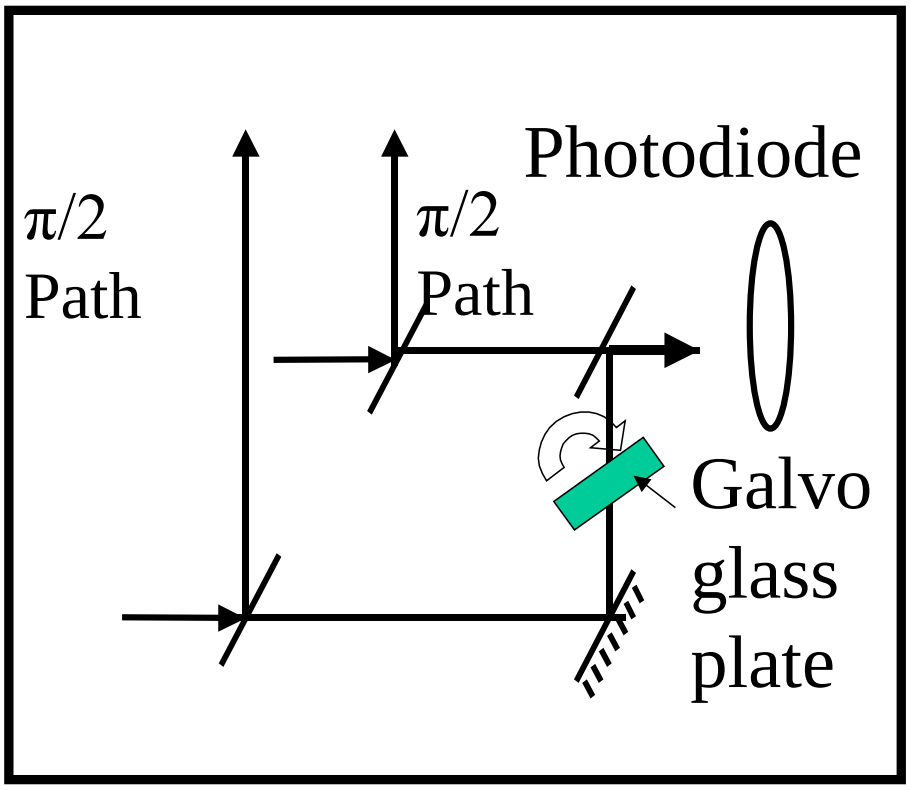

Figure 3.24 *Optical interferometer to characterize mechanical stability of the system*

beam in one direction of the counter propagating Raman beams to set up this interferometer. A photodiode with a small aperture was set up to look at only one fringe of the interference. We inserted a glass plate galvo in one leg of the interferometer. When we scan this galvo plate, the optical path length of that leg is changed and we expect that the photodiode should see the change of the intensity of that particular fringe as a function of the galvo scan voltage. If the system is stable and no mechanical vibration exist, we expect to see a time independent smooth curve of intensity vs. scan. Unfortunately, the time average of this signal approached zero due to the vibration. This means that the phase relation between the first $\pi/2$ and the second $\pi/2$ beams is random. In this case the atomic interference fringes would be completely wiped out by the mechanical vibration.

To solve this problem, we made some changes in our system. Two 1”x1’x9’ steel plates are mounted on the Unistruct, each weighs about 300 lb. They are connected by six 2”x4”x40” aluminum bars. Breadboards were mounted on top of these two steel plates. We also put vibration control pads under all the mechanical pumps to isolate the main sources of the mechanical vibration in the lab. See Figure 3.25 for the effect of the mechanical noise control. The interference signal on top is 32 times averaged Compared to the single shot interference signal, we still get about 80% of the amplitude left after the averaging. After the change, the short-term stability is greatly improved. However, the system is still very sensitive to the transient environmental noises, such as the slam of the door, or jumps on the floor. So if we average for a long time, the signal fluctuates. This is not perfect, but we have a reasonable chance to observe the atomic interference.

3.1.10.3 Laser intensity noise

When the Ti:sapphire laser is well aligned, the intensity noise is less than 1%. We don't have to worry about this noise source at least for now.

3.1.10.4 Laser Frequency drift

When we lock the Ti:sapphire laser to one of the saturation absorption peaks, the frequency noise is less than one MHz.

3.1.10.5 Raman beam difference frequency drift

What is important is the difference frequency between the two Raman beams in our experiment. We lock the RFsource, which drives the two 1.5 GHz AOMs for Raman beams, to a microwave frequency stabilizer which is in turn locked to a Rubidium clock.

3.1.11 Alignment

3.1.11.1 The alignment of the detection beam and the optical pumping beam

First we need to align the detection beam so it is perpendicular to the atomic beam and goes through the center of the atomic beam. We scan the laser over F=3 to F' frequencies and use the laser'sthe horizontal scan output to trigger the oscilloscope. We put the saturation absorption signal and the signal detected from the photo multiplier tube (PMT) into the oscilloscope's two input channels. Taking into account all the AOMs in the path of the detection beam, the peak of the detected signal should present itself at a particular position with respect to the saturation absorption peaks if the detection beam is perpendicular to the atomic beam

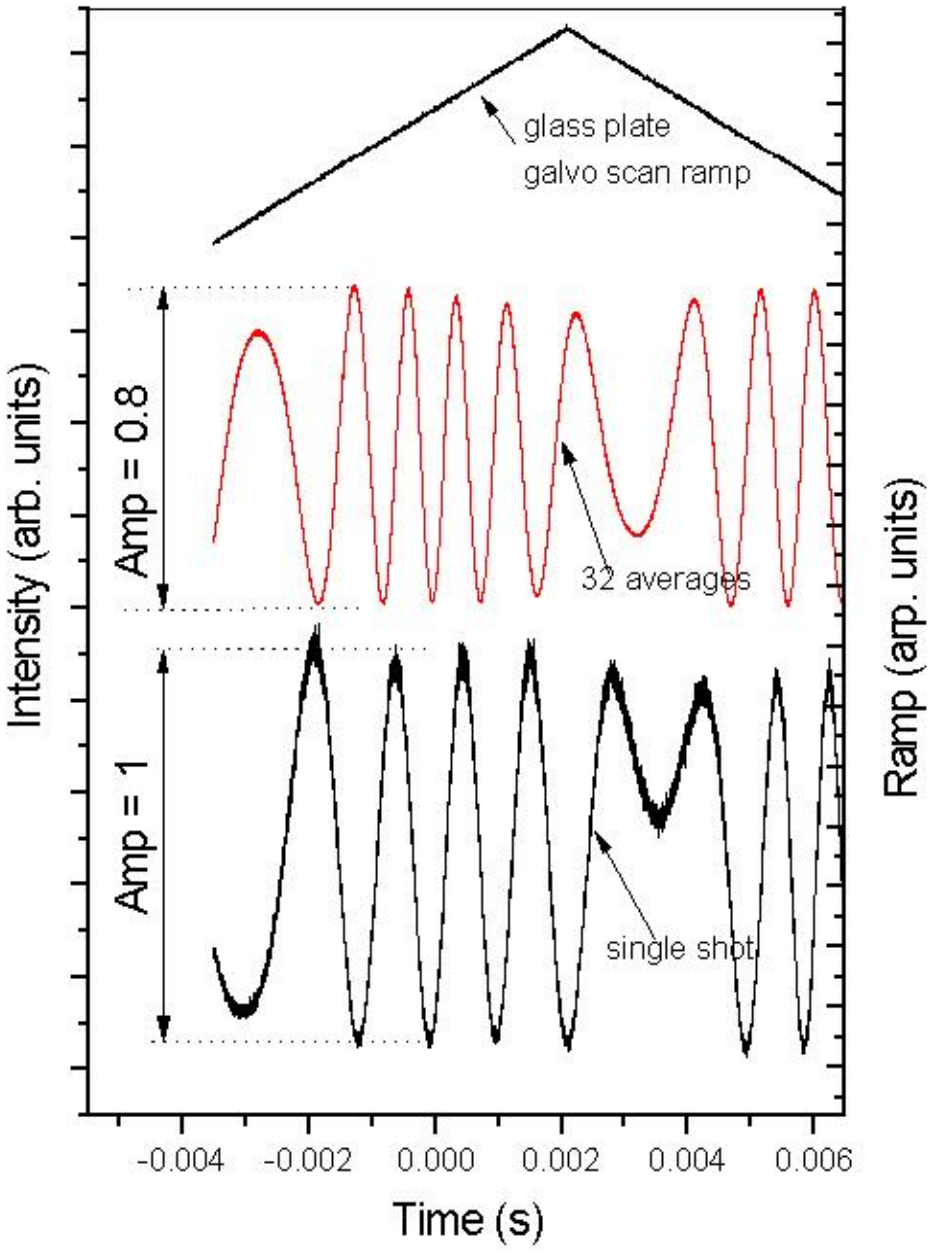

Figure 3.25 *The effect of mechanical noise control*

so there is no Doppler shift . We need to adjust the horizontal alignment to get the detected signal peaked at the expected position and adjust the vertical alignment so the detection beam goes through the center of the atomic beam. The detection beam is also retro reflected back so during the detection, the atoms won't get pushed to one side after a few cycles. We need to align the retro reflected detection beam so when we block the retro reflected beam, the fluorescence peak drop by half.

Next we need to align the optical pumping beam. Both optical pumping beams are vertical, perpendicular to the detection beam and Raman beams. We use the optical pumping beam F=3 to F'=3 to align and put F=2 to F'=2 on top of it. We want to make sure that the optical pumping beam pumps the same group of atoms that will be detected by the detection beam. We align the optical pumping beam so the detected signal will diminish and disappear. Since F=3 to F'=3 will pump atoms out of F=3 level and the detection beam detects atoms at F=3, therefore, when the optical pumping is the most efficient, we should see a minimum detection signal.

3.1.11.2 The alignment of the Raman beams

To roughly align the Raman beams, we use the same procedure as in the alignment of the detection beam.

The difference frequency of the two Raman beams is very important in our experiment. AC stark shift is proportional to the laser intensity, so if we don't cancel the AC stark shift, when the laser intensity fluctuates, the difference frequency will fluctuate too. To cancel the AC stark shift, we use Raman-Ramsey fringes and co-propagating signal. Raman-Ramsey fringes can be used to set the microwave source frequency right

so that the difference frequency of those two Raman beams is exactly the difference frequency of the two energy levels involved. After that, by adjusting the relative power of those two Raman beams, we will find a power ratio so that when we double the power of both beams, the peak position of the co-propagating Raman signal stays the same. Then we know that the AC stark shift is cancelled.

Next, we have to make sure that all three counter propagating Raman beams are aligned properly. After the rough alignment, we can use a big piece of glass with optical quality to make all three counter-propagating Raman beams parallel to each other. The glass has to be big enough to cover two beams at least. We mount the glass and insert it in front of two Raman beams. We adjust the glass tilting so that one of the Raman beams is reflected back to its incoming path and then we adjust the mirrors for the second Raman beam to make sure that it also reflects back to its incoming path. This way those two Raman beams are parallel to each other. We could use one of these two as standard and align the rest of the Raman beams the same way. To check that all Raman beams are not only parallel to each other but also overlapped well, we use counter-propagating Raman signals from each pair of the counter-propagating Raman beams. If the peaks of those counter-propagating Raman signals are lined up, we are ready to do the experiment.

3.1.12 Raman beam polarization, intensity

The polarization of the Raman beams plays an important role in this experiment. We found out that only cross-linear polarized Raman beams give us significant signal in both co-propagating and counter-propagating cases. In the co-propagating case, σ^+ - σ^+

and σ^{-} - σ^{-} pairs, in counter-propagating case, σ^{+} - σ^{-}, and σ^{-} - σ^{+} pairs produce significant signals.

The beam splitters for Raman beams are not polarization insensitive, so we inserted a half wave plate before they interact with the atomic beam to maximize the signals.

3.2 Diagnostic experiments

3.2.1 Resonant Raman transition without state preparation

Raman dip

This is the experiment performed to check our injection locking of the diode laser. The master laser, Ti:Sapphire laser is locked to F=3 to F'=3 and the diode laser output has the frequency F=2 to F'=3. Both legs of the Raman beams are on resonance. Optical pumping (without magnetic sublevel optical pumping) put atoms in state F=2 and we detect atoms at state F=3. When we scan the EOM driving RF frequency and the difference detuning is not zero, Raman interaction would move atoms from state F=2 to state F=3 so we expect to see a peak. When the difference detuning is exactly zero, we expect to see a Raman dip, as described in section 2.2, since a dark state is formed when exactly on resonance. See Figure 3.26 for the Raman dip.

Ramsey fringes

The Raman-Ramsey experiment is a very important diagnostic experiment in our case. We needed to go back to it again and again. It is used to test whether our microwave source is stable enough for Raman beams. It also helps to get rid of the AC stark shift.

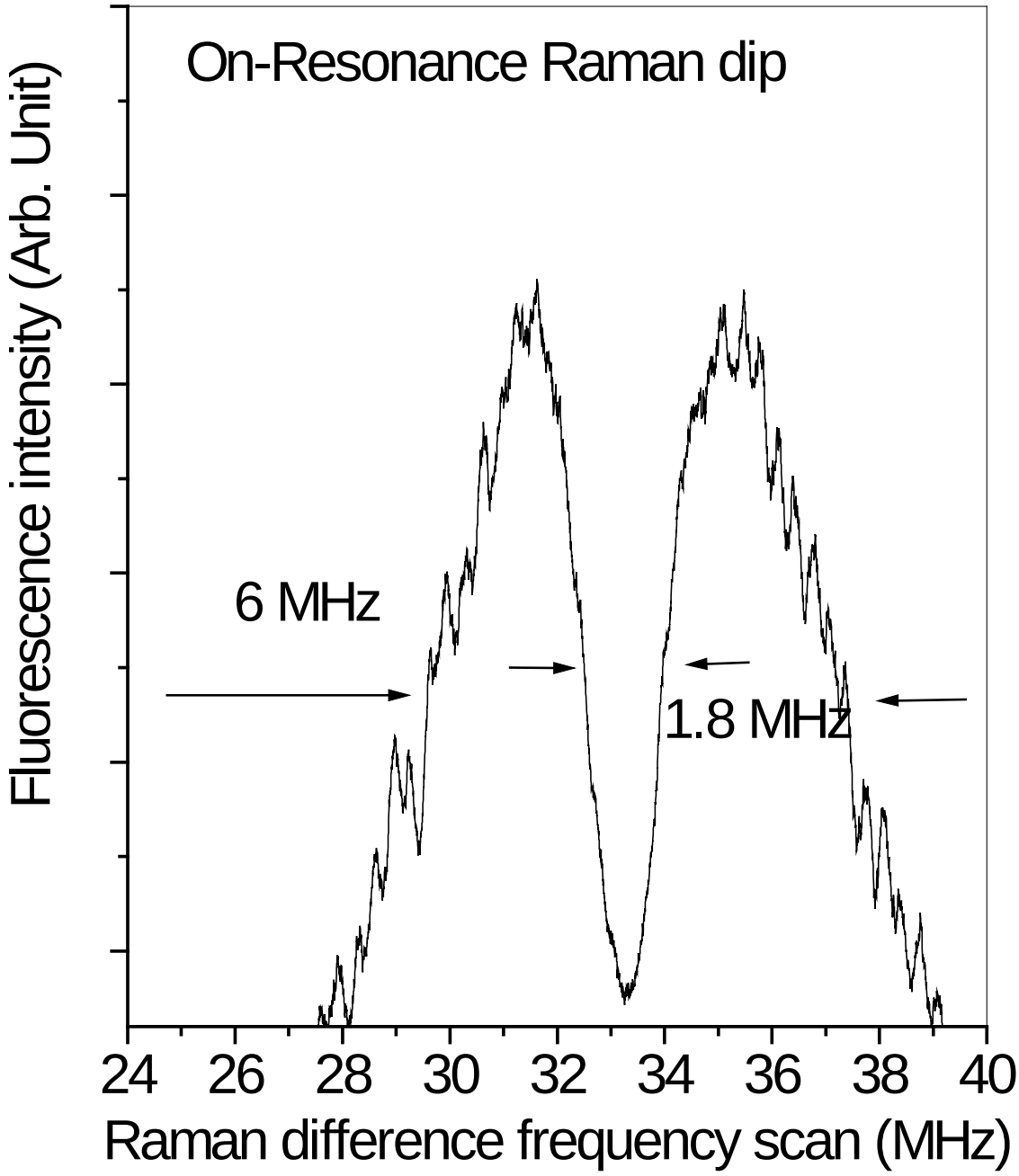

Figure 3.26 *On-resonance Raman dip*

Figure 3.27 shows the on-resonance co-propagating Raman Ramsey fringes[3] with a Raman beams separation about 30 cm.

3.2.2 Off-resonant Raman transition

Co-*propagating* Raman excitation

We use the co-propagating Raman signal to perfect our magnetic sublevel optical pumping. See Figure 3.9 for the effect of our magnetic sublevel optical pumping. Figure 3.28 shows a co-propagating signal without an applied magnetic field.

One way to find the π pulse duration is to use a co-propagating Raman signal. After setting the right relative intensity ratio of those two Raman beams (see next section), the Rabi frequency of those two Raman beams are the same, and we can measure the co-propagating signal strength as a function of the Rabi frequency (intensity) of the two Raman beams. We then can compare the measured data and the theoretical calculation to get the right intensity for a π pulse and get a π/2 pulse by cutting down the intensity by half.

***Ramsey* fringes**

As mentioned above, we need to use the off-resonant Raman-Ramsey fringes to find the proper transition frequency and to balance the relative intensity of those two Raman beams to get rid of the AC stark shift. We know that Raman-Ramsey fringes are located very close to the center of the zero difference frequency detuning, almost no AC stark shift exist compared to the co-propagating Raman signal envelope[22]. When the

Raman beam intensity ratio is too much off, we can't find the Raman-Ramsey fringes within the co-propagating Raman signal envelope.

AC stark shift could be caused by unbalanced intensities; it's also connected with the alignment since Doppler shift could also detune the interaction. Our goal is to adjust the intensity ratio and the alignment so that the Raman-Ramsey fringes occur at the peak of the co-propagating Raman envelope and that at the peak position the Raman difference detuning is really zero. In other words the frequency difference of the two Raman beams to be the same as the F=2 and F=3 level frequency difference.

Figure 3.29 shows an off-resonant Ramsey fringes.

Counter-propagating Raman excitation

The atom interferometer experiment would be performed in a counter-propagating configuration. We can use the counter-propagating Raman excitation to find the proper laser power and polarization and to check alignment. In the counter-propagating configuration, since we have to take into account the atom transverse velocity spread, the π pulse Raman beam intensity we measured using co-propagating Raman signal is a π pulse only for atoms with transverse velocity zero. To include some of the other atoms, we need to power broaden the Raman transitions.

As for the alignment and polarization check, we need to make sure that the first $\pi/2$ Raman beams produce the same counter-propagating Raman signal strength as that of the second $\pi/2$ Raman beams. We also have to make sure that the centers of the counter-propagating Raman signals for the two $\pi/2$ Raman beams and the middle π Raman beams are lined up.

Figure 3.30 shows a counter-propagating Raman signal. The width is a lot bigger than that of the co-propagating Raman signal due to the atom transverse velocity distribution.

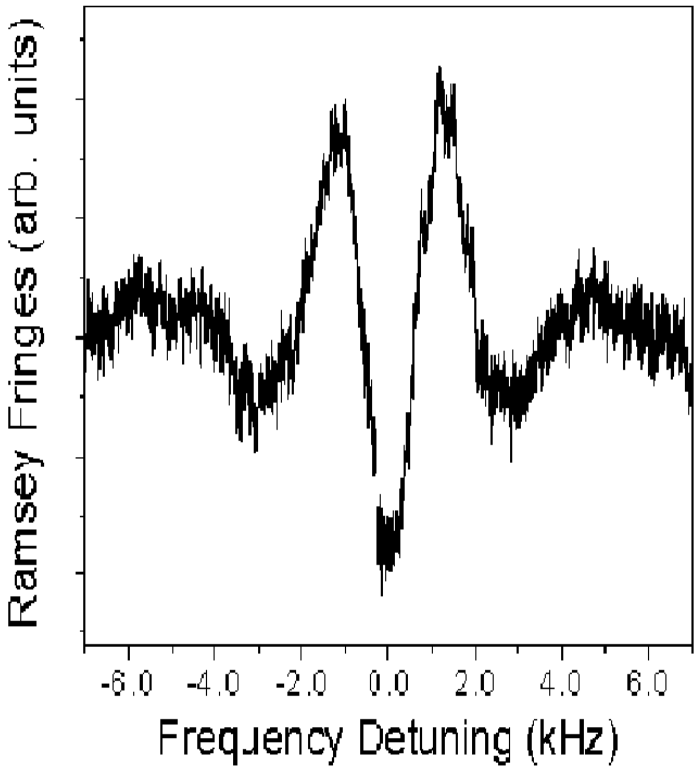

Figure 3.27 *On-resonance Raman-Ramsey fringes*

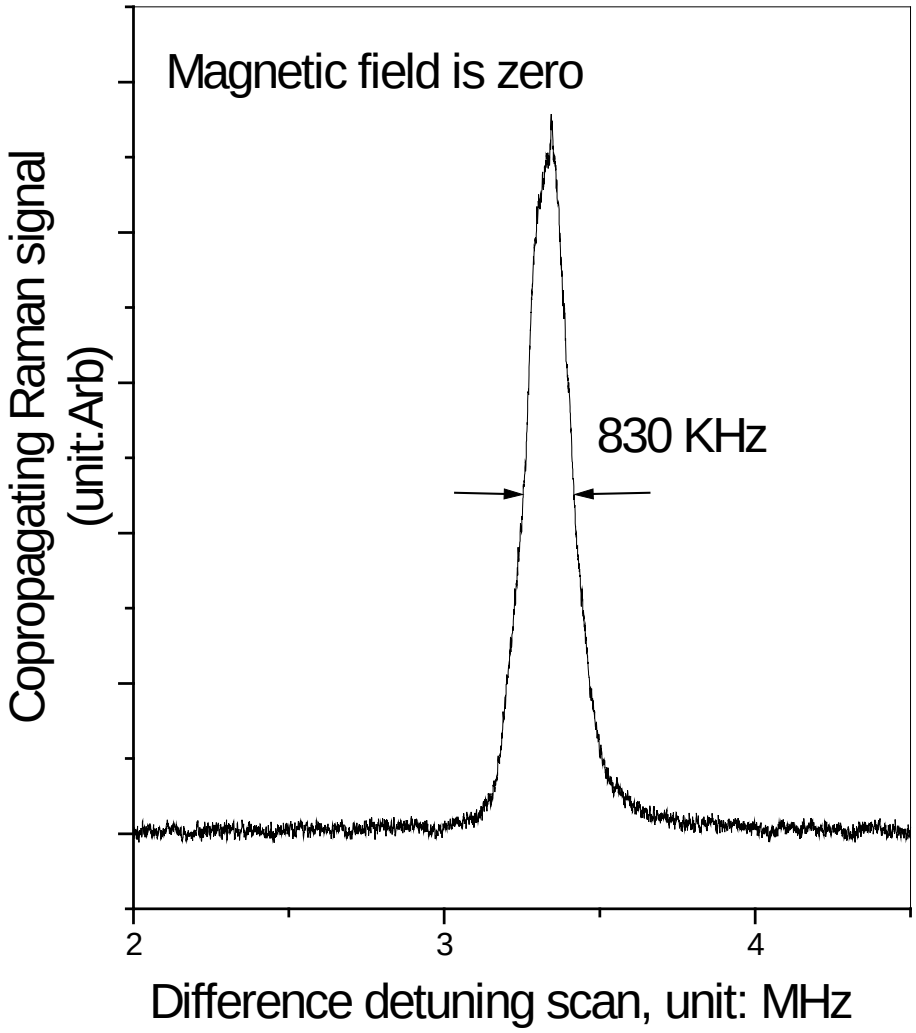

Figure 3.28 *Co-propagating Raman signal without an applied magnetic field*

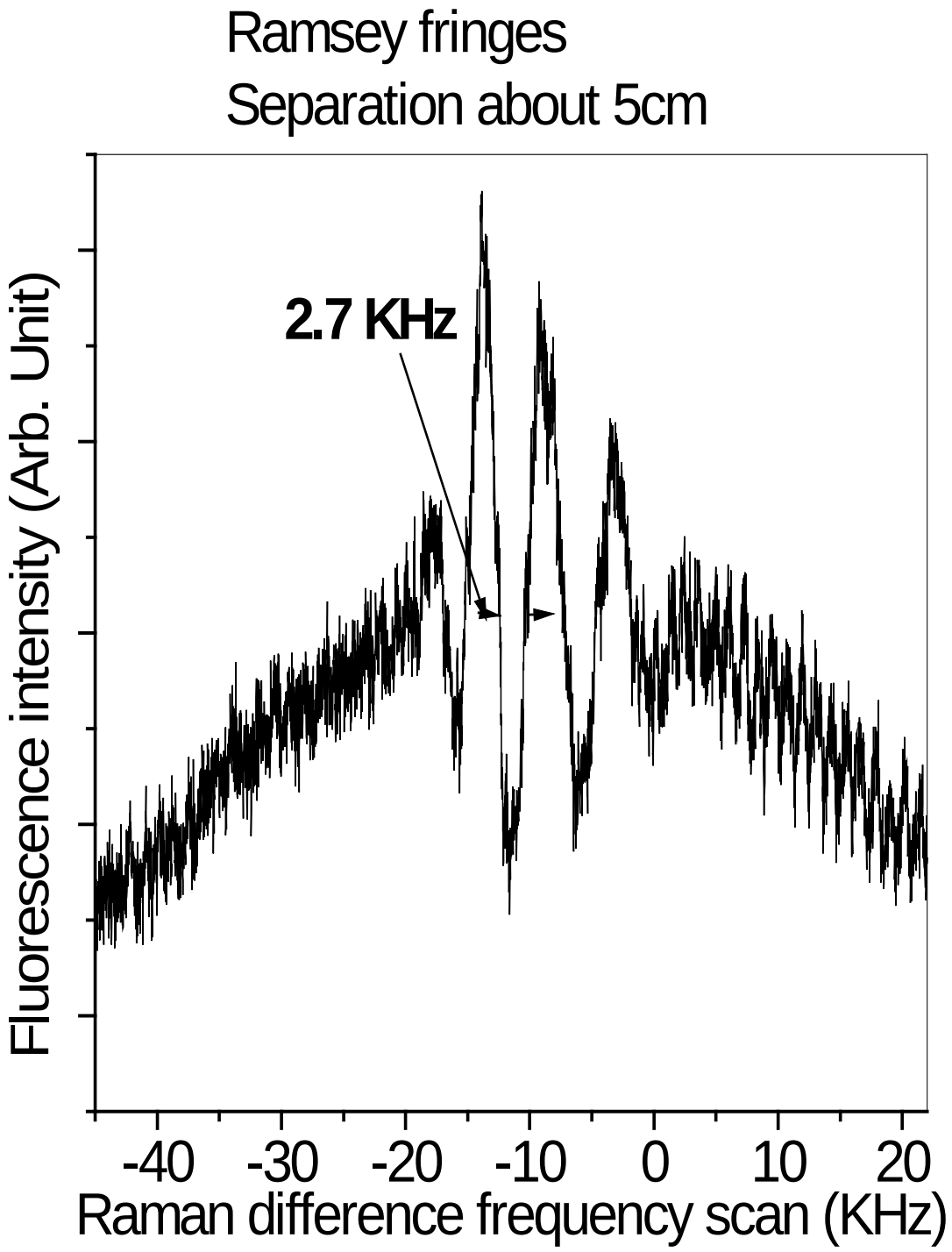

Figure 3.29 *Off-resonance Raman-Ramsey fringes*

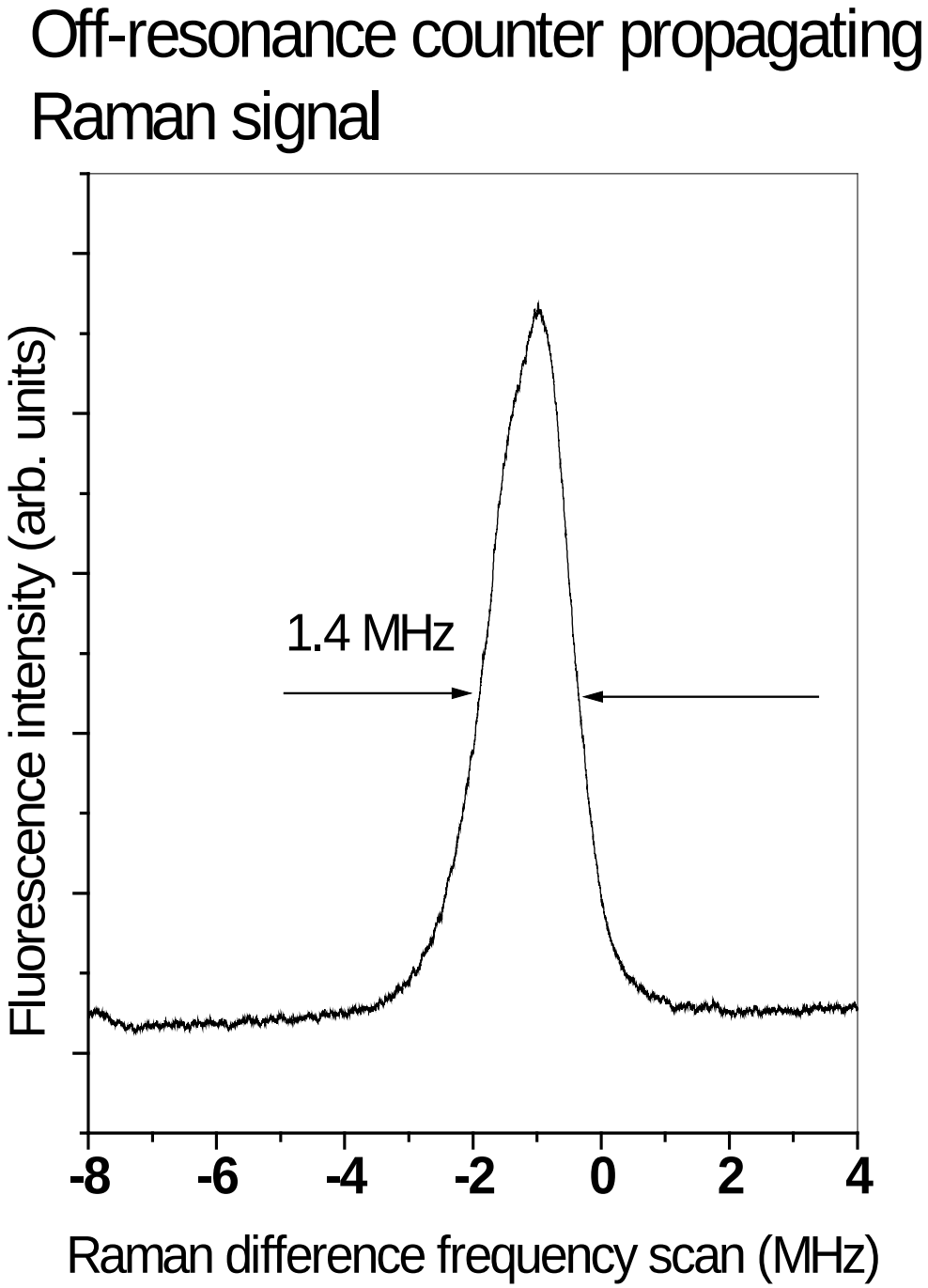

Figure 3.30 *Counter-propagating Raman signal*

3.3 Asbestos accident and the interruption of our experimental effort on this atomic beam machine for now

As described in Chapter one, after the asbestos accident happened, the vacuum system was destroyed completely and it's impossible to continue the experimental effort on this atomic beam machine for now. While we tried to recover this vacuum system, we build a small atomic beam and shift our experiment on that atomic beam.

Chapter Four:

Atom Interferometer Experiment on a New Atomic Beam

After the vacuum system of the big atomic beam was destroyed by the asbestos accident, the new compact atomic beam was built to continue the $\pi/2$- π - $\pi/2$ interferometer experiment we already started. As we went along, we observed atomic interference from single counter-propagating Raman beams and we discovered a better way to design an atom interferometer.

4.1 The structure of the new atomic beam

Figure 4.1 shows the structure of the new atomic beam. In a vacuum system, Rubidium atoms are emitted from an oven and form a thermal beam. Two nozzles are used to collimate the atomic beam. Since there is not enough length for us to do the aperturing as what we did for the big atomic beam machine, we use smaller nozzles to provide us with acceptable transverse velocity spread. By measuring the width of the counter-propagating Raman signal, we can estimate the atomic beam transverse velocity spread and therefore estimate whether the size of the nozzles is appropriate. After a few trials, we settled down with both the primary and the secondary nozzle diameters at about 330 μm. The distance between two nozzles is about 112 mm.

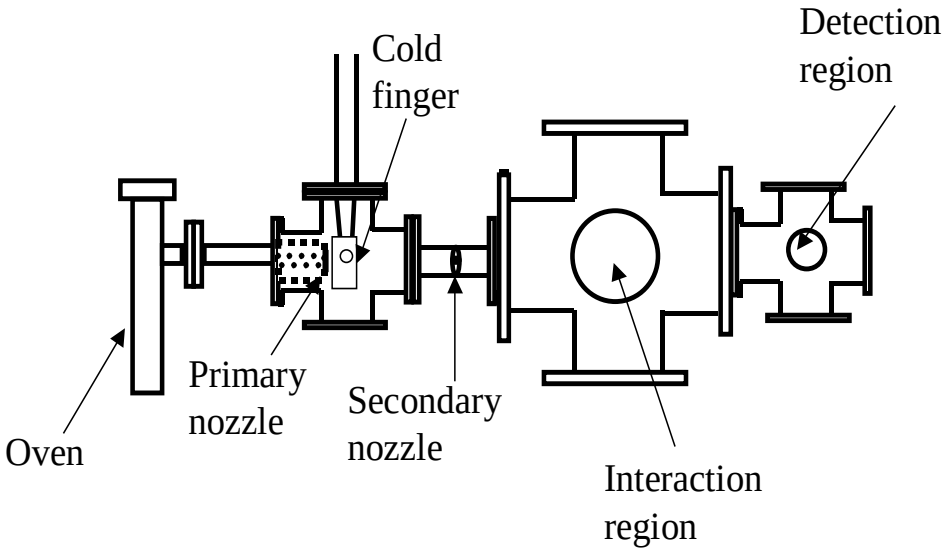

Figure 4.1 *Small atomic beam*

Due to the small size, the nozzle parts have to be very hot so they wouldn't clog easily. During the test run, we raised the temperature higher than what we actually need in the real experiment and found that the parts of our apparatus can endure high temperature without developing leaks. Now the running temperature profile is as follows:

Oven: 270 ^{o}C,

Oven top: 450 ^{o}C,

Nozzles: 560 ^{o}C.

There is a Helmholtz coil structure positioned around the interaction region to provide the bias magnetic field, which is along the direction of the Raman beams; see

Figure 4.1 for the interaction region. A μ metal shielding for the small atomic beam is wrapped around the interaction region, enclosing the Helmholtz coil structure.

4.2 The experiment and the result

In this experiment, we don't need to do magnetic sublevel optical pumping. We only need four different laser beams: an optical pumping beam, a detection beam and two Raman beams. One Ti:sapphire laser is all we need.

We set up acoustal optic modulators (AOMs) in the Ti:Sapphire laser frequency locking path so we can shift the Raman beam common detuning which would give us a bigger Rabi frequency for the Raman beam given the power constraint we have. As before, we use Rubidium 85 transitions. The Ti:sapphire laser is locked to the Rubidium 85 transition $5P_{3/2}$ (F=3) to $5S_{1/2}$ (F=3) through a saturation absorption of a Rubidium vapor cell. Part of the laser beam at this frequency is used for optical pumping which pumps Rb atoms to their initial state $5P_{3/2}$ (F=2) from $5P_{3/2}$ (F=3). Part of the laser beam passes through an acousto-optic modulator (AOM) (Isomet, model 1206C) with center frequency 110 MHz, upshift 120 MHz, which will tune the deflected beam to transition $5P_{3/2}$ (F=3) to $5S_{1/2}$ (F=4). This transition is a cyclic transition. We use it as the detection beam. By irradiating the atoms with this detection beam, we collect the fluorescence on a photomultiplier tube, which is mounted on top of the detection region and its position can be adjusted in three dimensions. The rest of the laser beam is split into two parts by a 50% beam splitter. One part goes through a 1.5 GHz AOM (Brimrose model GPF-1500-300-.795), upshift and another goes through a 1.5 GHz AOM (Brimrose model GPF-1500-300-.795), downshift. Those two 1.5 GHz AOMs are controlled by the same

microwave generator (Wavetek 1-4 GHz Micro Sweep model 962). Since the hyperfine splitting of Rubidium 85 ground states is about 3 GHz, both deflected beams after 1.5 GHz AOMs are red detuned by 1.5 GHz, from transitions $5P_{3/2}$ (F=2) to $5S_{1/2}$ (F=3) and $5P_{3/2}$ (F=3) to $5S_{1/2}$ (F=3), respectively.

We used the optical pumping method to set up Raman beam apertures so the Raman beams are roughly perpendicular to the atomic beam. The basic procedure of the alignment is very similar to what we did on the big atomic beam.

We scan the laser over transitions $5P_{3/2}$ (F=3) to $5S_{1/2}$. First we block all the beams except the detection beam to align and check to make sure that we have a good atomic beam. Then we let through and align the optical pumping beam. Since we detect the atom population in state $5P_{3/2}$ (F=3) and since the optical pumping beam moves atoms away from this state, we should see that the fluorescence signal is decreased and minimized when the alignment of the optical pumping beam is good as we gradually decrease the intensity of this beam. After this we can lock the laser to $5P_{3/2}$ (F=3) to $5S_{1/2}$ (F=3) and let the Raman beams through. To detect the Raman signal, we scan the difference detuning of the Raman beams by scanning the frequency of the microwave generator.

We performed two-zone Ramsey-Raman experiment with this new atomic beam. We tried to use one zone co-propagating Raman to get rid of the AC stark shift by changing the relative power of the two frequencies of the Raman beams and adjusting the overlap of the two. For this step we were limited by the stiffness of the mirror mounts we had. However, soon we found out that for the type of the atom interferometer we are interested in, canceling AC stark shift is not critical anymore. We also set up Counter-

propagating Raman beams, and tried $\pi/2$-π-$\pi/2$ by setting the middle beam twice as strong as each of the other two. We didn't see any interference signal. There could be many factors that defeated our effort. So we decided to start with a simpler configuration by using one enlarged beam separating into three beams by using two vertical wires. The idea is that this configuration should be equivalent to the case of $\pi/2$- π- $\pi/2$ with the separation between Raman beams almost zero if the total intensity is equivalent to a 2 π Raman pulse. The initial enlarged beam size is about 5 mm. To scan the phase of one part of one of the Raman beams, we used a galvo glass. The glass plate we had was too thick because we originally designed for separate Raman beams. So we used a piece of 1mm thick glass. It was attached to the side of the original glass plate by a piece of double sided tape. The galvo is directly mounted on a magnetic base and is driven by a function generator (BK Precision 5 MHz function generator). There is a loading effect.

When we scan the phase of the last part of one of the Raman beams, we observed the fringes on top of the counter-propagating Raman signal. However, when we block the middle part of the Raman beam, the amplitude of the fringes decreased but did not disappear. We have yet to figure out a way to test whether the fringe is the real interference signal or just the intensity modulation.

Then another idea came along. If we can use two pieces of wires to break one set of counter-propagating Raman pulses to $\pi/2$- π- $\pi/2$ configuration, why not just keep the Raman beams as they are and use a galvo glass to scan the last ¼ of one of the Raman beams. This configuration also should be equivalent to $\pi/2$- π- $\pi/2$ configuration. The experiment layout is shown in Figure 4.2.

When we get a good counter-propagating Raman signal, we can insert the galvo glass plate in one of the Raman beams and scan it. We then slow down the Raman difference-detuning scan to about 0.1 Hz. The interference fringes appear on top of the counter propagating Raman signal, see Figure 4.3 for this. Then we try to adjust the offset of the difference detuning scan and decrease this scan range to let the Raman signal sit at the peak position. At the same time we scan the galvo glass and carefully adjust the width of the Raman beam that the galvo glass cut through till we see the atomic interference. The galvo glass tilt angle is between 10^o and 20^o. When the galvo glass is completely in the Raman beam or when it's completely out of the Raman beam, we don't observe any atomic interference, which is we expected. Figure 4.4 shows this. When we change the tilt angle of the glavo glass or when we change the scan amplitude, in both cases, the phase shifts covered by one scan would change. Furthermore, we can see that the number of the atomic interference fringes also changes, accordingly. Figure 4.5 and 4.6 show the effect of varying the galvo scan amplitude. We can use a Mach-Zehnder optical interferometer to calibrate the phase shift caused by the galvo glass scanner by insert this galvo glass plate in one leg of the optical interferometer and scan it. The fringe period of this optical interferometer is a function of the phase of the Raman beam the galvo glass scanned over; the same is also true with the fringe period of our atomic interferometer. For the same tilt angle and the same scan amplitude, the fringe period we get from the optical interferometer should be the same as that of the atomic interferometer.

Figure 4.7 shows the best results of the atomic interference fringes and the optical interference fringes we got for the same galvo glass tilt angle.

For this type of the atomic interferometer to work, we do not need to do very complicated alignments since there is only one interaction area and all the components of the Raman beams are automatically parallel to each other. Just one set of counter-propagating Raman beams exist. We only need to make sure that they are roughly perpendicular to the atomic beam and are overlapped well. We don't have to balance the AC stark shift either. If we can extend this type of the atom interferometer to a larger area, and it will be a new approach to build atom interferometers.

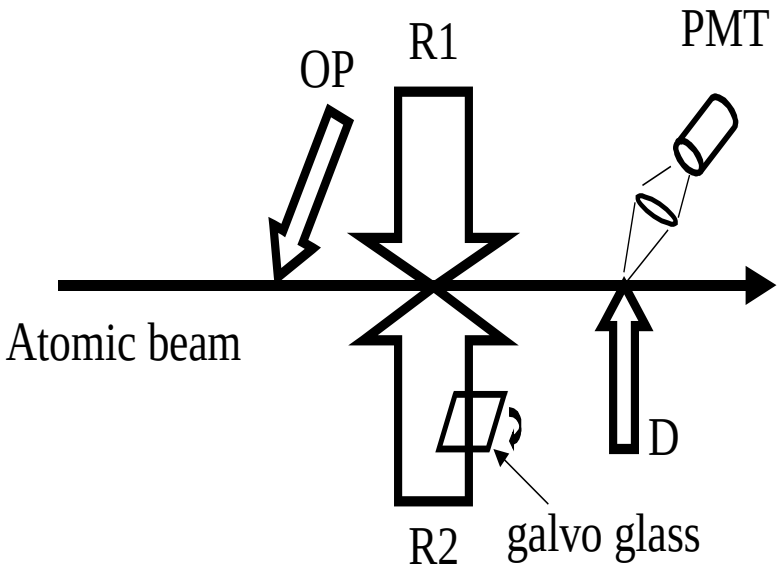

Figure 4.2 *Experimental layout*

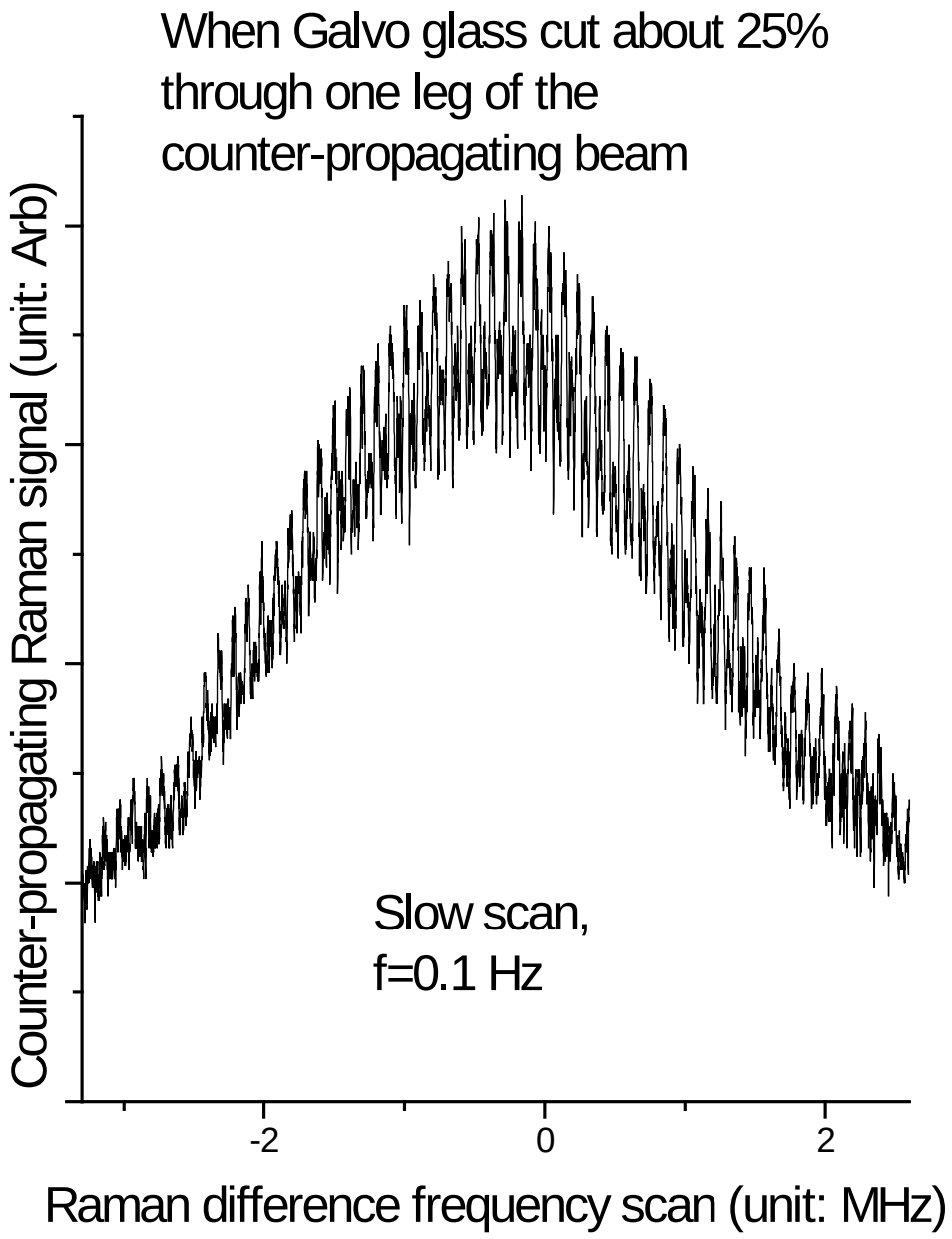

Figure 4.3 *Atomic interference fringes on top of the counter-propagating Raman signal*

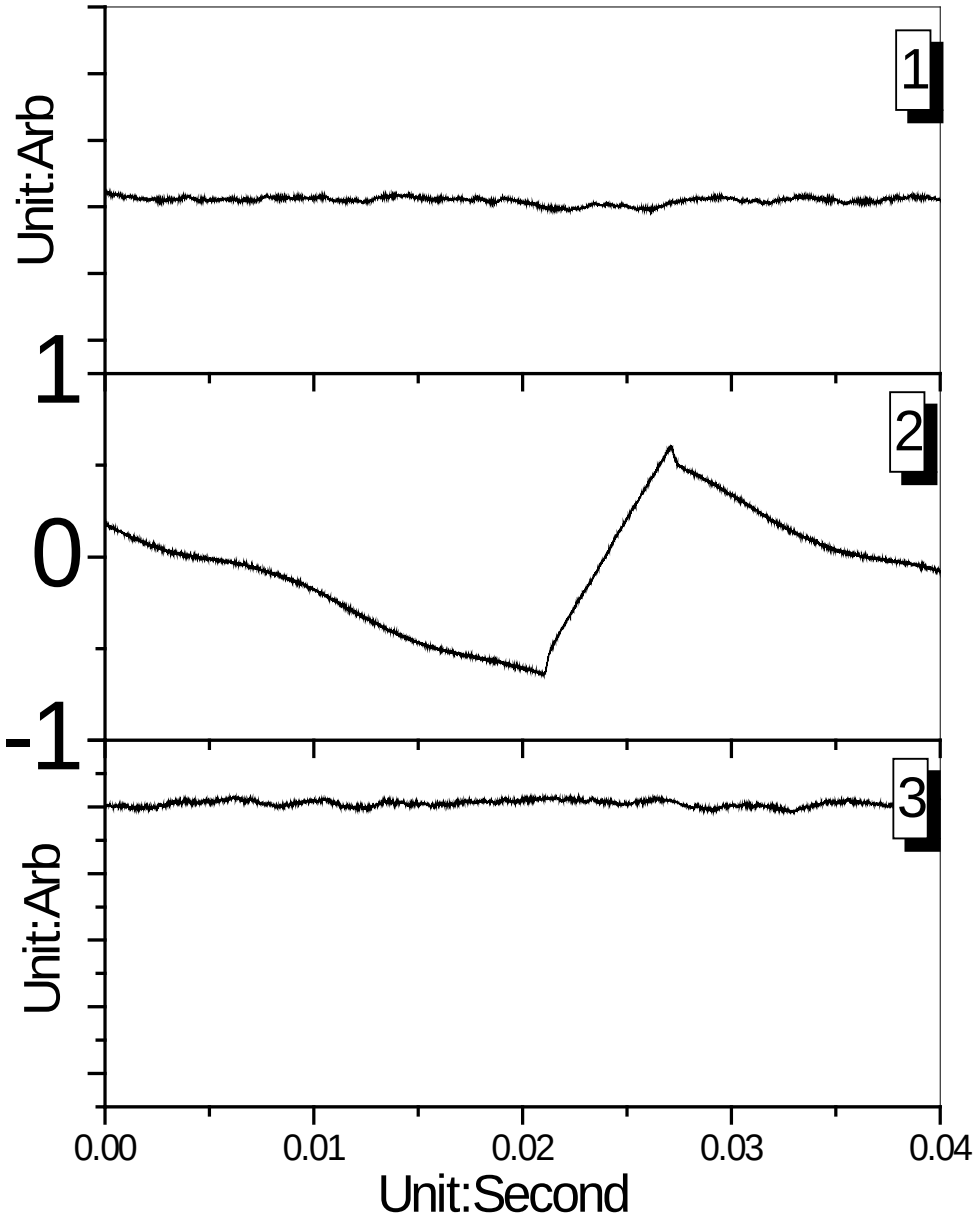

Figure 4.4 *No atomic interference fringes (1) when the galvo glass is completely in the Raman beam and (3) when the galvo glass is completely out of the Raman beam. (2) is the scan ramp for the galvo glass.*

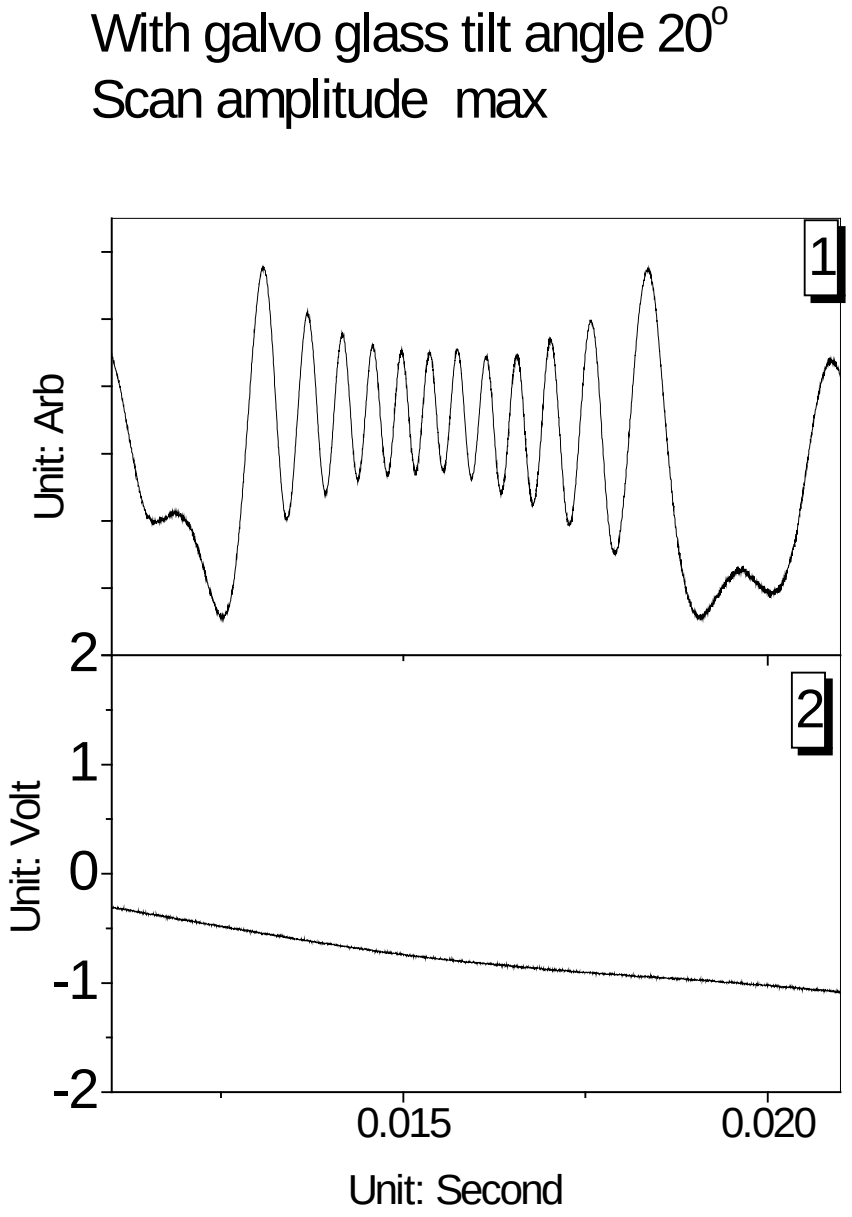

Figure 4.5 *(1) Atomic interference (2) Galvo scan ramp with galvo glass tilt angle 20° and scan amplitude maximum*

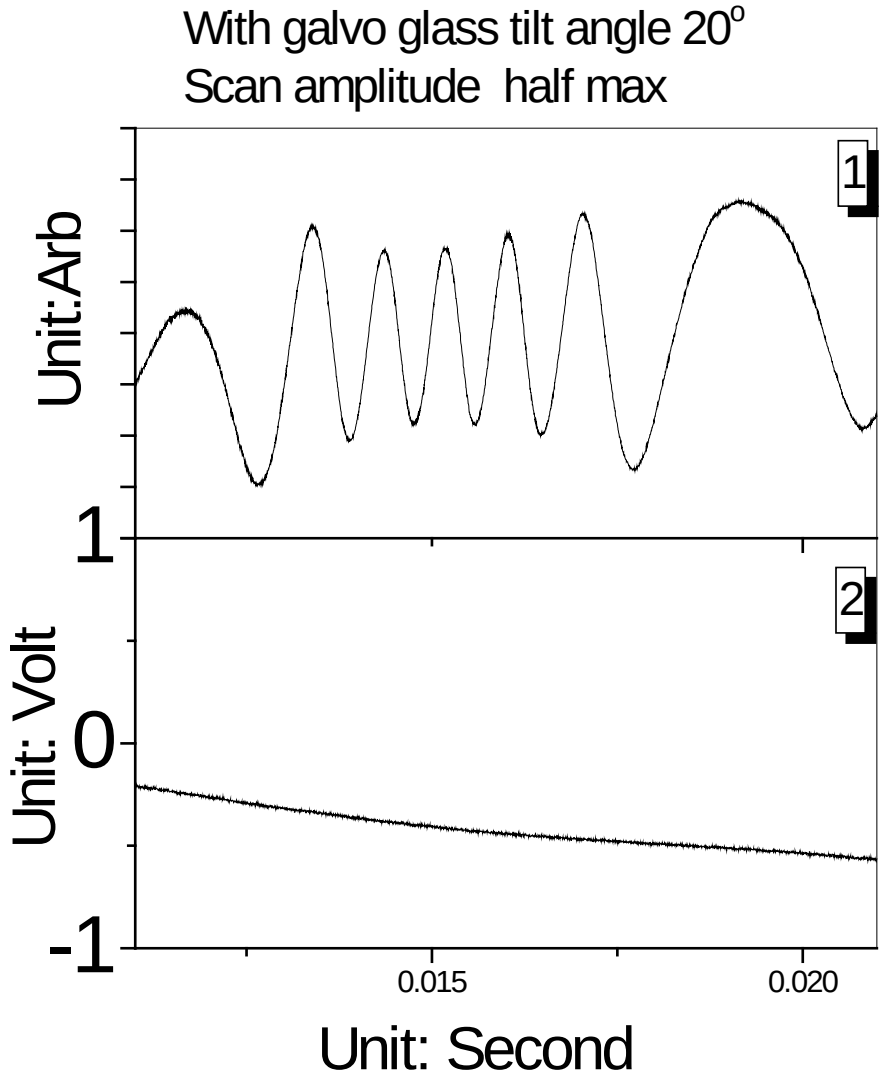

Figure 4.6 *(1) Atomic interference (2) Galvo scan ramp with galvo glass tilt angle 20° and scan amplitude half maximum*

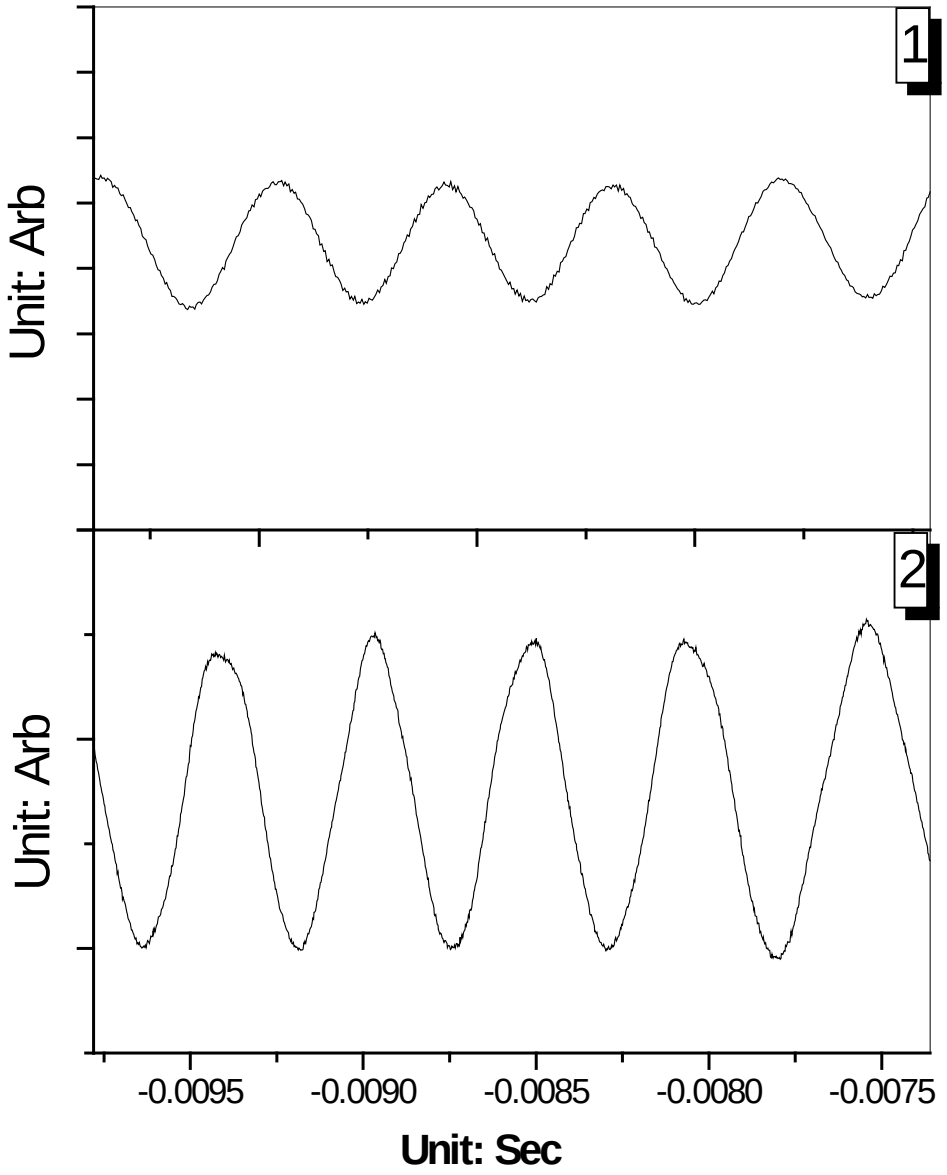

Figure 4.7 *Results of the atomic interference fringes and the optical interference fringes for the same galvo glass tilt angle (1): atomic interference (2): optical interference*

Chapter Five:

Numerical Simulations and the Investigation of the Possibility of Designing a New Type of Large Area Atom Interferometer Using Single Raman Pulse

Motivated by the experimental result we got in last chapter, we did some numerical simulation to see whether it is possible to design a large area atom interferometer based on a single counter-propagating Raman pulse.

5.1 The calculation method and approximations

In the case of the separated field Raman atom interferometer, we can always assume that the interaction time is much shorter than the atom free propagating time. Therefore in the calculation and simulation we can ignore the atom wave packet free propagation in the interaction region. This way the calculation of the atom light interaction and the atomic wave packet free propagation is separated. Obviously we cannot make the same approximation for the one field Raman atom interferometer.

To understand the problem physically and more intuitively, we can model the interaction and free propagation like this. Suppose that the Raman field is separated in many fine slices with the distance between each adjacent pair set to zero. Raman interaction will couple two states, $|g, \mathbf{p}, x\rangle$ and $|e, \mathbf{p}+2\hbar\mathbf{k}, x\rangle$. We assume that $(\mathbf{p}+2\hbar\mathbf{k})^2/2m - \mathbf{p}^2/2m \ll |\Omega|$, then for wave packet of state g and state e, we can analyze them in

momentum space, the Raman interaction will couple |g, $\mathbf{p}_i$> and |e, $\mathbf{p}_i$+2ħ **k** >, where $\mathbf{p}_i$ is the corresponding momentum components in momentum space, see Figure 5.1.

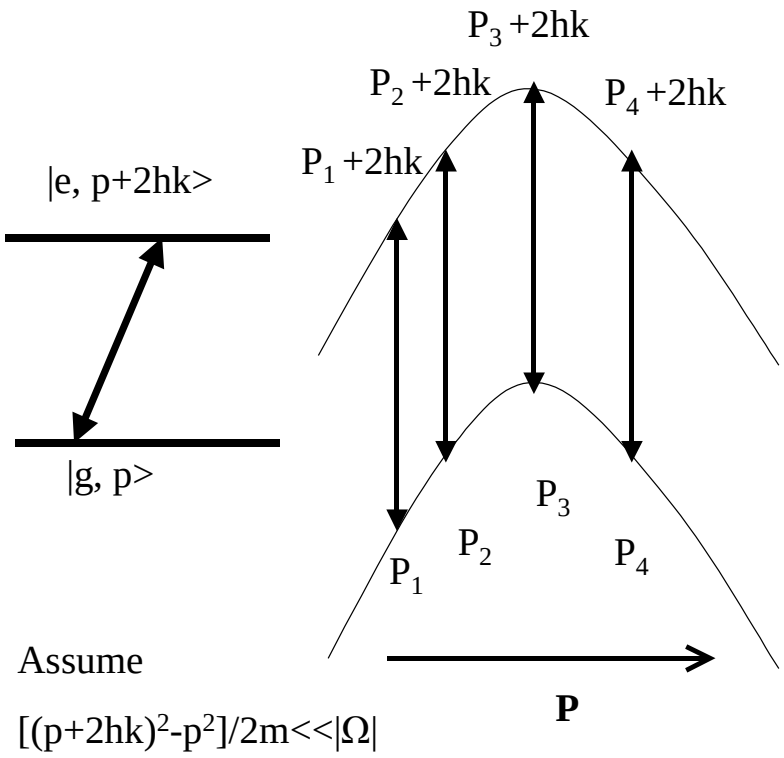

Figure 5.1 *Wave packets for States |g,* ***p****, x> and |e,* ***p****+2ħ* ***k****, x> are exactly the same except that in momentum space, all the momentum components are shifted by 2ħ* ***k*** *for |e,* ***p****+2ħ* ***k****, x> from that of |g,* ***p****, x>. Assume* $(\mathbf{p}+2\hbar\mathbf{k})^2/2m - p^2/2m << |\Omega|$ *and Raman interaction couple |g,* $\mathbf{p}_i$ *> and |e,* $\mathbf{p}_i+2\hbar\mathbf{k}$ *>.*

After each slice of Raman interaction and propagation, the part originally in state |g, **p**, x> will have some probability being in state |e, **p**+2ħ **k**, x>, and the part originally in state |e, **p**+2ħ **k**, x> will have some probability being in state |g, **p**, x>. The wave packets of both states will also free evolve, i.e. expand. We can combine the |g, **p**, x> state wave packets and the state |e, **p**+2ħ **k**, x> wave packets at the end of each slice of the Raman interaction and start over again for the next slice. See Figure 5.2 for the process. In the simulation, to simplify the calculation, we separate the Raman interaction part and the wave packet free evolution part. If the time step is fine enough, the result should be close to the reality. Since the three level system of far-detuned off-resonance Raman interaction can be simplified to an on-resonance two level system, as described in chapter two, we use two level system in the following calculation. Also we use natural units. Set ħ=1, mass of the atom m=1, effective Rabi frequency for the two level system Ω=1, wave number of the light k=1.

Assume for the first slice that the atom starts at the ground state |g, **p**=0, x>, where **p** is in the direction of the light beam and is perpendicular to the atom wave free propagation direction. At the end of the first slice, we will see a small population of excited state |e, **p**= ħ **k**, x>, of course the magnitude is dependent on the interaction time.

Assume that **p** is small and the change of the energies of states |g, **p**=0, x>, and state |e, **p**= ħ **k**, x> due to **p** can be ignored. For an on-resonance two-level system, after a rotating wave approximation and rotating wave transformation, as described in chapter two, the Hamiltonian becomes

$$H_R = \frac{\hbar}{2}\begin{bmatrix} 0 & -|\Omega| \\ -|\Omega| & 0 \end{bmatrix}. \qquad \text{(eq. 5.1)}$$

The wave function of the system is

$|\psi> = c_g |g, \mathbf{p}=0, x> + c_e |e, \mathbf{p}= \hbar \mathbf{k}, x> = c_g |g>|\mathbf{p}=0, x> + c_e |e>|\mathbf{p}= \hbar \mathbf{k}, x>.$ (eq. 5.2)

H_R will only have effect on the part of |g> and |e>. Applying Schrödinger equation

$$i\hbar \frac{\partial}{\partial t} |\Psi> = H |\Psi>, \quad \text{(eq. 5.3)}$$

we get

$$\begin{cases} \dot{c}_e = i \frac{|\Omega|}{2} c_g \\ \dot{c}_g = i \frac{|\Omega|}{2} c_e \end{cases}. \quad \text{(eq. 5.4)}$$

If in the beginning of the slice the atom starts at ground state C_g=1 and C_e=0 and the time duration of the slice is dt, at the end of the slice we have

$|\psi> = \cos(|\Omega|dt/2) \ |g>|\mathbf{p}=0, x> + i * \sin(|\Omega|dt/2) |e>|\mathbf{p}= \hbar \mathbf{k}, x>.$ (eq. 5.5)

If in the beginning of the slice the atom starts at excited state C_g=0 and C_e=1, at the end of the slice we have

$|\psi> = i * \sin(|\Omega|dt/2) \ |g>|\mathbf{p}=0, x> + \cos(|\Omega|dt/2) |e>|\mathbf{p}= \hbar \mathbf{k}, x>.$ (eq. 5.6)

States $|\mathbf{p}= 0, x>$ and $|\mathbf{p}= \hbar \mathbf{k}, x>$ will also propagate freely. Project the wave function in position space, we get

$$\Phi_g(x, k=0, t=0) = \frac{1}{\sqrt{a\sqrt{2\pi}}} e^{-\frac{x^2}{4a^2}}, \quad \text{(eq. 5.7)}$$

$$\Phi_e(x, k=k, t=0) = \frac{1}{\sqrt{a\sqrt{2\pi}}} e^{ikx} e^{-\frac{x^2}{4a^2}}. \quad \text{(eq. 5.8)}$$

Next, let's derive the general formula for the wave function free time evolution. Let the initial wave function be ψ (x,0). We can express ψ (x,0) as

$$\Psi(x,0) = \frac{1}{\sqrt{2\pi}} \int_{-\infty}^{\infty} b(k) e^{ikx} dk \qquad \text{(eq. 5.9)}$$

where

$$b(k) = \frac{1}{\sqrt{2\pi}} \int_{-\infty}^{\infty} \Psi(x,0) e^{-ikx} dx \qquad \text{(eq. 5.10)}$$

If Hamiltonian $\hat{H}$ is not a function of time, in this case

$$\hat{H} = \frac{\hat{p}^2}{2m}, \qquad \text{(eq. 5.11)}$$

we have

$$\Psi(x,t) = e^{\frac{i\hat{H}t}{\hbar}} \Psi(x,0) . \qquad \text{(eq. 5.12)}$$

$$\Psi(x,t) = \frac{1}{\sqrt{2\pi}} \int_{-\infty}^{\infty} e^{-\frac{i\hbar k^2 t}{2m}} b(k) e^{ikx} dk$$

$$= \frac{1}{\sqrt{2\pi}} \int_{-\infty}^{\infty} e^{-\frac{i\hbar k^2 t}{2m}} \frac{1}{\sqrt{2\pi}} \int_{-\infty}^{\infty} \Psi(x',0) e^{-ikx'} dx' e^{ikx} dk \quad \text{(eq. 5.13)}$$

$$\Psi(x,t) = \frac{1}{\sqrt{2\pi}} \sqrt{\frac{m}{i\hbar t}} \int_{-\infty}^{\infty} \Psi(x',0) e^{-\frac{m(x-x')^2}{2i\hbar t}} dx' \quad \text{(eq. 5.14)}$$

Using this equation, if we know the initial spatial wave function, we can propagate it easily. The whole simulation scheme works like this. An atom starts at ground state |g, **p**=0, x> with a Gaussian profile like the one in eq. 5.7 . In the first slice, after the atom light interaction the wave function will have a small component in the excited state. That part of the spatial wave function will have an extra phase factor exp (ikx). Then, we free propagate the spatial wave functions corresponding to the ground state and the excited state. By the end of the slice, the |g> state wave packet center position won't change but the wave packet will spread out a little. The little wave packet in state |e> will behave slightly differently. Since it has an extra phase factor exp(ikx), the center position of that wave packet will move to the right at the speed of ħk/m and the wave packet will also spread a little. At the end of the next slice, the initial ground state part of the wave function would have a small component of the excited state with an extra phase factor exp (ikx) for that part of the wave function. The large part of the wave

function will stay in the ground state. The initial excited state part of the wave function will have a small component of the ground state with an extra phase factor exp (-ikx) for that part of the wave function. The large part of the wave function will stay in the excited state. Then we group the two parts of the ground state wave functions and let it propagate freely. The same will be done for the two parts of the excited state wave function. The process will repeat itself as we go along all the slices.

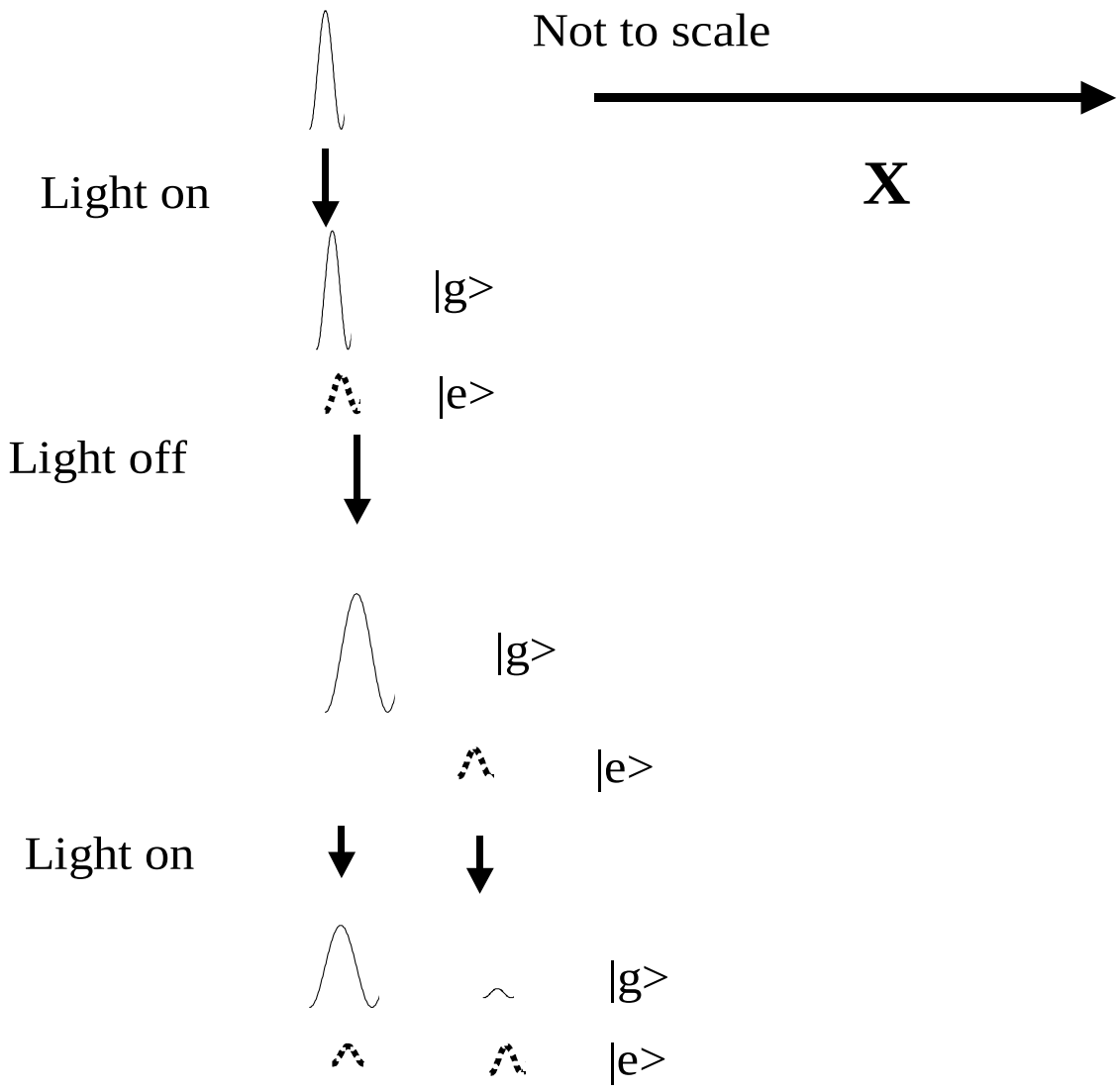

Figure 5.2 *The exaggerated version of the scheme of the simulation process. The solid line represents the ground state and the dotted line represents the excited state.*

To detect the atomic interference, we need to scan the phase of part of light beam. Describe this in physics, which is the Rabi frequency that will have a phase factor. Suppose we change the phase by δ, Hamiltonian will become

$$H_R = \frac{\hbar}{2}\begin{bmatrix} 0 & -|\Omega| e^{i\delta} \\ -|\Omega| e^{-i\delta} & 0 \end{bmatrix}. \qquad \text{(eq. 5.15)}$$

Apply rotating wave transformation, as what we did before in section 2.1, by applying a transformation matrix Q where

$$Q = \begin{bmatrix} e^{-\frac{i\delta}{2}} & 0 \\ 0 & e^{\frac{i\delta}{2}} \end{bmatrix} \qquad \text{(eq. 5.16)}$$

$$H_R' = Q^{-1} H_R Q = \frac{\hbar}{2}\begin{bmatrix} 0 & -|\Omega| \\ -|\Omega| & 0 \end{bmatrix} \qquad \text{(eq. 5.17)}$$

and

$$|\Psi>_R = Q|\Psi>. \qquad \text{(eq. 5.18)}$$

In matrix form, we have

$$\begin{bmatrix} c_e' \\ c_g' \end{bmatrix} = \begin{bmatrix} e^{-\frac{i\delta}{2}} & 0 \\ 0 & e^{\frac{i\delta}{2}} \end{bmatrix}\begin{bmatrix} c_e \\ c_g \end{bmatrix} = \begin{bmatrix} c_e e^{-\frac{i\delta}{2}} \\ c_g e^{\frac{i\delta}{2}} \end{bmatrix} \qquad \text{(eq. 5.19)}$$

5.2 Simulation results

Figure 5.3 shows the trajectory of the ground state and the excited state, the total interaction time is $4\pi/5$. Figure 5.4 shows the population of the ground state and the excited state at each time step, corresponding to the trajectory in Figure 5.3.

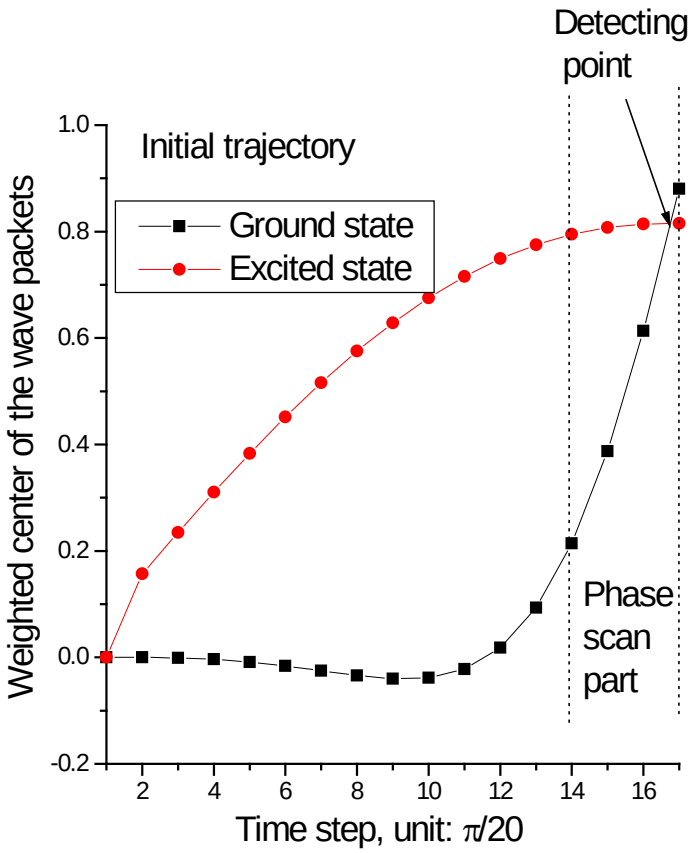

Figure 5.3 *The initial trajectory of the center of the ground state and excited state wave packet. The total interaction time is $4\pi/5$.*

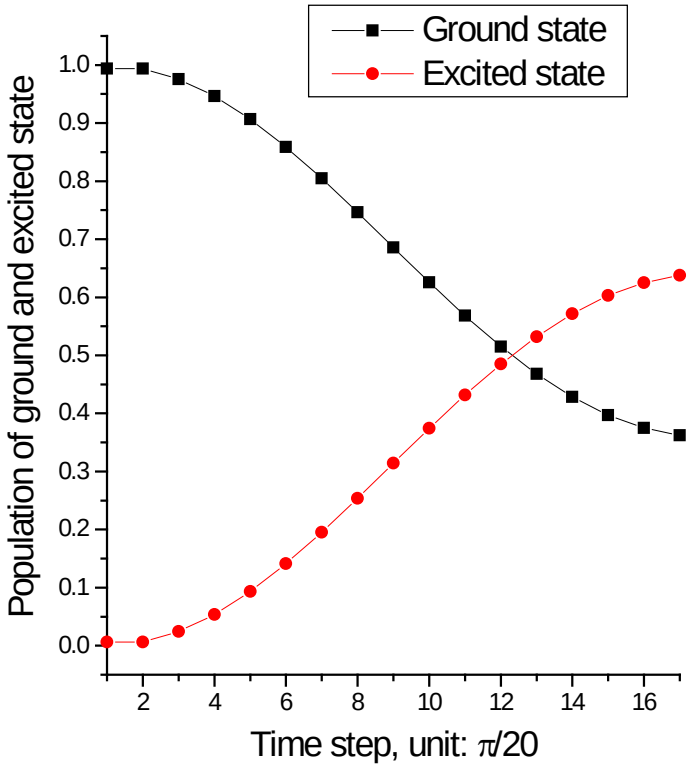

Figure 5.4 *The population of the ground state and the excited state at each time step.*

Figure 5.5 shows the population of excited state at the detecting point of Figure 5.3 as a function of the phase scanned over the part indicated in Figure 5.3.

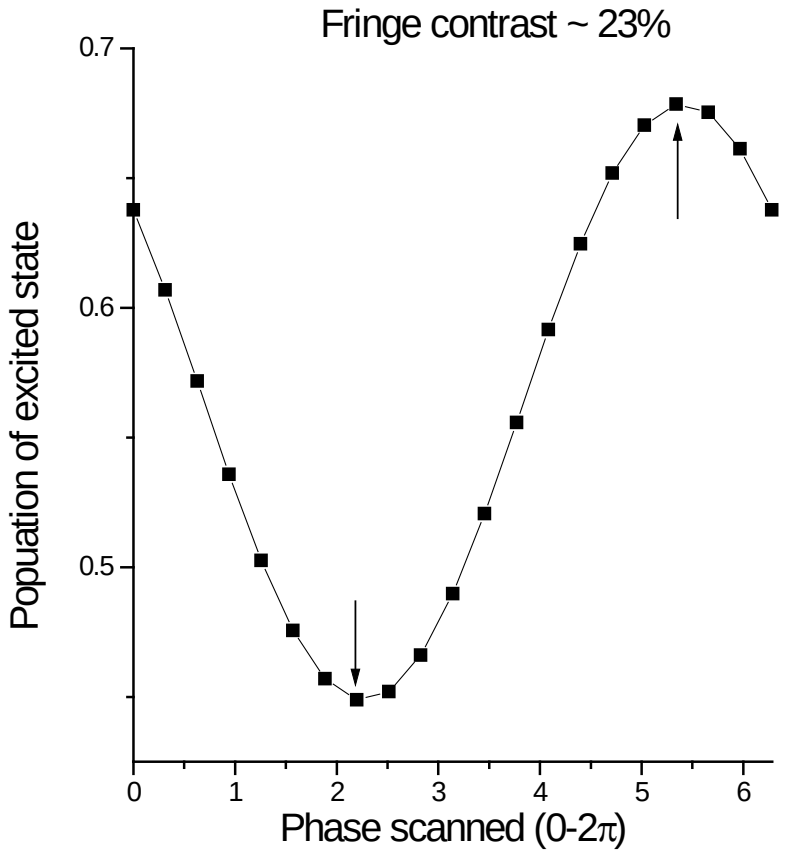

Figure 5.5 *The population of excited state we can detect at the end of the trajectory as a function of the phase scanned over the last part of the trajectory, as indicated in Figure 5.3*

Figure 5.6-5.10 show the wave packets of the ground state and the excited state evolve at each time step along the initial trajectory.

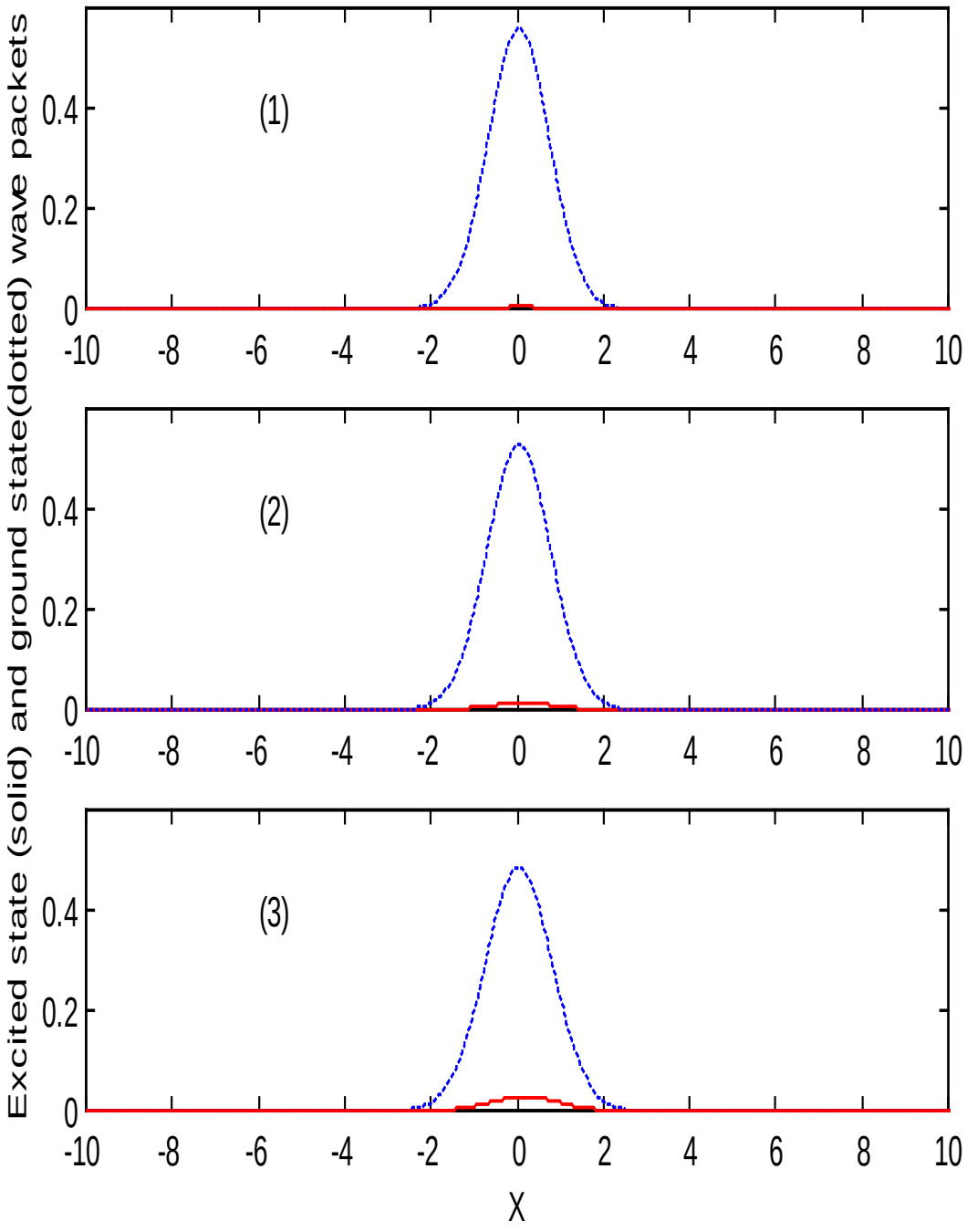

Figure 5.6 *The wave packets of the ground state and the excited state of the first three time steps.*

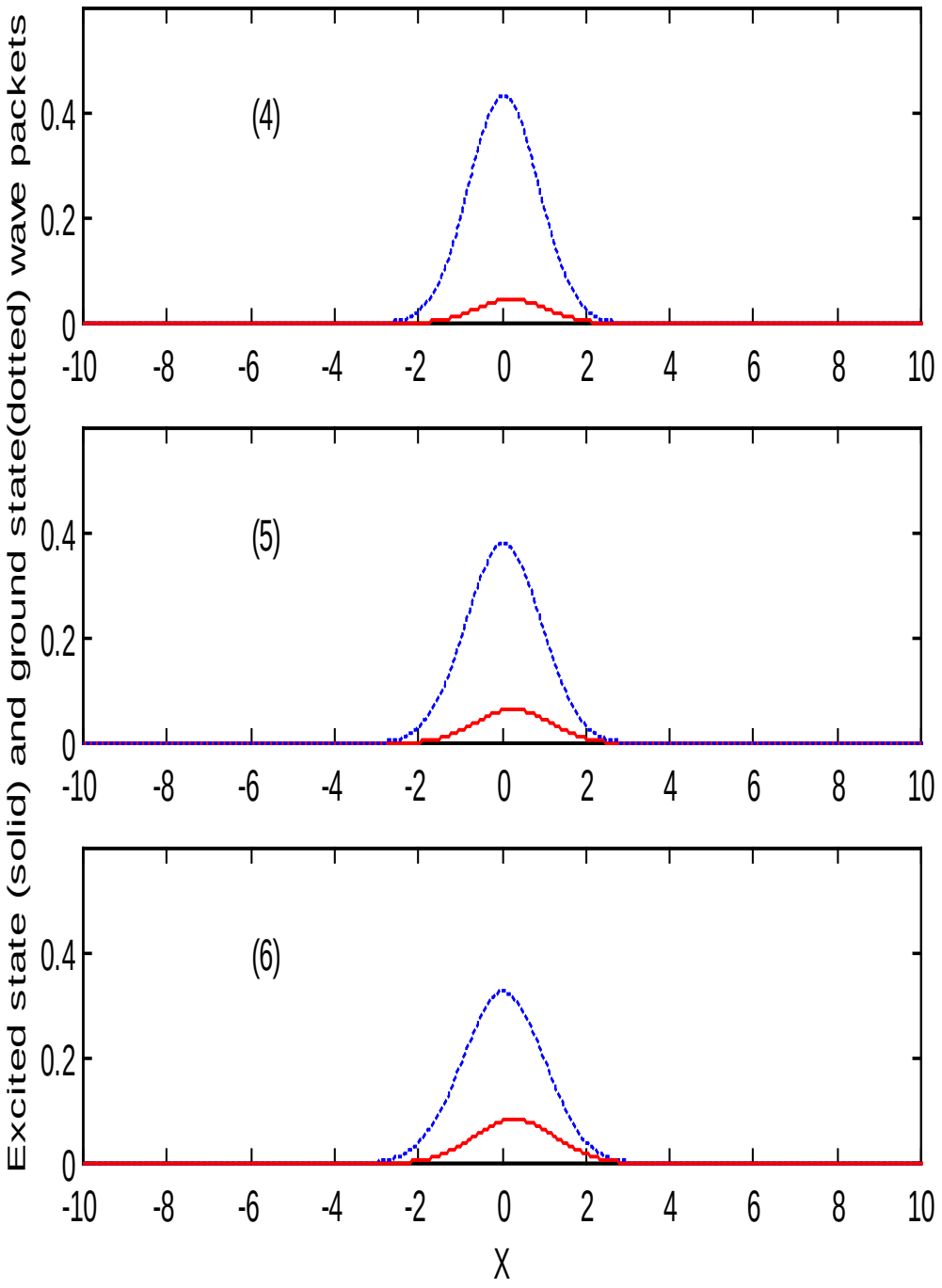

Figure 5.7 *The wave packets of the ground state and the excited state of the second three time steps.*

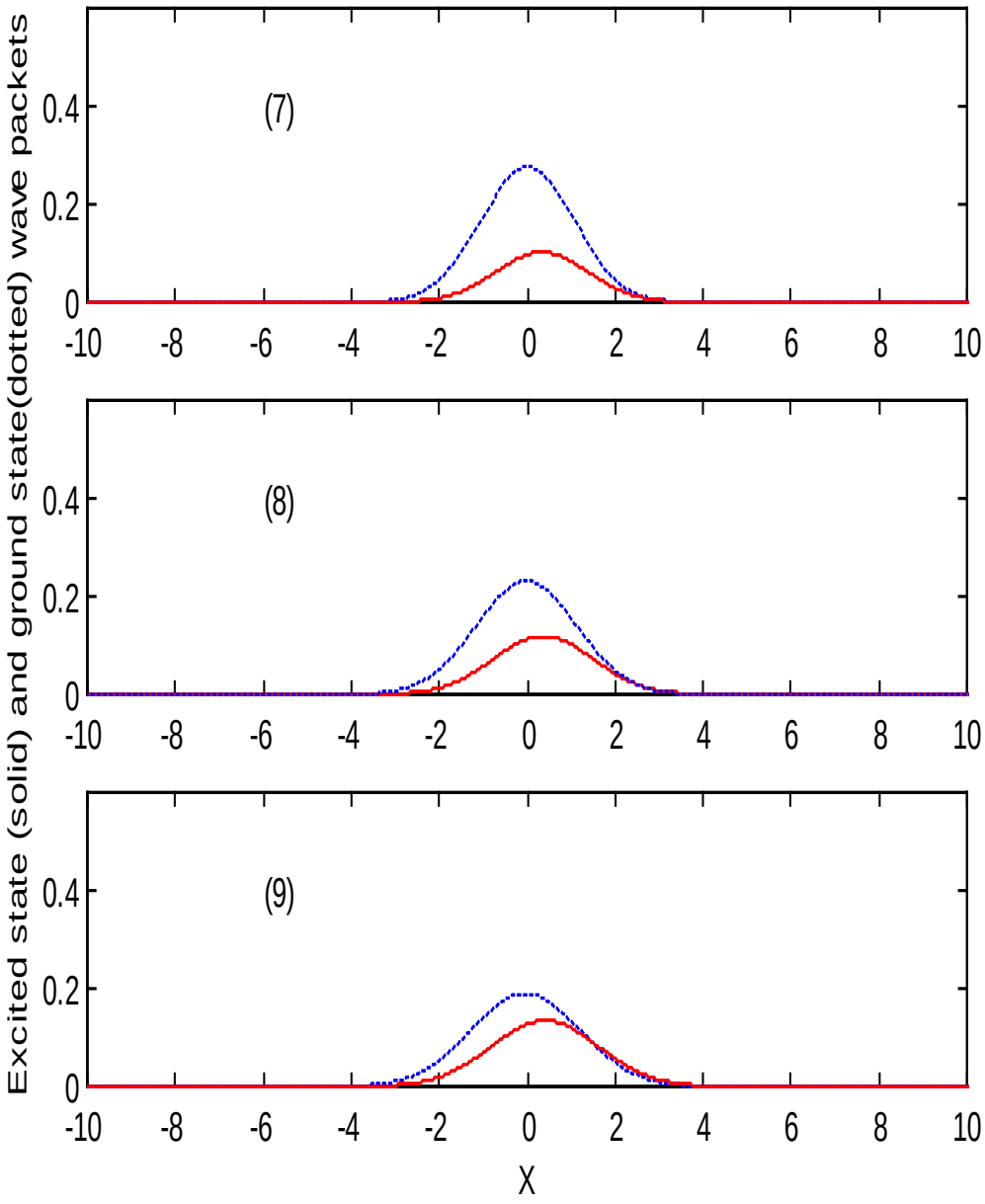

Figure 5.8 *The wave packets of the ground state and the excited state of the third three time steps.*

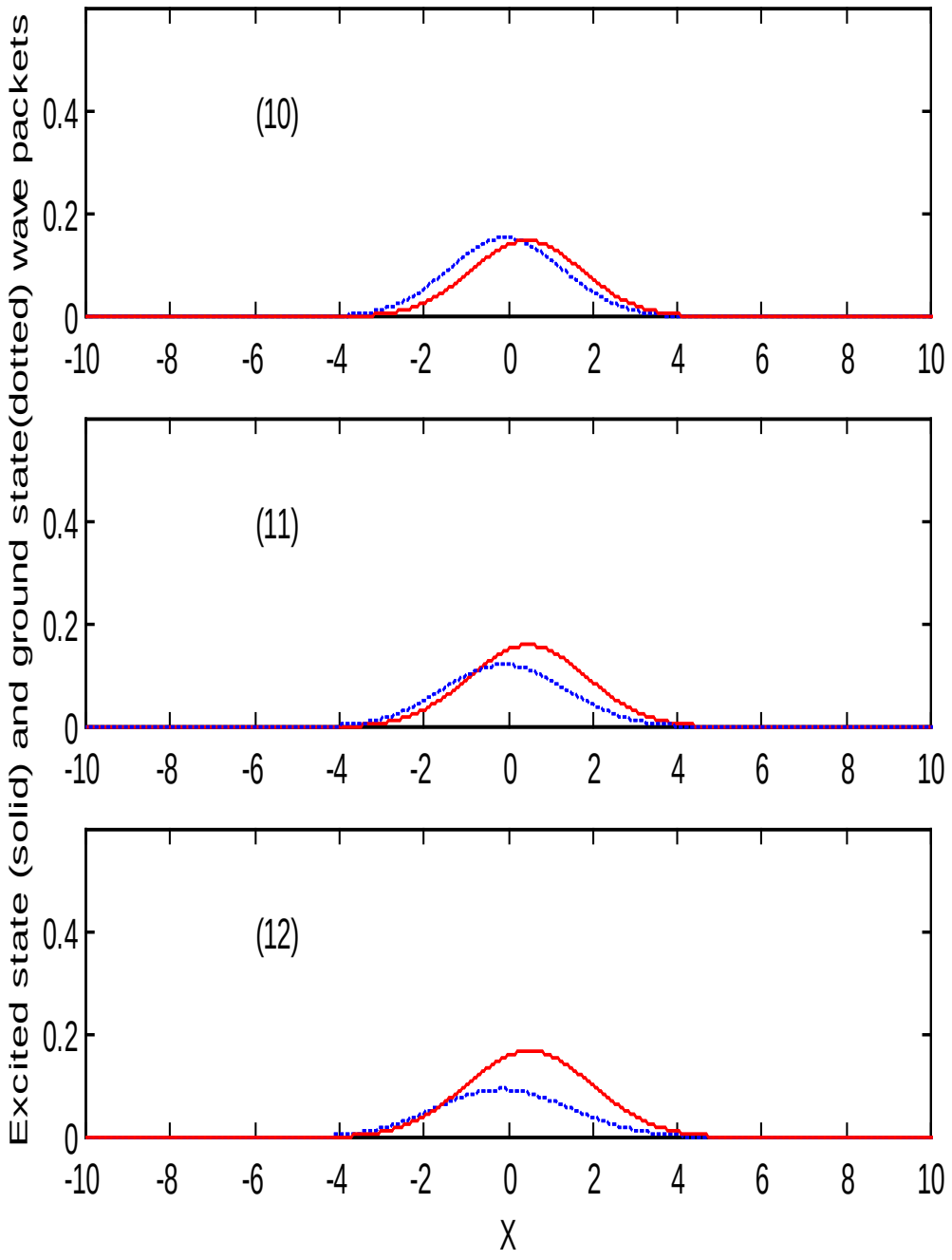

Figure 5.9 *The wave packets of the ground state and the excited state of the fourth three time steps.*

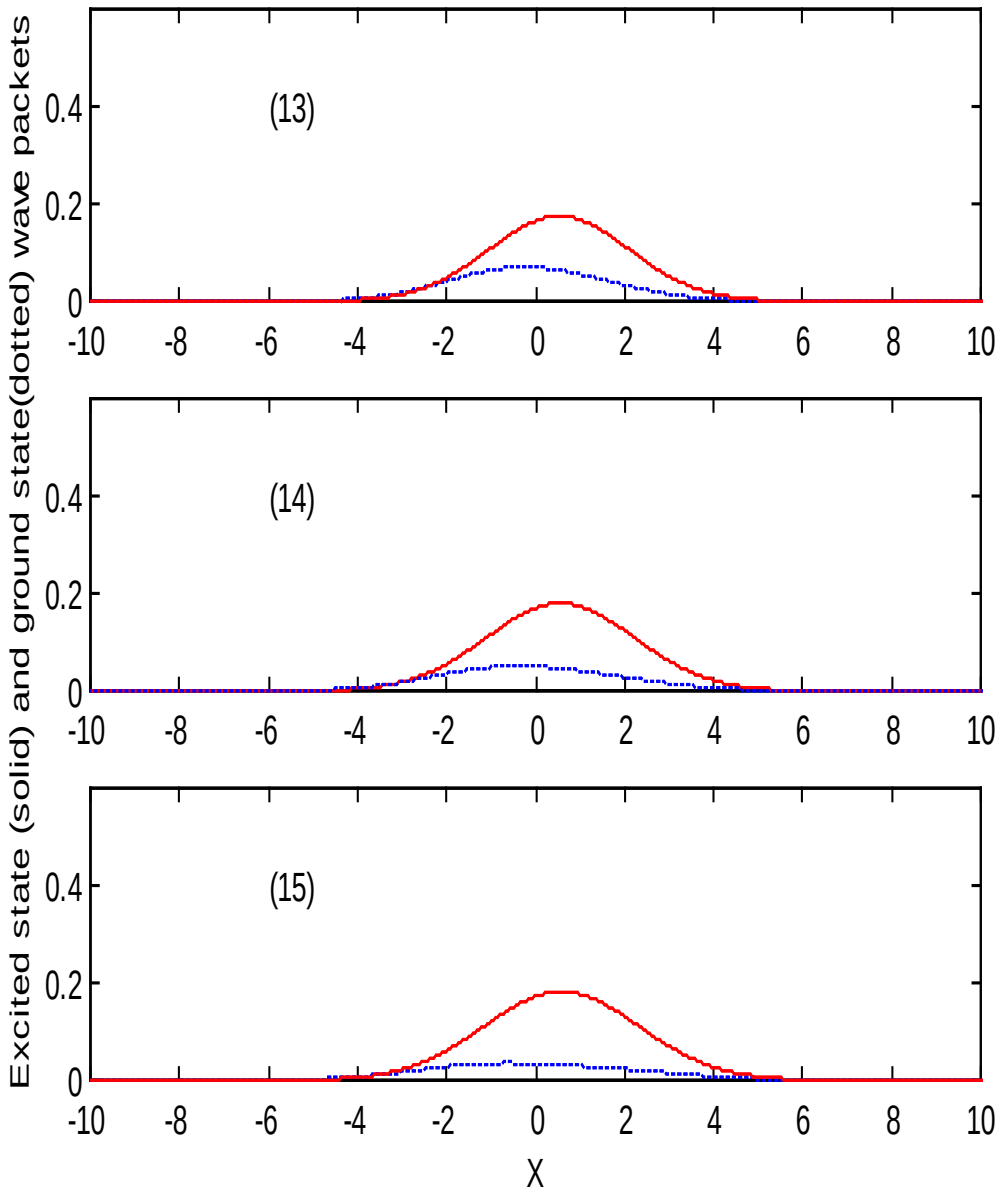

Figure 5.10 *The wave packets of the ground state and the excited state of the fourth three time steps.*

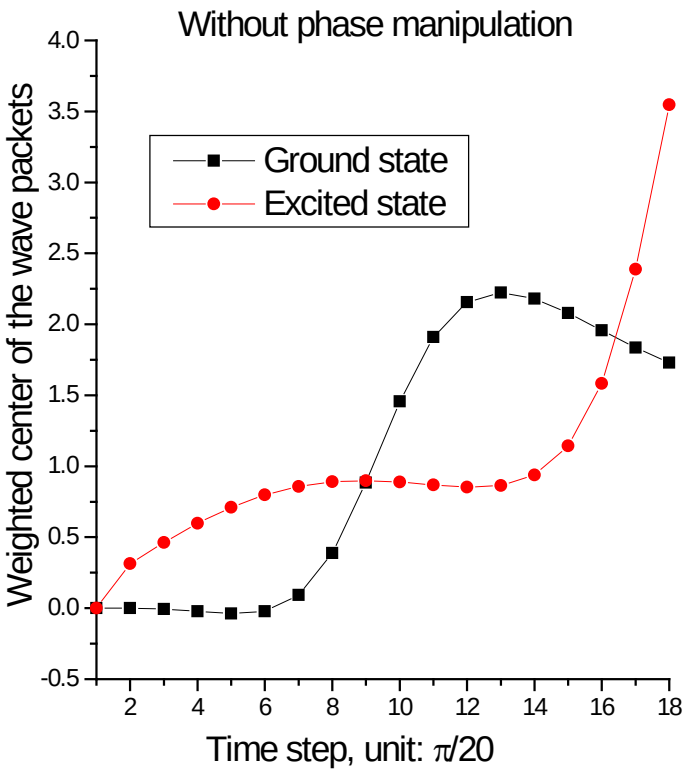

Figure 5.11 *Without phase manipulation, the trajectory of the excited state and the ground state will cross each other again and again as we apply longer and longer Raman pulse.*

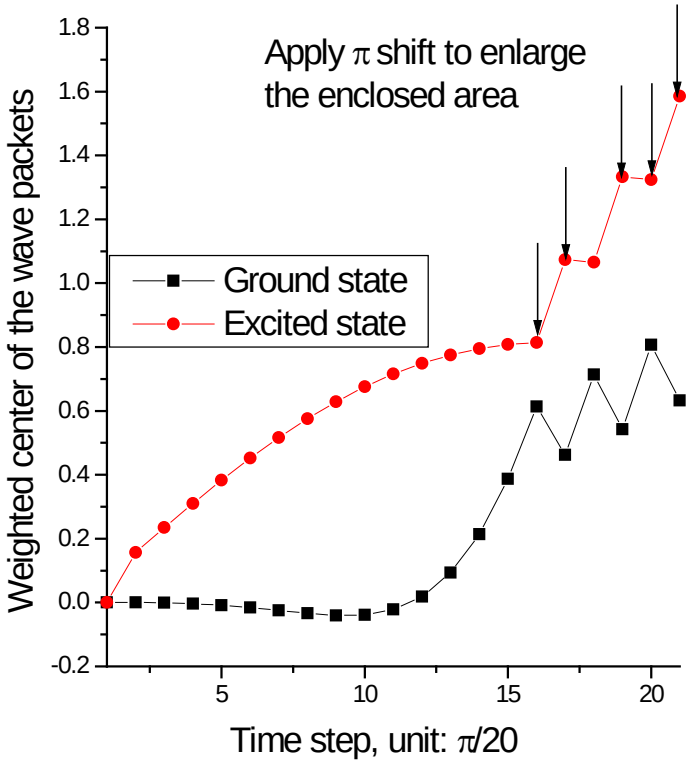

Figure 5.12 *Manipulating the trajectory by applying π shift.*

We want to investigate whether we can enlarge the enclosed area of the interferometer. Figure 5.11 shows the trajectory when we make the Raman pulse longer. Without any manipulation, we see that the trajectory of the ground state and the excited state will cross each other. Figure 5.12 shows that by applying π shift to part of the Raman beam, we can effectively change the trajectory. Figure 5.13 shows why the phase shift of the Raman beam would bend the trajectory.

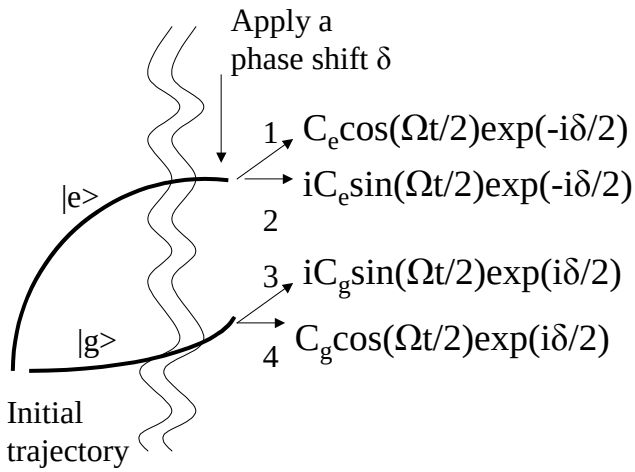

Figure 5.13 *Along the trajectory, the next center positions of the wave packets for state |e> and |g> are determined by the interference of wave packets 1 and 3, 2 and 4. Phase shift plays an important role in determine where the constructive interference will be.*

Figure 5.14 shows the trajectory of the ground state and the excited state with a bigger enclosed area; the total interaction time is 2π. There are a few π shifts applied in the earlier part of the Raman beam.

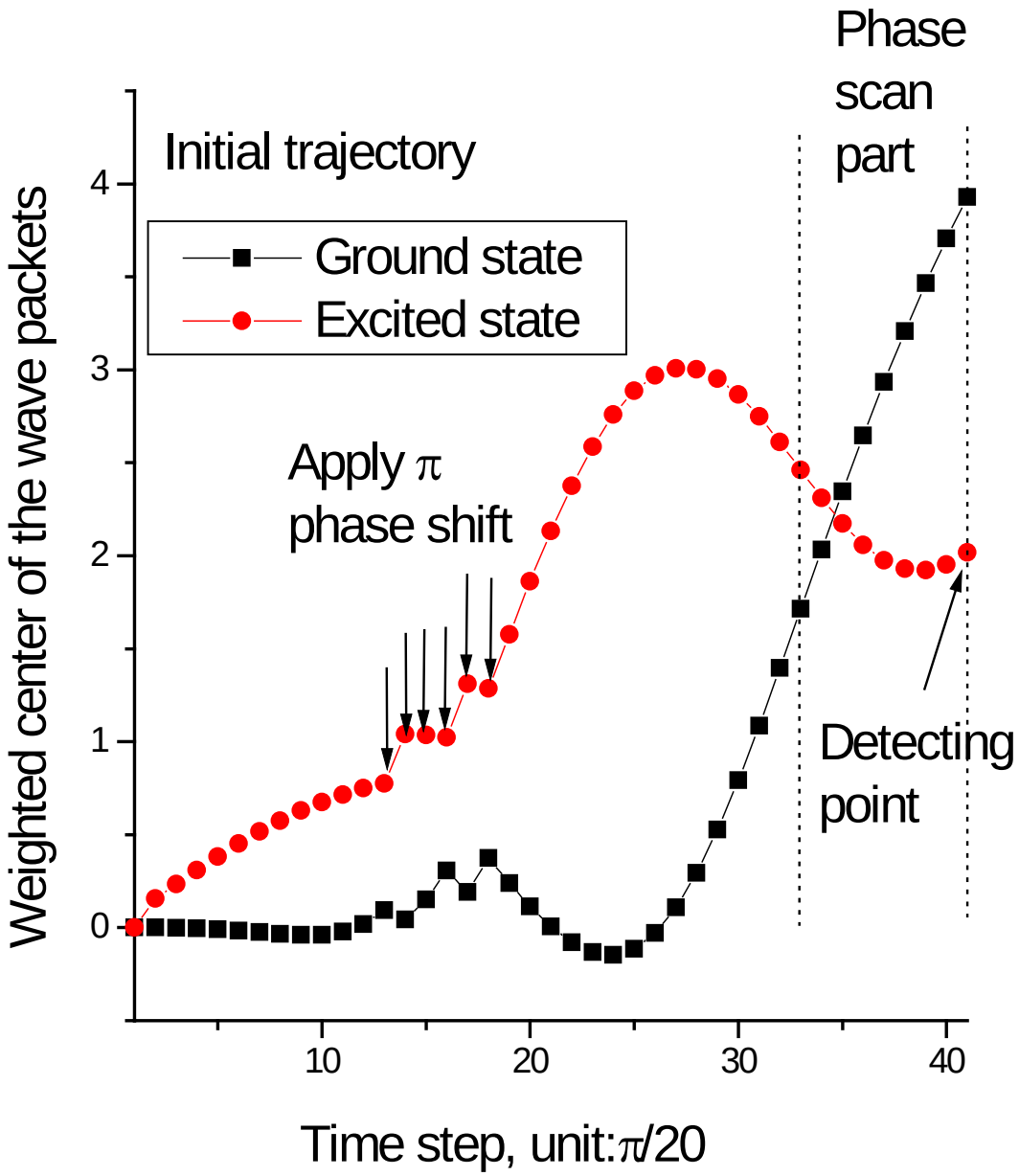

Figure 5.14 *The initial trajectory of the center of the ground state and excited state wave packet. The total interaction time is 2π. At the time steps with black arrows, a π phase shift is applied to change the trajectory so that the interferometer can enclose bigger area.*

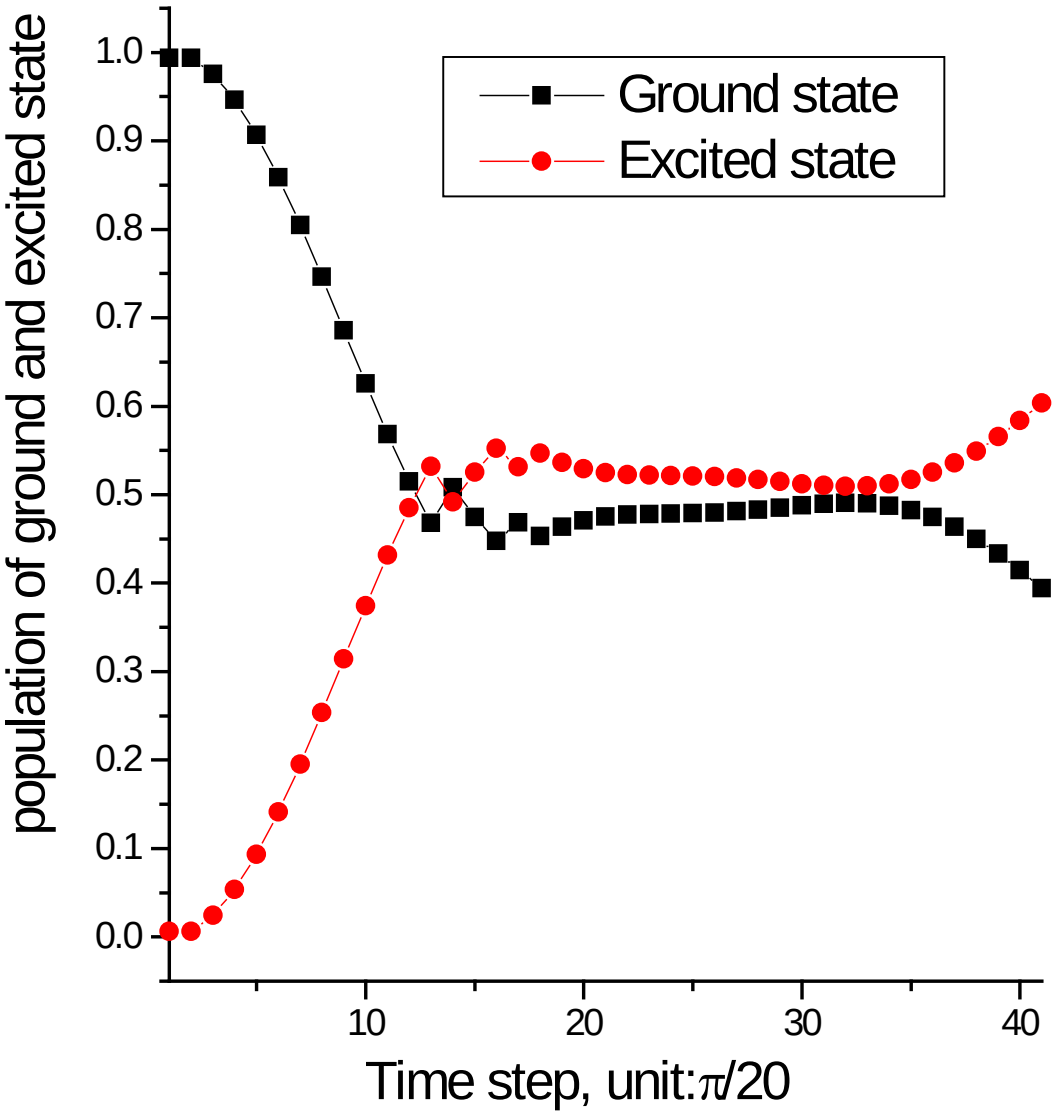

Figure 5.15 *The population of the ground state and the excited state at each time step.*

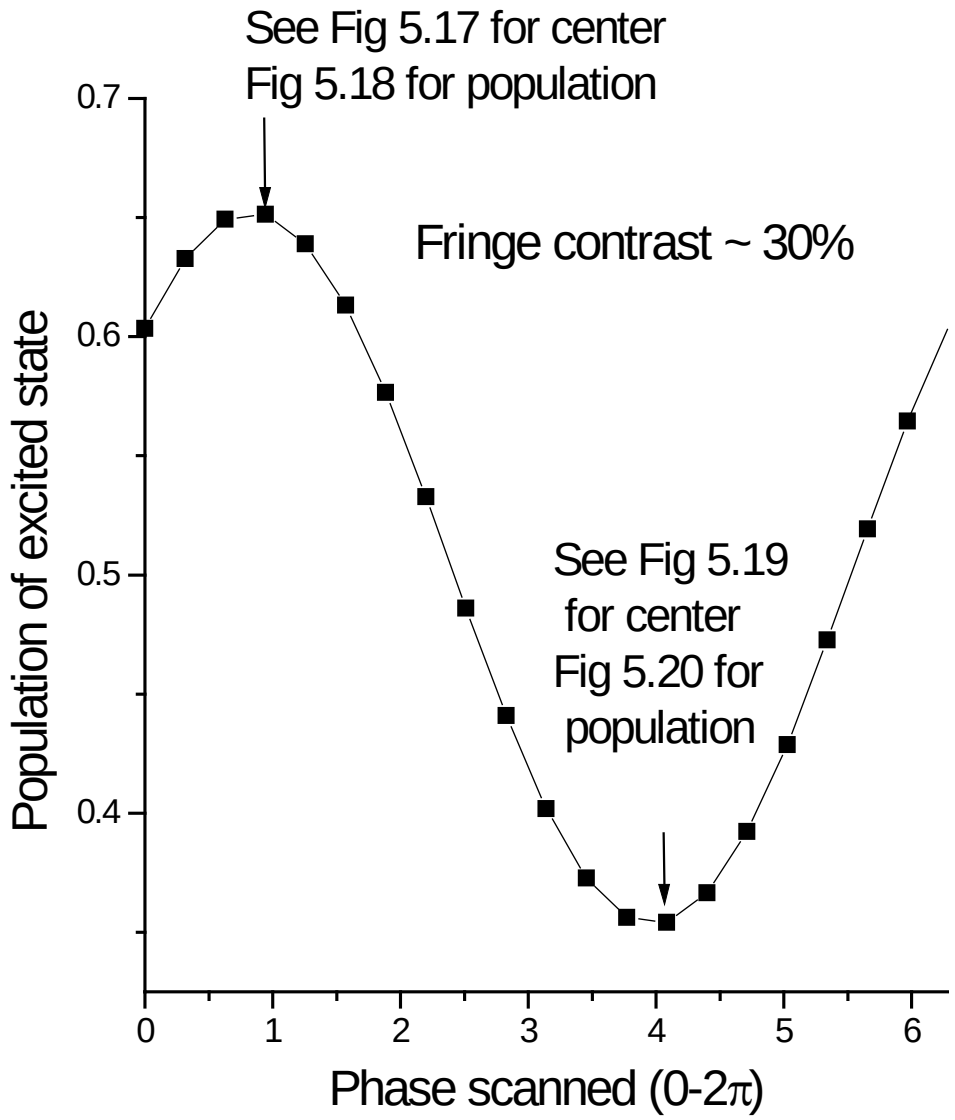

Figure 5.16 *The population of excited state we can detect at the end of the trajectory as a function of the phase scanned over the last part of the trajectory, as indicated in Figure 5.14*

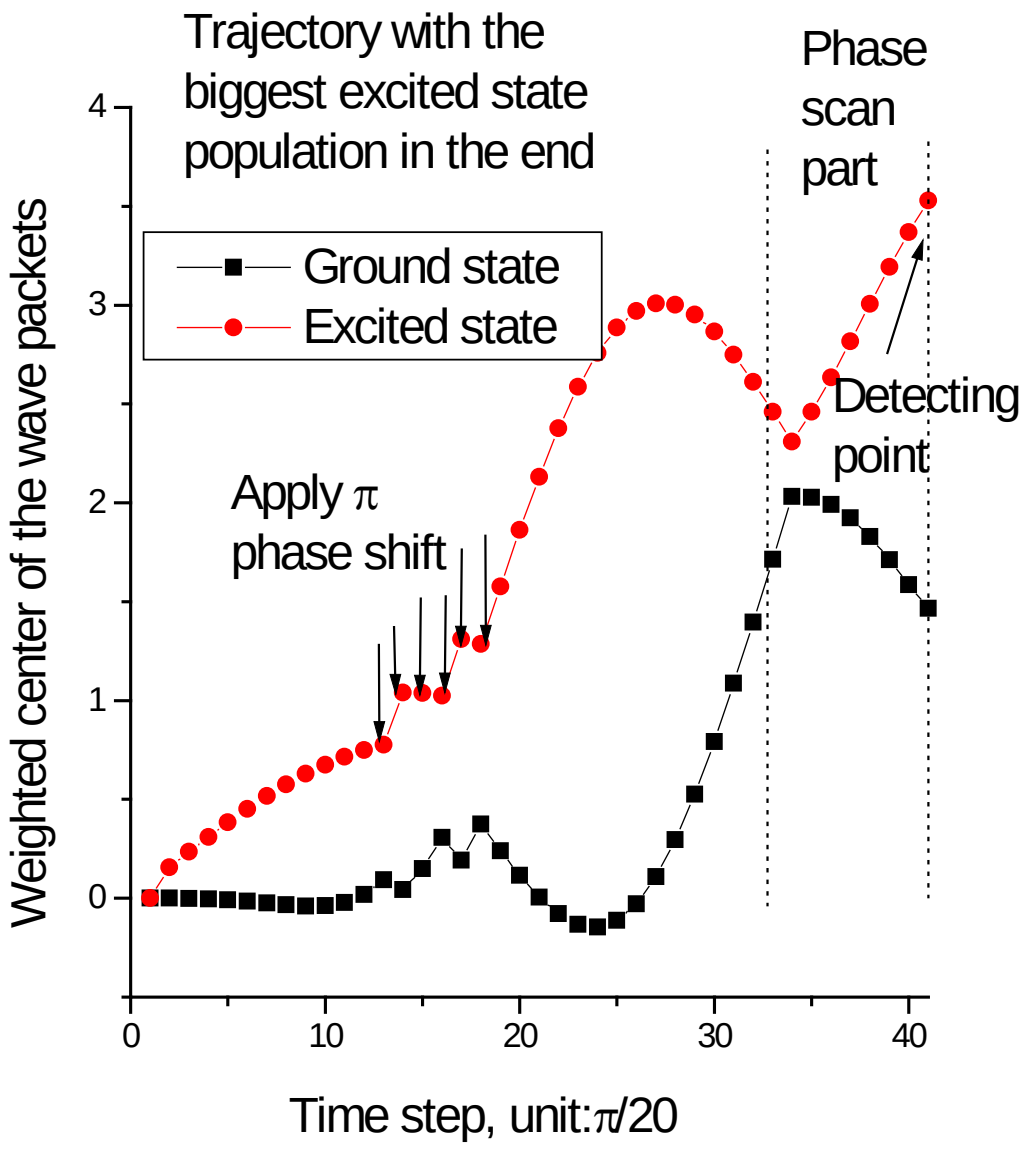

Figure 5.17 *The trajectory of the center position of the ground state and the excited state of the biggest population point in Figure 5.16*

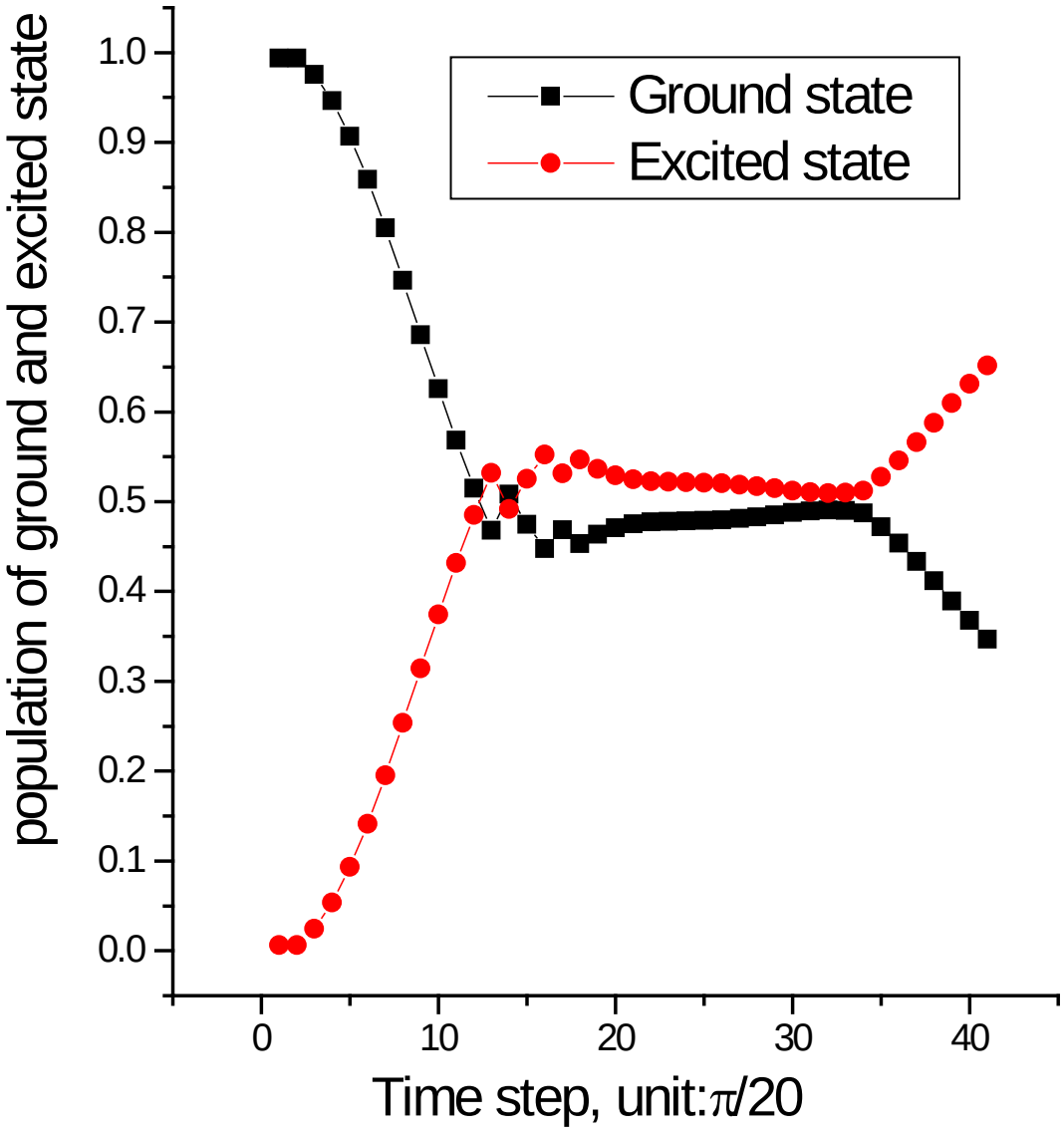

Figure 5.18 *The corresponding population for the trajectory in Figure 5.17*

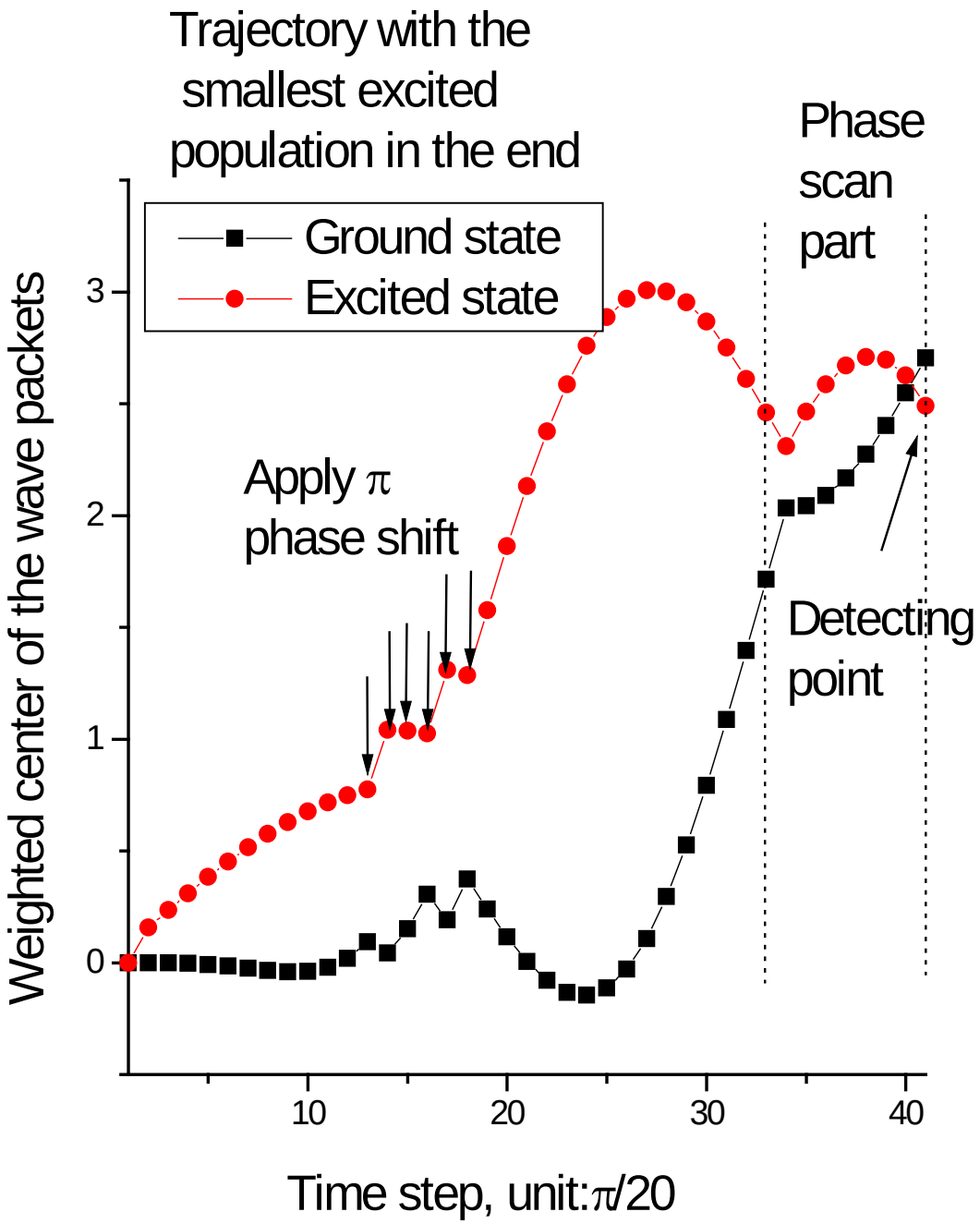

Figure 5.19 *The trajectory of the center position of the ground state and the excited state of the smallest population point in Figure 5.16*

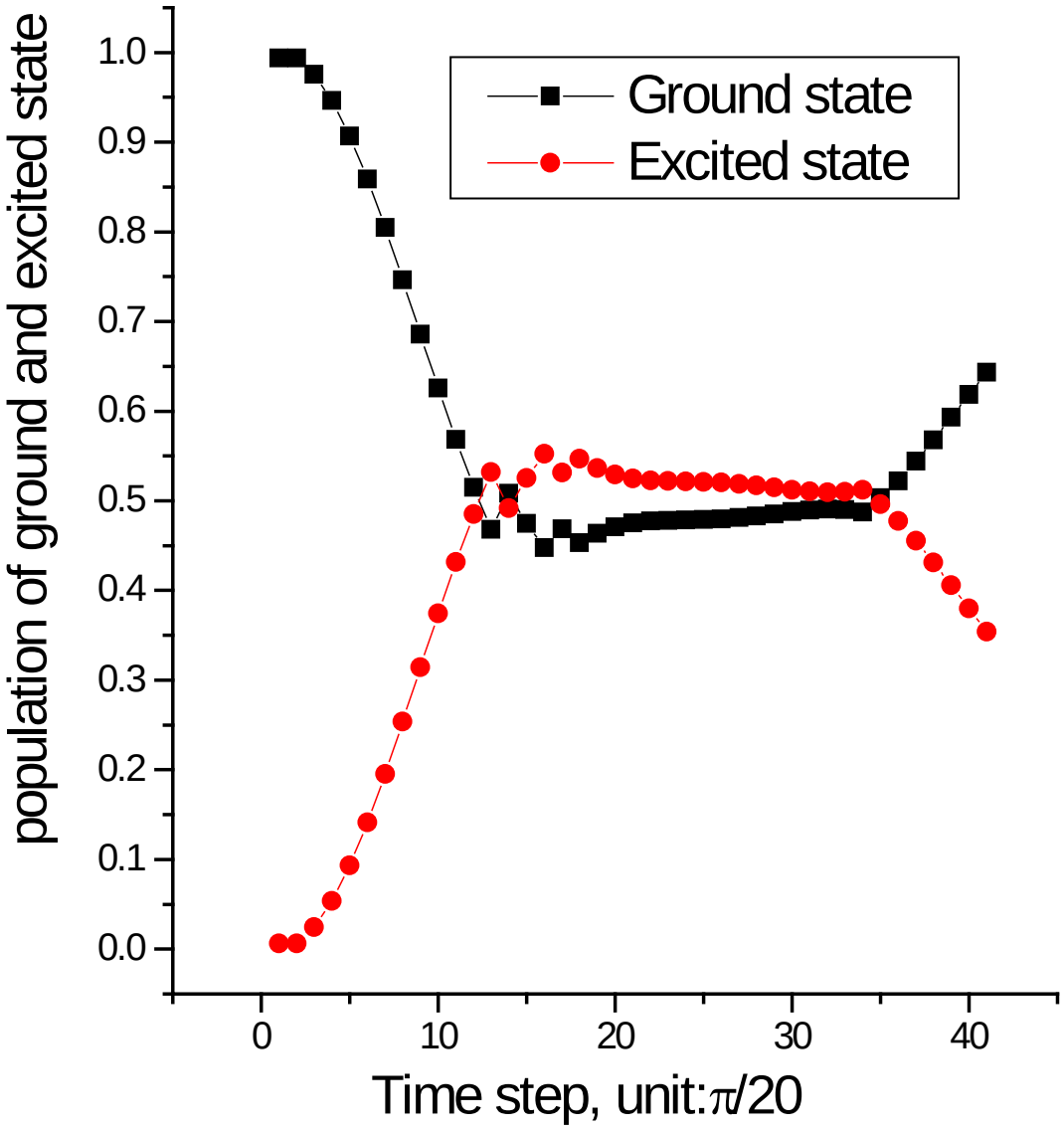

Figure 5.20 *The corresponding population for the trajectory in Figure 5.19*

Figure 5.15 shows the population of the ground state and excited state at each time step. Figure 5.16 shows the population of excited state we can detect at the end of the trajectory as a function of the phase scanned over the last part of the trajectory, as indicated in Figure 5.14. The contrast of the atomic interference fringe in this case is about 30%. Figure 5.17 shows the trajectory of the center position of the ground state and the excited state of the biggest population point in Figure 5.16, while Figure 5.19 shows the smallest point. Figure 5.18 shows the corresponding population for the trajectory in Figure 5.17, while Figure 5.20 shows the corresponding population for the trajectory in Figure 5.19.

Figure 5.21 shows another trajectory with the same interaction time but initially has one more π phase shift point. Figure 5.22 shows the corresponding population at each time step. Figure 5.23 shows the population of the excited state at the end of the trajectory as a function of the phase scanned over the part indicated in Figure 5.21.

Comparing to the trajectory in Figure 5.14 and in Figure 5.21, we see that applying a π phase shift to the light beam would definitely change the trajectory of the center of the ground state and the excited state. If we let the atom interact with the light without changing any light phase, the trajectory of the ground state and the excited state will eventually form an enclosed loop. However, if we can apply a π phase shift to the light beam at some points, we can make the enclosed loop bigger and bigger.

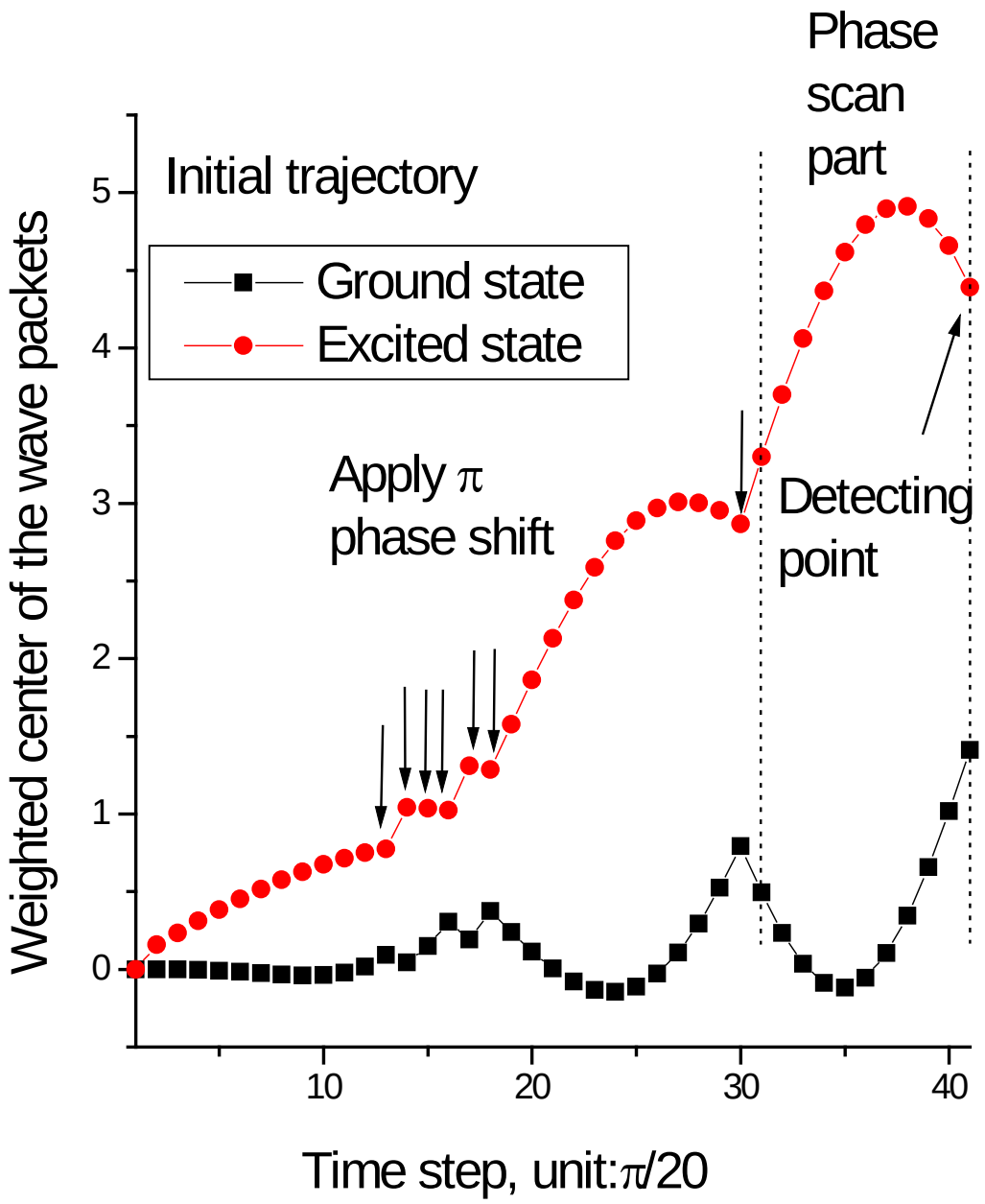

Figure 5.21 *Another trajectory with the same interaction time but initially have one more π phase shift point, compare to Figure 5.3*

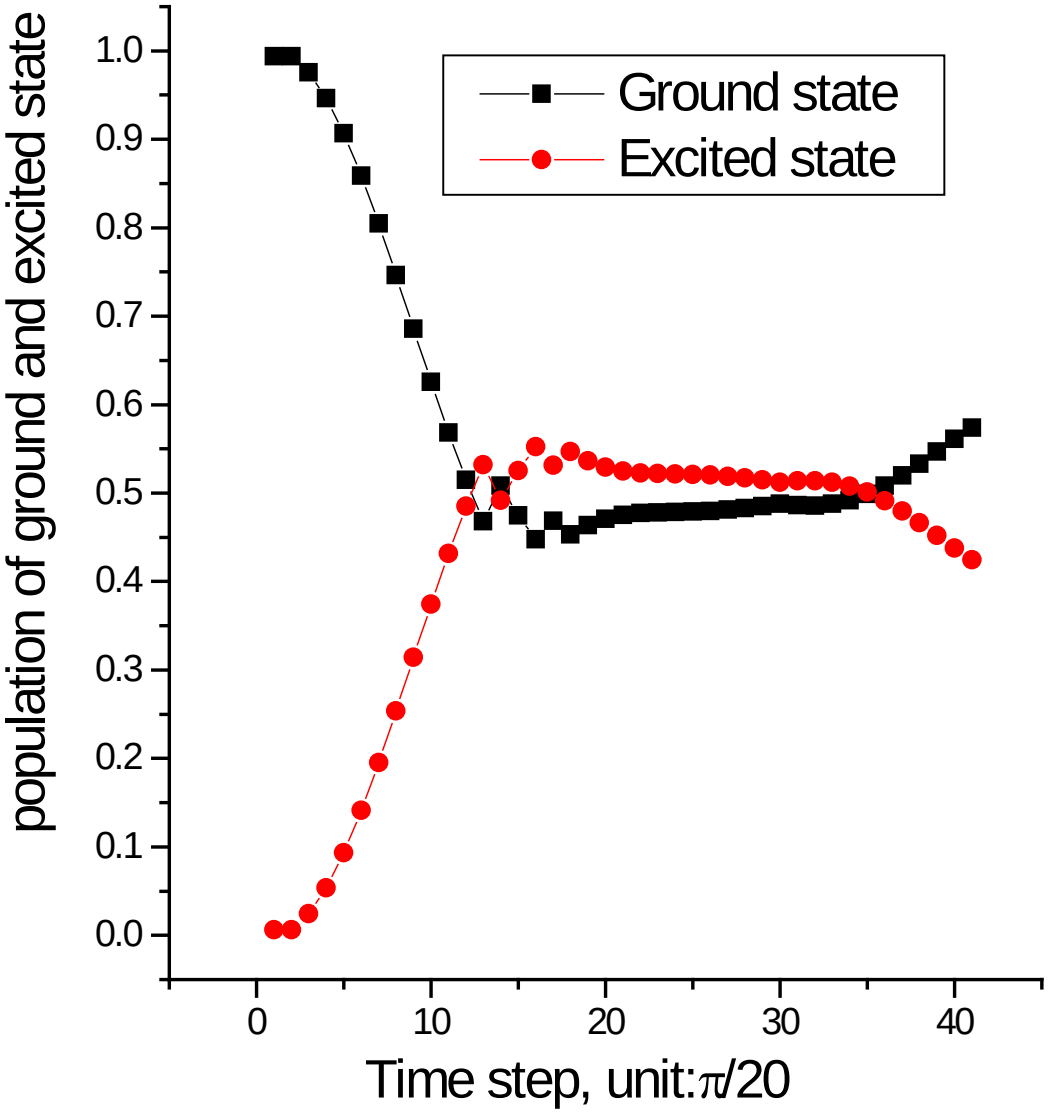

Figure 5.22 *The population of the ground state and the excited state of the trajectory shown in Figure 5.10 at each time step.*

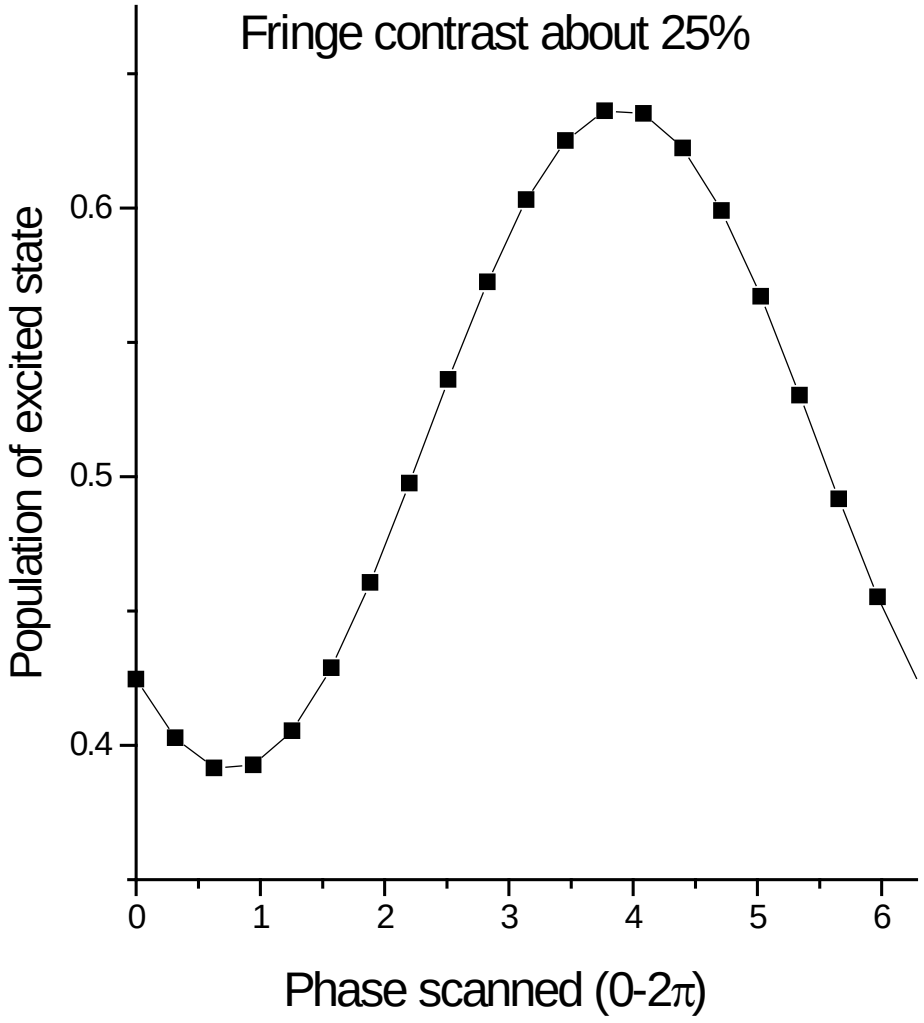

Figure 5.23 *The population of the excited state at the end of the trajectory as a function of the phase scanned over the part indicated in Figure 5.10.*

Chapter Six:

Conclusion and Future Work

The goal of this project, to investigate the possibility of building a large angle, large area atom interferometer has come a long way. We started with a Bichromatic standing wave method and discovered the scheme's limitations, the most serious one being that we were limited by the available laser power to completely carry through that method. Subsequently we moved on with our work on the multiple Raman pulses scheme. While we were struggling with the technical difficulties of this experiment, another research group succeeded with the $\pi/2$- π- $\pi/2$ experiment. We chose to extend this idea further and proceeded to implement the multiple π pulses scheme. Unfortunately, after considerable effort was put into this project our vacuum system was completely destroyed by an accident out of our control. Nevertheless, since further work along this line is worthwhile because this scheme can be extended to two-dimensional atom interferometers or even further, to generate arbitrary pattern nanolithography, someone else in our group is continuing this work and is studying the theoretical aspects of arbitrary pattern generation using this type of atom interferometer.

To resume the experimental investigation of the work that we had already carried out and to apply our knowledge gained from the previous systems, we built a completely new small-scale atomic beam machine. To our great relief we saw the atomic interference on this small atomic beam machine.

Looking at the experimental results that we obtained in chapter four and the simulation results in chapter five, it seems reasonable to conclude that there is a very good possibility to design a successful large angle and large area atom interferometer based on the novel scheme of using single Raman pulse. The experimental implementation of this new scheme should be a lot easier than the original one which was based on multiple Raman pulses since in the new scheme only one Raman pulse is needed which simplifies the alignment considerably. To enlarge the enclosed area, one only needs to apply at predetermined positions π phase shifts to one of the Raman beams. This could be done using phase plates with adjustable positions.

It definitely seems worthwhile to continue the investigation of this project to gain a more thorough theoretical and experimental understanding of its aspects.

Reference:

[1]Special Issue Atom Optics (1994). Optics and Interferometry with Atoms (Special issue) J. Phys.II **4**.

[2] Special Issue Atom Optics (1992). Atom Optics (Special issue) Appl. Phys. B **54**

[3] Edited by Paul R. Berman, "Atom Interferometry", Academic Press,1997

[4] T. wong, M.K. Olsen, S.M. Tan, D.F. Walls "Bichromatic beam splitter for three-level atoms" phys. Rev. A vol 52, number 3 (1995)

[5] Todd L. Gustavson, Ph.D thesis, " Precision rotation sensing using atom interferometry"

[6] T.L. Gustavson, P.Bouyer, and M.A. Kasevich, Phys. Rev. Lett. **78**, 2046 (1997)

[7] reference for other ways to do nanolithography

[8] Sze M. Tan, Daniel F. Walls "Analysis of the bichromatic atomic beam splitter" , Opt. Commun. 118 (1995)

[9] Steven chu's experiment,our paper.

[10] Tanya's thesis

[11] our paper

[12] Murray Sargent III, Marlan O. Scully, Willis E. Lamb, Jr. "Laser physics"

[13] Paul R. Berman edited, "Atom Interferometry"

[14] C. J. Bordé : Phys. Lett. A **140**, 10(1989)

[15] L. Allen, J. H. Eberly "Optical Resonance and Two Level Atoms"

[16] Rodney Loudon "The quantum theory of light", second edition

[17] M. S. Shahriar, P. R. Hemmer, D.P. Katz, A. Lee, and M. G. Prentiss "Dark-state-based three-element vector model for the stimulated Raman interaction" phys. Rev. A. **55,** 2272(1997)

[18] Y. Tan, J. Morzinski*, A.V. Turukhin, and M.S. Shahriar "Two-Dimensional Atomic Interferometry for Creation of Nanostructures", submitted to phy.s. Rev. A
[19] Ti:sapphire laser manual and communication with Coherent technical support staff
[20] W. Demtroder, Laser Spectroscopy, Springer, 1996.
[21] M.S.Shahriar, A.V. Turukhin, T.Liptay, Y.Tan, P.R.Hemmer "Demonstration of injection locking a diode laser using a filtered electro-optic modulator sideband", Opt. Commun. 184 (2000)

[22] Philip Robert Hemmer's Ph.D thesis " Precision studies of stimulated resonance Raman scattering in atomic beams." 1984, MIT